Physik-Department

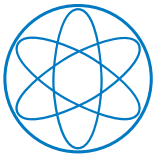

Neutrino Masses and Mixings in Future Experiments

Diploma Thesis
written by
Alexander Merle

July 2006

Technische Universität München
Physik-Department T30d
Theoretical Elementary Particle Physics
Prof. Dr. Manfred Lindner

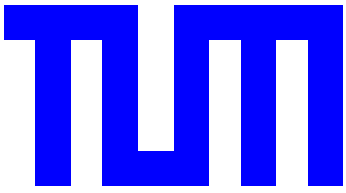

“Staunen ist der erste Schritt zu einer Erkenntnis.”
– Louis Pasteur

“There’s a lot goin’ on.”
– GNR

Abstract

In this thesis, we study what can be learned about neutrino masses and mixings in future experiments. After a short introduction, the relevant basics of neutrino physics, namely mass terms and neutrino oscillations, as well as some methods to measure the neutrino mass are explained. Then we introduce one possibility for a future precision measurement of the solar neutrino oscillation parameters, θ_{12} and $\Delta m^2_{\odot}$. This could be done using a Large Liquid Scintillator Detector in combination with a nuclear reactor. Therefore, a detailed statistical analysis has been performed, with the inclusion of possible backgrounds and different systematical errors. With the right setup, even sub–percent precision can be possible. In the next chapter, present and upcoming direct measurements of the neutrino mass are presented. These are the kinematical mass determination using single β–decay and the interesting process called neutrinoless double beta decay ($0\nu\beta\beta$), as well as possible alternatives. Finally, the neutrino mass matrix is discussed in detail with special focus on a future improved limit on the yet unknown neutrino mixing angle θ_{13}. Its most important entry is the effective neutrino mass $|m_{ee}|$, which is the observable quantity in $0\nu\beta\beta$. $|m_{ee}|$ shows an interesting behavior, which is analyzed for normal and inverted mass ordering, and could also help to distinguish between these two possibilities. Furthermore, for some special cases, there can even be an interplay with cosmology, which could be nicely used as cross–check. For the sake of completeness, also the other elements of the neutrino mass matrix as well as correlations coming from possible texture zeros are investigated.

Kurzfassung

Diese Arbeit beschäftigt sich mit der Frage, was man von zukünftigen Experimenten über Neutrinomassen und –mischungen lernen kann. Nach einer kurzen Einleitung werden sowohl die relevanten Grundlagen der Neutrinophysik, nämlich Massenterme und Neutrinooszillation, erklärt, als auch einige Methoden zur Messung der Neutrinomasse. Danach wird eine mögliche zukünftige Methode zur Präzisionsbestimmung der solaren Neutrinooszillations–Parameter, θ_{12} und $\Delta m^2_{\odot}$, vorgestellt. Dies könnte mittels eines großen Flüssigszintillator–Detektors in Kombination mit einem Kernreaktor geschehen. Hierzu wurde eine detailgenau statistische Analyse unter Miteinbeziehung möglicher Hintergrundprozesse und verschiedener systematischer Fehler durchgeführt. Mit dem richtigen Aufbau wäre damit sogar eine relative Genauigkeit von unter einem Prozent machbar. Im darauf folgenden Kapitel werden jetztige und kommende direkte Messmethoden der Neutrinomasse aufgezeigt. Hierzu gehören die kinematische Massenbestimmung mittels des einfachen β–Zerfalls und der interessante Prozess namens neutrinoloser Doppel–β–Zerfall ($0\nu\beta\beta$), sowie mögliche Alternativen hierzu. Schließlich wird noch die Neutrino–Massenmatrix diskutiert, mit speziellem Hinblick auf eine zukünftig verbesserte obere Grenze für den noch unbekannten Neutrino–Mischungswinkel θ_{13}. Ihr wichtigster Eintrag ist die effektive Masse $|m_{ee}|$, welche durch $0\nu\beta\beta$ gemessen wird. $|m_{ee}|$ zeigt ein interessantes Verhalten, welches für die normale und für die invertierte Massenanordnung untersucht wird und auch zur Unterscheidung dieser beiden Möglichkeiten hilfreich sein könnte. Weiterhin kann in bestimmten Spezialfällen auch ein Zusammenspiel mit der Kosmologie auftreten, welches gut als Gegenprobe benutzt werde könnte. Der Vollständigkeit halber werden auch die anderen Elemente der Neutrino–Massenmatrix untersucht und Zusammenhänge, die sich aus möglichen Null–Einträgen ergeben, werden diskutiert.

Contents

Chapter 1

Introduction

In 1930, Wolfgang Pauli postulated the existence of a neutral particle with a tiny mass, that nearly does not take part in any interaction [1]. Since Pauli knew that this particle cannot have an electrical charge, he gave it the name "neutron". His assumptions were based on his strong belief in the physical laws.

At that time, physicists thought that in β^-–decay a nucleus $B(A, Z)$ decays into a daughter nucleus $C(A, Z + 1)$ via emission of only an electron e^-. Since there is a well-defined mass difference between the two nuclei, the spectrum of the β–particle should be completely mono–energetic. But what had been observed was approximately the spectrum from Fig. 1.1, where the energy distribution of the electron is clearly continuous and not discrete as expected.

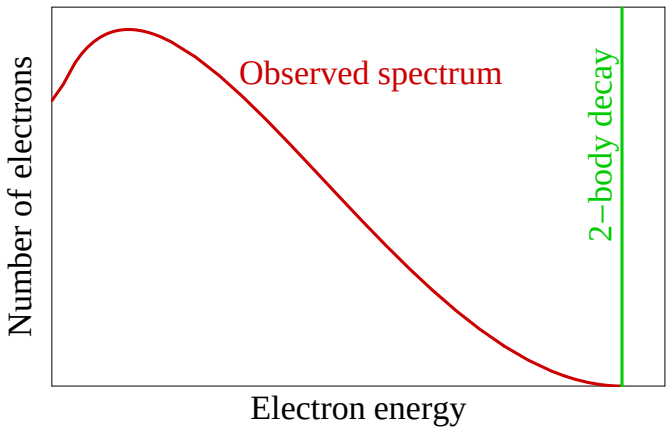

Figure 1.1: The expected 2–body energy spectrum of the electron in β^-–decay compared to the spectrum that has been observed. The missing energy of the electron is carried away by the electron–antineutrino.

Because of this spectrum, Niels Bohr originally wanted to reject even the conservation of energy [2], but Pauli understood that – if the spectrum was correct – also the quantum mechanical conservation of angular momentum and hence the spin statistics would be violated (since the nuclei had both integer spins that cannot couple to a half-integer spin like the electron has). So he postulated a hypothetical particle with small mass, spin $\frac{1}{2}$, and electrical charge zero.
Two years later, in 1932, the "real" neutron was discovered by James Chadwick and people immediately understood that this cannot be that hypothetical particle because of its too large mass. Taking this into account, Enrico Fermi started to call Pauli's particle "neutrino", which means "small neutron" in Italian, and this name has been retained until now.
In 1956, two years before his death, Pauli could finally witness the discovery of "his" particle by Fred Reines (Nobel prize 1995) and Clyde Cowans [1,3], using inverse β–decay of electron antineutrinos on free protons,

$$\overline{\nu}_e + p^+ \rightarrow e^+ + n^0.$$

From that, it is clear that the β^-–decay, from which Pauli concluded the existence of the neutrino must in fact look like

$$n^0 \rightarrow p^+ + e^- + \overline{\nu}_e,$$

which explains the continuous energy spectrum of the electron (since energy is carried away by the neutrino) as well as saves the correct spin statistics (since the neutrino is a fermion with spin $\frac{1}{2}$).
Neutrinos have fascinating properties and are a beautiful part of nature. One just has to imagine that the unbelievable number of 10^{11} neutrinos [4] coming from the sun penetrate every area of 1cm^2 (which is just a thumbnail) on Earth per second. But neutrinos only take part in the weak interaction, which means that they basically do nothing. In the whole life of a human being, only about one (!) of these neutrinos causes a reaction in the body (such as giving an electron of a particular atom a slight hit). But on the other hand, if neutrinos just had slightly different properties (such as a larger mass), our Universe would not look like it does and our whole existence would perhaps be in question.
Let us discover part of the world of neutrinos in the following pages of this thesis. The outline is as follows: in Chapter 2, some basics of neutrino physics will be introduced, such as mass terms, oscillations, and methods for the mass determination. Then, in Chapter 3, we will present a possible future precision measurement of the solar oscillation parameter using a reactor in combination with a Large Liquid Scintillator. Afterwards, Chapter 4 will introduce direct methods of a measurement of the neutrino mass and Chapter 5 will explain what can be learned about the nature of neutrino masses from such experiments. We finally conclude in Chapter 6.

Chapter 2

Neutrino properties and phenomenology

In this chapter, some basics of neutrino physics will be discussed. Since the nature of neutrino masses is still a big riddle, we start at first by introducing different mass terms for neutrinos as well as the famous seesaw mechanism. Afterwards, neutrino oscillations will be explained, whose observation revealed that neutrinos indeed have non–vanishing masses (at least not all existing neutrinos can be massless). Finally, some current experimental methods for the mass determination as well as the actual limits on neutrino masses will be reviewed.
In the common literature, one finds these considerations e. g. in Refs. [1, 5] or any other textbook (or review) on neutrinos.

2.1 Neutrino mass terms

2.1.1 The Dirac mass term

For fermions (like e. g. quarks), the Lagrangian,

$$\mathcal{L} = \overline{\Psi}(i\partial\!\!\!/ - m)\Psi, \tag{2.1}$$

normally contains a so–called mass term, that has its origin in the Dirac equation, where Ψ denotes the (Dirac-) spinor of the particle and $\partial\!\!\!/$ is defined as $\gamma^\mu\partial_\mu$ with the γ-matrices obeying the Clifford algebra $\{\gamma^\mu, \gamma^\nu\} = \gamma^\mu\gamma^\nu + \gamma^\nu\gamma^\mu = 2g^{\mu\nu}\mathbb{1}$. $\overline{\Psi}$ is the adjoint spinor with $\overline{\Psi} = \Psi^\dagger\gamma^0$ and the metric of the Minkowski spacetime is $g^{\mu\nu} = (1, -1, -1, -1)$. For the γ-matrices, there exist different respresentations.
One now can divide the Dirac spinor Ψ into its chiral components, the right– and left–handed fields $\Psi_{\mathrm{R,L}}$, where

$$\Psi_{\mathrm{R,L}} \equiv \mathcal{P}_{\mathrm{R,L}}\Psi = \frac{1 \pm \gamma^5}{2}\Psi, \tag{2.2}$$

where $\gamma^5 \equiv i\gamma^0\gamma^1\gamma^2\gamma^3$. From the Clifford algebra, it follows that $\mathcal{P}^2_{\mathrm{R,L}} = \mathbb{1}$ and $\mathcal{P}_\mathrm{R}\mathcal{P}_\mathrm{L} = \mathcal{P}_\mathrm{L}\mathcal{P}_\mathrm{R} = 0$, and hence for the mass term

$$\mathcal{L}_{\mathrm{mass}} = -m\overline{\Psi}\Psi = -m(\overline{\Psi}_\mathrm{L}\Psi_\mathrm{R} + \overline{\Psi}_\mathrm{R}\Psi_\mathrm{L}). \tag{2.3}$$

This is the so–called Dirac mass term. One can clearly see that the mass term connects a left–handed field with its right–handed partner, and vice versa, so it flips the chirality of a particle.
In the Standard Model (SM) of elementary particle physics, such a term would be forbidden, since it breaks the gauge invariance[1]. This is a problem for all fermion fields, but the gauge invariance can be retained using the Higgs mechanism, where all SM fermions have a so–called Yukawa coupling to a bosonic Higgs field Φ. The quantum numbers of this field are chosen in such a way that the coupling terms,

$$\mathcal{L}_{\mathrm{Yukawa}} = -Y\overline{\Psi}_\mathrm{L}\Phi\Psi_\mathrm{R} + \mathrm{h.c.}, \tag{2.4}$$

with the Yukawa coupling matrix Y, are singlets. Through the spontaneous symmetry breaking of the $SU(2)_L \times U(1)_Y$ symmetry to $U(1)_{\mathrm{em}}$, the Higgs field gets a non–vanishing vacuum expectation value $v/\sqrt{2}$ which produces fermion mass terms,

$$\mathcal{L}_{\mathrm{Yukawa}} = -Y\frac{v}{\sqrt{2}}(\overline{\Psi}_\mathrm{L}\Psi_\mathrm{R} + \overline{\Psi}_\mathrm{R}\Psi_\mathrm{L}) + \mathrm{interactions}. \tag{2.5}$$

In the SM, all fermions get their masses from this mechanism. The only exception is the neutrino, since there exist no right–handed neutrino fields in the Standard Model of elementary particle physics. Hence, the neutrino is massless in the minimal model. However, if one introduces right–handed neutrinos, then there can be a Dirac mass term for neutrinos, too. This little extension of the SM is the easiest way to generate neutrino masses, but immediately a new question arises: the masses of neutrinos are much smaller than the ones of the other elementary particles (e. g. the electron, which has the lightest mass of all charged fermions, is still at least about 5 orders of magnitude heavier then all the three known neutrinos) and this large deviation from the masses of all the other Dirac particles seems to indicate that the nature of neutrino masses could indeed be different.

2.1.2 The Majorana mass term

For neutrinos, another interesting possibility besides the Dirac mass term arises. At first, let us have a look at the charge conjugation operator $\mathcal{C}$, that

[1] right–handed fermion fields are $SU(2)_L$ singlets, while left–handed ones are doublets, and hence the mass term, as a doublet, is not invariant under $SU(2)_L$ gauge transformations; see e. g. Ref. [6].

translates a particle into its corresponding antiparticle. For a spinor Ψ, the charge conjugation is defined as

$$\Psi^{\mathcal{C}} = \mathcal{C}^{\dagger}\Psi\mathcal{C} = C\overline{\Psi}^{T}, \tag{2.6}$$

where $C = i\gamma^2\gamma^0$ and hence

$$\Psi^{\mathcal{C}} = i\gamma^2\Psi^*. \tag{2.7}$$

Now, taking the charge conjugation of a left– or right–handed spinor flips the chirality of the field because of the anti–commutation $\{\gamma^2, \gamma^5\}$=0:

$$(\Psi_{\mathrm{R,L}})^{\mathcal{C}} = \left(\frac{1 \pm \gamma^5}{2}\Psi\right)^{\mathcal{C}} = i\gamma^2\frac{1 \pm \gamma^5}{2}\Psi^* = \frac{1 \mp \gamma^5}{2} \cdot i\gamma^2\Psi^* = (\Psi^{\mathcal{C}})_{\mathrm{L,R}}. \tag{2.8}$$

The structure of a mass term is $\overline{\Psi}_{\mathrm{L}}\Psi_{\mathrm{R}}$ (or the Hermitean conjugate) and with Eq. (2.8) one has an additional left–handed field that can be used in the mass term.
This can be pointed out more clearly by using the Weyl representation of the spinors, where the Dirac spinor Ψ is represented by the two-component Weyl spinors η and ξ. Using the corresponding representation for the Dirac matrices, one finds for the spinor and its left– and right–handed components:

$$\Psi = \begin{pmatrix} \xi \\ \eta \end{pmatrix}, \ \Psi_{\mathrm{L}} = \begin{pmatrix} 0 \\ \eta \end{pmatrix}, \ \Psi_{\mathrm{R}} = \begin{pmatrix} \xi \\ 0 \end{pmatrix}. \tag{2.9}$$

For the charge–conjugated fields, this gives:

$$(\Psi_{\mathrm{L}})^{\mathcal{C}} = \begin{pmatrix} i\sigma_2\eta^* \\ 0 \end{pmatrix}, \ (\Psi_{\mathrm{R}})^{\mathcal{C}} = \begin{pmatrix} 0 \\ -i\sigma_2\xi^* \end{pmatrix}. \tag{2.10}$$

The Majorana condition now postulates, that a particle is identical with its antiparticle, and hence, for a four-component spinor

$$\chi^{\mathcal{C}} = \pm\chi. \tag{2.11}$$

For neutrinos, this condition can be fulfilled, because they carry no electrical charge. From the Dirac fields, Ψ_{L} and Ψ_{R}, one can construct two such fields:

$$\chi \equiv \Psi_{\mathrm{L}} + \Psi_{\mathrm{L}}^{\mathcal{C}} \ \text{ and } \ \omega \equiv \Psi_{\mathrm{R}} - \Psi_{\mathrm{R}}^{\mathcal{C}}. \tag{2.12}$$

Projecting out the left– and right–handed components of these two new fields, one gets

$$\begin{aligned} \chi_{\mathrm{L}} &= \tfrac{1-\gamma^5}{2}\chi = \Psi_{\mathrm{L}}, & \chi_{\mathrm{R}} &= \tfrac{1+\gamma^5}{2}\chi = \Psi_{\mathrm{L}}^{\mathcal{C}}, \\ \omega_{\mathrm{L}} &= \tfrac{1-\gamma^5}{2}\omega = -\Psi_{\mathrm{R}}^{\mathcal{C}}, & \omega_{\mathrm{R}} &= \tfrac{1+\gamma^5}{2}\omega = \Psi_{\mathrm{R}}. \end{aligned} \tag{2.13}$$

Now one can write down the mass term for the Majorana field, which gives

$$\mathcal{L}_{\text{mass}} = -\frac{m}{2}\overline{\chi}\chi, \tag{2.14}$$

where m is assumed to be real. One can in principle generalize the Majorana construction to $\chi = e^{i\alpha}\Psi_{\text{L}} + e^{i\beta}\Psi_{\text{L}}^{\mathcal{C}}$ which then would lead to a complex mass M whose phase could be absorbed in the definition of Ψ_{L}. The mass term would then look like

$$\mathcal{L}_{\text{mass}} = -\frac{M}{2}\overline{\Psi_{\text{L}}^{\mathcal{C}}}\Psi_{\text{L}} + \text{h.c.}, \tag{2.15}$$

which clearly breaks lepton number (= number of leptons - number of antileptons) as expected, since such a number makes no sence when particles and antiparticles are equal.

2.1.3 The seesaw mechanism

One can also combine both possible mass terms to a more general one. Assuming the existence of right-handed neutrinos and including all 3 generations of elementary particles (which does not change the notation, except for the mass eigenvalues, which are now matrices, and the mass term hence a scalar product of two vectors with a matrix), the (type I) seesaw mass term becomes:

$$\mathcal{L}_{\text{mass}} = -\overline{\nu}_{\text{R}} m_{\text{D}} \nu_{\text{L}} - \frac{1}{2}\overline{\nu}_{\text{R}} m_{\text{R}} \nu_{\text{R}}^{\mathcal{C}} + \text{h.c.}. \tag{2.16}$$

The Dirac mass matrix m_{D} is a complex 3×3 matrix and the Majorana mass matrix m_{R} is additionally symmetric. One can now make use of the identity $\overline{\nu_{\text{L}}^{\mathcal{C}}} m_{\text{D}}^T \nu_{\text{R}}^{\mathcal{C}} = \overline{\nu}_{\text{R}} m_{\text{D}} \nu_{\text{L}}$ (fermion fields anti–commute!) and write the mass term in a more convenient form:

$$\mathcal{L}_{\text{mass}} = -\frac{1}{2}(\overline{\nu}_{\text{R}} m_{\text{D}} \nu_{\text{L}} + \underbrace{\overline{\nu_{\text{L}}^{\mathcal{C}}} m_{\text{D}}^T \nu_{\text{R}}^{\mathcal{C}}}_{=\overline{\nu}_{\text{R}} m_{\text{D}} \nu_{\text{L}}}) - \frac{1}{2}\overline{\nu}_{\text{R}} m_{\text{R}} \nu_{\text{R}}^{\mathcal{C}} + \text{h.c.} \equiv -\frac{1}{2}\overline{\Psi^{\mathcal{C}}} M \Psi + \text{h.c.}, \tag{2.17}$$

where

$$\Psi \equiv \begin{pmatrix} \nu_{\text{L}} \\ \nu_{\text{R}}^{\mathcal{C}} \end{pmatrix} \quad \text{and} \quad M \equiv \begin{pmatrix} 0 & m_{\text{D}}^T \\ m_{\text{D}} & m_{\text{R}} \end{pmatrix}. \tag{2.18}$$

Dirac particles in the SM have very roughly similar masses and hence the entries of m_{D} should be of the same order, while the masses m_{R} can have any value. Assuming $m_{\text{R}} \gg m_{\text{D}}$, one then gets three neutrinos with very light masses $m_{\text{D}} m_{\text{R}}^{-1} m_{\text{D}}^T$ and three heavy (and decoupled) neutrinos with masses of approximately m_{R}. This is the so–called seesaw mechanism which leads to a very natural explanation of the still not understood smallness of the neutrino masses.

2.2 Neutrino oscillations

From the observation of neutrino oscillations, we know that neutrinos must indeed have non–vanishing masses. Here, the theory and observations of neutrino oscillations are shortly reviewed.

2.2.1 The oscillation formula

A short derivation of the famous neutrino oscillation formula will be given in this subsection. For more information, one can e. g. make use of Refs. [7–9]. Assuming three generations of neutrinos (for other numbers of generations the formalism is analogous), one can classify neutrinos by their flavours, i.e. the states which participate in the weak interaction. In the SM, these flavours are ν_e, ν_μ, and ν_τ. As can be seen from the Standard Model Lagrangian, each of these flavours is associated with a certain charged lepton, which means that the creation or annihilation of e. g. a ν_e or its antiparticle via a charged current interaction will always appear together with the creation or annihilation of an electron or a positron. Equivalently, the neutrinos can be classified by their different mass eigenstates (assuming that their eigenvalues are non–zero) given by ν_1, ν_2, and ν_3. Trying to diagonalize the interactions for the SM states, it turns out that, in general, the neutrino flavours and the mass eigenstates cannot be diagonalized simultaneously and are hence related by a rotation matrix, the so–called PMNS matrix U, which gives

$$|\nu_\alpha\rangle = \sum_{i=1}^{3} U^*_{\alpha i} |\nu_i\rangle. \tag{2.19}$$

Here, flavours are denoted by Greek and mass eigenstates by Latin indices. If now all the mass eigenvalues of the neutrinos were zero, every linear combination of mass eigenstates, in particular the three flavours, would have zero a mass eigenvalue and the rotation in Eq. (2.19) (and hence neutrino mixing and oscillations) would not exist.
Now one can try to figure out the amplitude for detecting a neutrino (that has been produced as flavour α) as a flavour β after some propagation as mass eigenstate (only mass eigenstates can propagate; their propagator will be denoted here as $\pi(\nu_i)$). At first, the flavour eigenstate ν_α can be decomposed into mass eigenstates ν_i (see Eq. (2.19)), and, vice versa, $U_{\beta i}$ is the probability for ν_i to be observed as flavour β. In between, the eigenstate with mass m_i has to propagate, which gives for the total amplitude

$$A(\alpha \to \beta) = \sum_{i=1}^{3} U_{\beta i} \pi(\nu_i) U^*_{\alpha i}. \tag{2.20}$$

To evaluate the propagator $\pi(\nu_i)$, one first goes into the rest frame of the

neutrino and has a look at Schrödinger's equation,

$$i\frac{\partial}{\partial\tau_i}|\nu_i\rangle = H|\nu_i\rangle = m_i|\nu_i\rangle, \tag{2.21}$$

where τ_i is the proper time of the considered neutrino. Since the Hamiltonian here consists only of the mass m_i, it is time–independent, and hence the time evolution of the neutrino state is

$$|\nu_i(\tau_i)\rangle = e^{-im_i\tau_i}|\nu_i(0)\rangle \equiv \pi(\nu_i)|\nu_i(0)\rangle. \tag{2.22}$$

Taking into account that the distance as well as the time from the neutrino's production to its detection can be set experimentally, one can write (for simplicity we consider only one spatial dimension) $m_i\tau_i = E_it - p_iL \equiv (p_i)(x)$, where $(a)(b)$ is the scalar product of two 4–vectors.
Normally, neutrinos are ultra–relativistic after their production, simply because the Q–values in normal nuclear reactions are much larger than the neutrino masses. So one can approximate E_i by $p_i + \frac{m_i^2}{2p_i}$. Furthermore, the transition probability for a flavour change from flavour α to β is given by $P(\alpha\to\beta) = |A(\alpha\to\beta)|^2$, and hence one can always multiply the amplitude A by a complex number with absolute value 1, e^{iq} with real q, that does not depend on the index i. From that, one obtains:

$$e^{-i(p_i)(x)} \to e^{-i((p_i)-(p_1))(x)}, \tag{2.23}$$

where

$$((p_i)-(p_1))(x) = (E_i-E_1)t-(p_i-p_1)L \approx (p_i-p_1)t+\frac{m_i^2}{2p_i}-\frac{m_1^2}{2p_1}-(p_i-p_1)L. \tag{2.24}$$

Since the mass eigenvalues are very small compared to all involved momenta, one can write $p \approx p_i \approx p_1$ in all denominators, which then, with $\Delta m_{i1}^2 \equiv m_i^2 - m_1^2$, leads to

$$((p_i)-(p_1))(x) \approx \underbrace{(p_i-p_1)}_{\sim\, m_1^2}\underbrace{(t-L)}_{\sim\, m_i^2}+\frac{\Delta m_{i1}^2}{2p}\cdot t \approx \frac{\Delta m_{i1}^2}{2E}\cdot L, \tag{2.25}$$

where L denotes the baseline, the distance to the place, where the neutrino has been produced.
From this, one gets for the oscillation probability

$$P(\alpha\to\beta,L) = |A(\alpha\to\beta,L)|^2 = \Big|\sum_{i=1}^{3} U_{\beta i}U_{\alpha i}^* e^{-i\frac{\Delta m_{i1}^2}{2E}t}\Big|^2. \tag{2.26}$$

In the standard parametrization for 3 neutrino flavours, the PMNS matrix

$$U = \begin{pmatrix} U_{e1} & U_{e2} & U_{e3} \\ U_{\mu1} & U_{\mu2} & U_{\mu3} \\ U_{\tau1} & U_{\tau2} & U_{\tau3} \end{pmatrix} \tag{2.27}$$

is then given by

$$U = \begin{pmatrix} c_{12}c_{13} & s_{12}c_{13} & s_{13}e^{-i\delta} \\ -s_{12}c_{23} - c_{12}s_{23}s_{13}e^{i\delta} & c_{12}c_{23} - s_{12}s_{23}s_{13}e^{i\delta} & s_{23}c_{13} \\ s_{12}s_{23} - c_{12}c_{23}s_{13}e^{i\delta} & -c_{12}s_{23} - s_{12}c_{23}s_{13}e^{i\delta} & c_{23}c_{13} \end{pmatrix} \cdot \cdot \mathrm{diag}(1, e^{i\alpha}, e^{i\beta}), \quad (2.28)$$

where $s_{ij} \equiv \sin\theta_{ij}$ and $c_{ij} \equiv \cos\theta_{ij}$. The parameters involved are the mixing angles θ_{ij}, the CP-violating phase δ, and the two Majorana phases α and β, which are zero in the case of Dirac neutrinos. However, note that in the oscillation probability Eq. (2.26), there is no contribution of any of the Majorana phases, since there only appear terms proportional to e. g. $e^{i\alpha}e^{-i\alpha} = 1$. Hence, by using oscillation experiments, one can never get any information on whether the neutrinos are Dirac or Majorana particles.
In the 2–flavour case, the mixing matrix is (for Dirac neutrinos) simply given by the 2–dimensional rotation,

$$\begin{pmatrix} |\nu_e\rangle \\ |\nu_\mu\rangle \end{pmatrix} = \begin{pmatrix} \cos\theta & \sin\theta \\ -\sin\theta & \cos\theta \end{pmatrix} \begin{pmatrix} |\nu_1\rangle \\ |\nu_2\rangle \end{pmatrix}, \quad (2.29)$$

which results in the well–known oscillation probability for two neutrino flavours,

$$P(\nu_\mu \to \nu_e, L) = \sin^2 2\theta \sin^2 \frac{\Delta m^2 L}{4E}, \quad (2.30)$$

where $\Delta m^2 = m_2^2 - m_1^2$ (see also Fig. 2.1). From this formula, one can easily see, that this transition probability vanishes in case that all neutrinos are exactly massless.

2.2.2 The oscillation parameters

As discussed in the previous subsection, the parameters relevant for neutrino oscillations are the three mixing angles θ_{12}, θ_{13}, and θ_{23}, as well as the two mass square differences, $\Delta m^2_{\odot} \equiv \Delta m^2_{21}$ and $\Delta m^2_{\mathrm{atm}} \equiv |\Delta m^2_{31}|$, and the CP–phase δ.
In general, there are 2 types of neutrino oscillation experiments, the so–called appearance and disappearance experiments. In the latter, just a decreasing neutrino flux of one kind of neutrinos is measured. E.g. the Homestake experiment [10] has only been sensitive to ν_e's and has measuered a decreased flux of neutrinos coming from the sun which leads to the famous solar neutrino puzzle. The other type of experiment tries to detect neutrinos of the flavour into which the produced neutrino has oscillated and to measure the corresponding flux. One example for such kinds of experiments is the future OPERA experiment [11, 12].

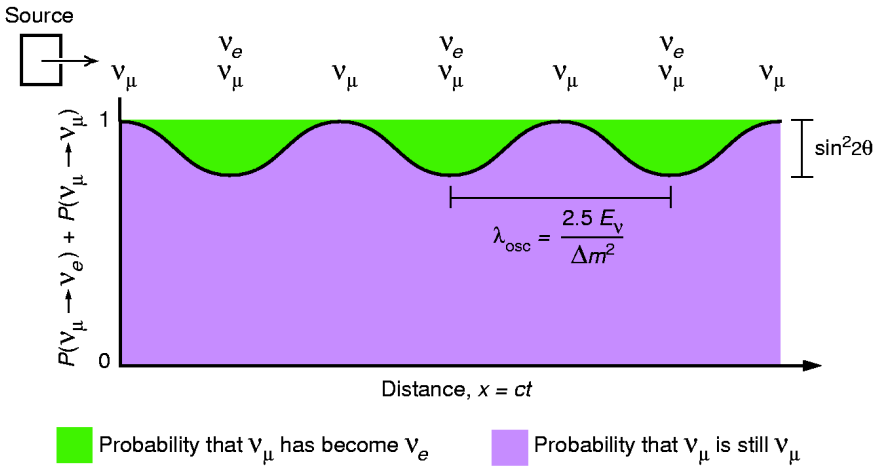

Figure 2.1: The neutrino flavour change as a function of the baseline x indeed has the form of a squared sine–function. That is why this effect is called "oscillation". (Figure taken from [3].)

At the moment, not all parameters are known. Using the oscillation of solar resp. reactor neutrinos, e. g. the experiments SNO [13–15] and KamLAND [16,17] have measured the "solar parameters" θ_{12} and $\Delta m^2_{\odot}$. Due to the observed MSW effect [18,19] in matter, also the sign of $\Delta m^2_{\odot}$ is known to be positive. The "atmospheric parameters", θ_{23} and Δm^2_{atm}, are known from measurements of atmospheric (Super–Kamiokande: [20, 21]) and accelerator neutrinos (K2K: [22, 23], MINOS: [24, 25]). However, the sign of $\Delta m^2_{\text{atm}}$is currently not known.
Less well known is the third mixing angle θ_{13}, which is at the moment only constrained from above to be very small ($\sin^2 2\theta_{13} \lesssim 0.1$) by the CHOOZ experiment [26]. The CP-violating phase δ which is basically the asymmetry between matter and antimatter is currently completely unknown. One reason for that are the CPT constraints on the oscillation probabilities: $P(\nu_\alpha \to \nu_\beta) = P(\overline{\nu}_\beta \to \overline{\nu}_\alpha)$ [7,27], which implies $P(\nu_\alpha \to \nu_\alpha) = P(\overline{\nu}_\alpha \to \overline{\nu}_\alpha)$ and hence $P(\nu_\alpha$ disappearance$) \equiv P(\overline{\nu}_\alpha$ disappearance). So, the phase δ cannot be measured in a disappearance experiment and this kind of experiments is exactly what has mostly been performed until now.
One example set of global fit values for the oscillation parameters is [28]

$$\begin{aligned} \Delta m^2_{\odot} &= 7.9^{+0.3,1.0}_{-0.3,0.8} \cdot 10^{-5}\text{eV}^2 \ , \\ \sin^2\theta_{12} &= 0.31^{+0.02,0.09}_{-0.03,0.07} \ , \\ \Delta m^2_{\text{atm}} &= 2.2^{+0.37,1.1}_{-0.27,0.8} \cdot 10^{-3}\text{eV}^2 \ , \\ \sin^2\theta_{23} &= 0.50^{+0.06,0.18}_{-0.05,0.16} \ , \\ \sin^2\theta_{13} &= 0 \ \text{ resp. } < 0.012 \ (0.046) \ . \end{aligned} \tag{2.31}$$

Here, the best–fit, 1σ, and 3σ values are given. As one can see, one has two large mixing angles (θ_{23} even seems to be maximal) and just one small angle. This is completely different from the mixing in the quark sector. Since the sign of Δm^2_{atm} is still unknown, it is at the moment also not clear, if the neutrino masses have a normal ($m_1 < m_2 < m_3$) or inverted ($m_3 < m_1 < m_2$) mass ordering (see Fig. 2.2). However, the second mass eigenstate has definitely a larger mass than the first one because of the sign of $\Delta m^2_{\odot}$. Other global fit values can be found e. g. in [29–32].

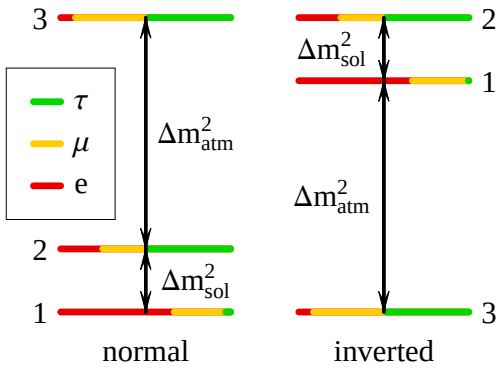

Figure 2.2: The two possible hierarchies for three neutrinos. Since $\Delta m^2_{\odot}$ is known to be positive, the second mass eigenstate has to have a larger mass than the first one. However, it is not yet clear, if the third mass eigenstate is the heaviest or the lightest one.

2.3 Measurements of the neutrino mass

Measuring the mass of the neutrino is one of the most important tasks of future elementary particle physics. The smallness of neutrino masses is still a mystery and knowing the exact values can maybe help to understand the origin of particle masses in general. The Higgs mechanism seems to give an explanation, but in fact it is just a re–arrangement of the same problem (finding the origin of the particle masses is the same task as finding the one for the Yukawa couplings).
There exist several approaches for the determination of neutrino masses. The most common ones are kinematical measurements from tritium beta decay as well as from neutrinoless double beta decay. The explanation of these two methods will be postponed to Chapter 4, because it is strongly related to the work done afterwards. The remaining methods are to limit the neutrino mass by cosmological considerations as well as time–of–flight

measurements of supernova neutrinos. These two possibilities will be briefly reviewed here to give an outlook to other methods. More detailed descriptions can e. g. be found in [33–35].

2.3.1 Cosmological bounds on neutrino masses

The fascinating interplay between particle physics and cosmology can be demonstrated in a nice way by having a look at Big–Bang Nucleosynthesis (BBN). The number of effective light degrees of freedom (and hence the number of light neutrinos) affects the expansion rate of the Universe: the larger the number of light degrees of freedom the larger that rate. This, in turn, results in a higher freeze–out temperature of the weak interaction that converts protons and neutrons, and hence, the neutron to proton ratio as well as the corresponding primordial helium yield would be higher, which can be measured. However, at the time when these events have taken place, the Universe had a temperature of about 1 MeV and this is much higher than the current bound for light neutrino masses ($\lesssim 1$ eV). As a consequence, no information on the absolute value of neutrino masses can be gained from that early epochs of the Universe. But, in spite of that, from BBN one can deduce a limit on the number of light neutrino species [36]: $N_\nu \leq 4$.
The remaining possibilities to get information on neutrino masses from cosmology are the Cosmic Microwave Background (CMB), the Large Scale Structure Surveys (LSS), and studies of the Lyman α forest (Lyα):
The CMB fills the whole Universe nearly completely isotropically with a 2.725 K temperature electromagnetic radiation [37]. The origin of the CMB is the decoupling of radiation and matter in the early universe (or, more precisely, at the time of the "re"–combination of electrons and protons to hydrogen). At this time, there must already have been certain inhomogeneities, caused by quantum fluctuations, which finally resulted in today's inhomogeneous structure of the Universe. These fluctations can be seen in the CMB spectrum as relative temperature differences of about 10^{-5}. The harmonic structure of the spectrum comes from the fact that, before the production of the CMB, there has been an equilibrium between radiation and gravitational pressure in the primordial photon–baryon plasma. If one calculates the power spectrum of the CMB, as it is possible in linear perturbation theory which is used to describe the fluid, one will get the harmonic modes of the oscillation. Odd peaks correspond to compression maxima and even ones to compression minima (= rarefaction maxima). Non–zero neutrino masses affect the positions of the different peaks as well as their amplitudes. This is because their mass affects their freeze–out temperature and hence the decoupling, which has to effect the peaks in the power spectrum. However, the effect of non–vanishing neutrino masses on the CMB spectrum is much smaller than other influences (e. g. curvature, baryon density, cosmological constant). In spite of that, the CMB is important for extract-

ing information on neutrino masses from cosmology: at first, it provides a very good consistency check for other cosmological measurements and on the other hand, one can apply the so–called Gerstein–Zeldovich limit. This limit is based on the fact that the density of neutrinos in the Universe must be less than the matter density in total, $\Omega_\nu < \Omega_m$, which already gives a bound of $\sum_i m_i < 14$ eV for the sum of all (light) neutrino masses and hence $m_i < 5$ eV for each neutrino species [35].
The second piece of information can be gained by structure formation. Clearly, relativistic particles cannot cluster due to their large kinetic energies. However, if neutrinos became non–relativistic at a certain point of the evolution of the Universe, they could in principle build clusters and this transition point from relativistic to non–relativistic motion is in turn related to the neutrino mass. One possibility to get a clue of the structure in our Universe is simply by observing the distribution of galaxies that should trace the matter density of the Universe. This is done by the so–called Galaxy Redshift surveys (e. g. 2dF [38]), where the redshift of the light from distant galaxies caused by the cosmic expansion is measured. The other type of measurement is the study of the Lyman α forest, where the distribution of gas clouds in the Universe is measured. Light emitted by quasars gets redshifted when travelling through space and hence even very energetic radiation can reach a point where it has exactly the wavelength to perform a $1s \rightarrow 2p$ transition in hydrogen (which forms most of the gas in the Universe). Since the re–emission of the radiation is isotropic, a gap in the light spectrum will remain, which gets further redshifted on the way to the Earth. Hence – since the wavelength of the Lyman α transition is well known – the spectrum carries information about at which distance gas clouds are located. According to [36], current cosmological bounds for the sum $\Sigma \equiv \sum_i m_i$ of all neutrino masses lie between 0.17 eV [39] and 1.8 eV [40], depending on the group that has done the analysis. Since there are several sources of uncertainties involved in such studies, we will take here the conservative limit of 1.8 eV for our considerations (see Chapter 5).

2.3.2 Supernovae and neutrino masses

A more astrophysical method to get constraints on the neutrino mass is by performing a time–of–flight measurement of neutrinos coming from supernova explosions. The basic idea is quite a few years old [41, 42]: if neutrinos have non–zero masses, they cannot have exactly the velocity of light. Under normal conditions, this deviation is so small, that it can never be observed, but since neutrinos coming from a distant supernova travel a long way, even this small difference can become visible.
From simple kinematic considerations, one can relate the neutrino mass to measurable quantities: if the neutrino energy E can be measured, the distance D to the supernova explosion is known, and if the width ΔE of the

neutrino energy spectrum is taken into account, one can relate the neutrino mass to the observed duration $\Delta T_{\rm obs}$ of the neutrino burst (which is always larger than the intrinsic duration) by [35]

$$m_\nu \lesssim E\sqrt{\frac{E}{\Delta E}\frac{\Delta T_{\rm obs}}{D}}. \tag{2.32}$$

A supernova is essentially a black–body source of neutrinos, so e. g. having a look at the spectrum of $\overline{\nu}_e$, one should see a thermal spectrum [43]. Now taking into account neutrino mixing, one realizes that the distance of a typical supernova to the Earth is much larger than the neutrino oscillation length (= smallest distance, after which a neutrino produced as a certain flavour consists again completely of its original flavour), it is clear that the oscillation cannot be seen anymore, since the coherence is completely lost. Due to the decoherence, neutrinos produced as $\overline{\nu}_e$'s will reach us at most as mass eigenstates $\overline{\nu}_1$'s, since they have the largest mixing with the flavour e [44].
Having a look at different analyses of the supernova explosion SN1987A in the Large Magellanic Cloud ($D \approx 50$ kpc), the upper bounds on the neutrino masses reach from 5.7 eV [45] up to 30 eV [46] with $E \simeq 15$ MeV, $\Delta E \sim 15$ MeV, and $\Delta T_{\rm obs} \sim 10$ sec. Hereby, the latter limit is obtained without making specific model assumptions on the supernova.

Chapter 3

Future measurement of the solar oscillation parameters with reactor neutrinos

Now that we have gone through some basics of neutrino physics, we can proceed to what can be learned from neutrino oscillations. As can be seen from Eq. (2.32), the values of the parameters involved in neutrino oscillations are not yet known very precisely. One method for measuring these parameters better are long baseline experiments (LBLs), e. g. with a reactor as neutrino source. In this section, at first reactor neutrino experiments will be introduced and then details of such a measurement will be discussed. For the simulation of LBLs, a sophisticated treatment of statistics is necessary as well as the careful implementantion of detector properties and the inclusion of all important backgrounds. The numerical calculation has been performed using a modified version of the GLoBES software package [47] and as example for a Large Liquid Scintillator Detector (LLSD) the proposed LENA detector [48] is taken. The goal of the simulation is to show how one can improve the knowledge on the so–called "solar parameters" of neutrino oscillations, namely $\Delta m^2_{\odot}$ and θ_{12}. The results of this analysis can also be found in [49].

3.1 The basics of reactor neutrino experiments

Reactor experiments have always played a crucial role in neutrino physics. The first evidence for the existence of neutrinos has been given by the Reines–Cowan experiment [50] in 1956 and since then, reactor experiments have been used to try to detect neutrino oscillations (e. g. Gösgen [51]) as well as to measure the oscillation parameters (e. g. KamLAND [16, 17]; see Sec. 2.2.2).
Neutrinos produced in reactors are emitted by β^-–decays of neutron–rich

isotopes and are hence electron–antineutrinos ($\overline{\nu}_e$). The typical detection reaction of such neutrinos is the so–called "inverse beta decay" on protons,

$$\overline{\nu}_e + p^+ \rightarrow e^+ + n^0. \tag{3.1}$$

This process also traces the energy E_ν of the incoming neutrino, since the positron is a prompt signal with energy $E_\nu - 0.77$ MeV and – inside the right material – the neutron can be captured on e. g. a second free proton and form a deuteron,

$$n^0 + p^+ \rightarrow d^+ + \gamma. \tag{3.2}$$

The emitted photon has a well–defined energy of 2.2 MeV and yields a delayed signal, which completes the experimental signature for the inverse beta reaction. Since a neutron has a larger mass than a proton and also a positron has to be produced, the reaction (3.1) has a threshold of 1.8 MeV neutrino energy. The relevant part of the energy spectrum of reactor neutrinos ranges from these 1.8 up to about 10 MeV[1] and is lower for higher energies [16,52]. The cross sections are of order 10^{-42} cm^2 and are larger for higher energies [53]. As can be seen from Fig. 3.1, these values lead to the highest event rates for neutrinos with an energy slightly lower than 4 MeV. To make use of this detection reaction, it is necessary to detect charged particles (in this case the positron) as well as light, which is best done using a scintillator. This is why we take an LLSD as example detector in our simulation, namely the proposed LENA detector [48, 54]. It is an LLSD filled with PXE ($C_{16}H_{18}$), it has a fiducial mass of 45 kt, and its possible location could be the Pyhäsalmi mine in Finland which is taken into account in the calculation of the backgrounds. However, we want to stress that LENA is just an example for such a measurement. Other LLSDs could provide similar results, depending on their fiducial mass, their energy resolution, and other experimental properties.

Important to note is also that what is measured is the disappearance of electron–antineutrinos $\overline{\nu}_e$. This means, that – from this kind of experiment – one cannot conclude into which type of neutrino the original $\overline{\nu}_e$'s have oscillated. It could be $\overline{\nu}_\mu$, $\overline{\nu}_\tau$, or also some sterile neutrino. However, if one is able to measure the L/E-dependence of the signal, it is still possible to conclude that one has really seen neutrino oscillations and no other sources for a reduced neutrino flux, such as neutrino decay or decoherence [55].

The full oscillation probability for $\overline{\nu}_e$–disappearance can be derived from Eqs. (2.26) and (2.28), which gives:

$$\begin{aligned} P(\overline{\nu}_e \rightarrow \overline{\nu}_e) = 1 - \sin^2 2\theta_{13} \sin^2 \Delta_{\text{atm}} - (\cos^4 \theta_{13} \sin^2 2\theta_{12} + \sin^2 \theta_{12} \sin^2 2\theta_{13}) \sin^2 \Delta_\odot + \\ + \sin^2 \theta_{12} \sin^2 2\theta_{13} (\frac{1}{2} \sin 2\Delta_\odot \sin 2\Delta_{\text{atm}} + 2 \sin^2 \Delta_{\text{atm}} \sin^2 \Delta_\odot), \end{aligned} \tag{3.3}$$

[1] It should be mentioned that the spectrum is not very well known for larger energies, but the general belief is that the flux in this region is anyway too low to cause any differences for reactor neutrino experiments.

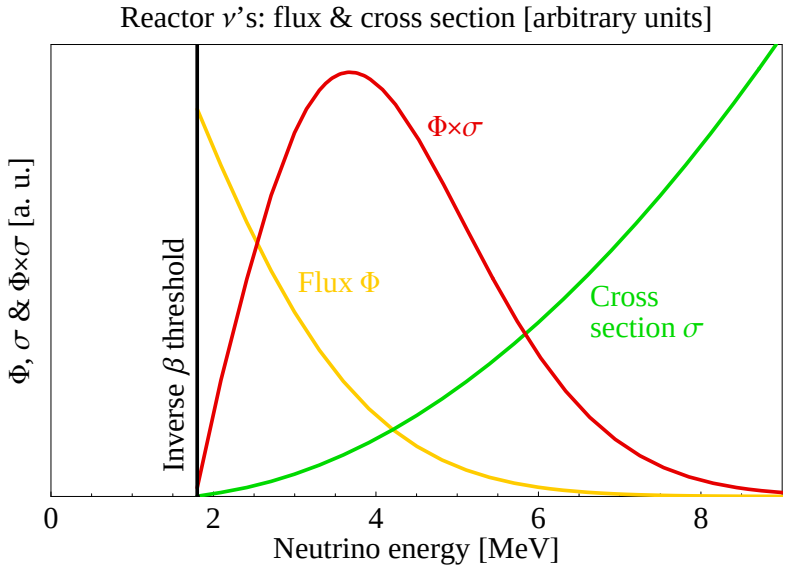

Figure 3.1: Reactor neutrino spectrum [16, 52], cross section [53] for inverse β–decay, and the product of both in arbitrary units as functions of the neutrino ($\overline{\nu}_e$) energy in MeV.

where $\Delta_\odot \equiv \Delta m^2_\odot L/(4E)$ and $\Delta_{\text{atm}} \equiv \Delta m^2_{\text{atm}} L/(4E)$. For analytical considerations, the 2–flavour approximation to Eq. (3.3) is used,

$$P_{\text{sol}}(\overline{\nu}_e \to \overline{\nu}_e) \approx 1 - \sin^2 2\theta_{12} \sin^2 \Delta_\odot, \tag{3.4}$$

which is a sufficiently good approximation for analatical calculations. The reason for that is, that the superposed smaller 13–oscillation has a much shorter oscillation length[2] than the considered 12–oscillation and because of the smallness of θ_{13}, the amplitude of the 13–oscillation can simply be considered as small perturbation.

3.2 The χ^2 function

The goal of this analysis is to determine the sensitivity of the experiment to certain parameters. In our case, these are the solar parameters of neutrino oscillations, $\Delta m^2_\odot$ and θ_{12}. This is done using a χ^2 test. The basics of such a test can e. g. be found in [56].
The χ^2 function contains the differences between the theoretical and the "observed" event rates as well as so–called pull terms for a proper treatment of systematical uncertainties, which are the normalization of the reactor and the detector fluxes, errors in the assumed background rates, and an energy

[2] This is the distance, after which the oscillation phase has changed from 0 to π.

calibration error. The events are assumed to follow a Poisson distribution, for which one can relate the event rate N to the standard deviation σ by $N = \sigma^2$. However, for analytical calculations, it is enough to consider a Gaussian approximation, for which the same relation for the standard deviation holds. Our complete χ^2 expression is then:

$$\chi^2 = \sum_{i=1}^{n} \frac{1}{N_i} \left[T_i(a_{\text{norm}}, a_{\text{det}}, a_{\text{reac}}, a_{\text{U}}, a_{\text{Th}}, b; \Delta m^2_{\odot}, \theta_{12}) - N_i \right]^2 + \\ + \frac{a^2_{\text{norm}}}{\sigma^2_{\text{norm}}} + \frac{a^2_{\text{det}}}{\sigma^2_{\text{det}}} + \frac{a^2_{\text{reac}}}{\sigma^2_{\text{reac}}} + \frac{a^2_{\text{U}}}{\sigma^2_{\text{U}}} + \frac{a^2_{\text{Th}}}{\sigma^2_{\text{Th}}} + \frac{b^2}{\sigma^2_b}. \tag{3.5}$$

There are many different quantities involved, so we should take some time and discuss all of them: Let us start with the statistical part of the χ^2 function, which corresponds to the first line of Eq. (3.5). This part compares the (hypothetical) observed rates N_i with the theoretically predicted ones T_i. The energy is binned and hence the index i runs over all bins from 1 to n. The calculation of the N_i's is done by using the full oscillation probability for vacuum, Eq. (3.3). These "true" event rates are calculated using the "true" values of the oscillation parameters (details on the numerical values can be found in Sec. 3.4). The T_i's are the theoretically predicted rates assuming certain values for the oscillation parameters and for the systematical errors a_j resp. b.

The systematical part corresponding to the second line of Eq. (3.5) contains the so–called pull terms. Through the standard deviations which are included in these terms, prior knowledge on certain systematics parameters is implemented. The way this works can be understood easily: the larger the deviation from the assumed value, the further away is a_j from zero, which gives a positive contribution to the χ^2 function. Since this function has to be minimized, the favored solution should pull all a's (and b) down to zero. The systematics parameters taken into account in this analysis are normalization errors a_{norm} of the reactor and a_{det} of the detector, the fluxes of the various backgrounds by surrounding reactors (a_{reac}) and by Geo–neutrinos which are again devided into those originating from uranium (a_{U}) and those from thorium (a_{Th}), and a bias in the overall energy calibration, b.

With a wrong energy calibration, it can of course also be that part of the events are binned into the wrong energy bins due to non–zero b. Hence, the theoretical rates T_i consist of the not correctly binned rates for the signal, $\tilde{S}_i(b)$, and for the different backgrounds, $\tilde{B}_{\text{reac},i}(b)$, $\tilde{B}_{\text{U},i}(b)$, and $\tilde{B}_{\text{Th},i}(b)$. The complete dependence of the T_i's on these rates and on systematics is

$$T_i = (1 + a_{\text{norm}} + a_{\text{det}})\tilde{S}_i(b) + (1 + a_{\text{reac}} + a_{\text{det}})\tilde{B}_{\text{reac},i}(b) + \\ + (1 + a_{\text{U}} + a_{\text{det}})\tilde{B}_{\text{U},i}(b) + (1 + a_{\text{Th}} + a_{\text{det}})\tilde{B}_{\text{Th},i}(b). \tag{3.6}$$

What is left now is to explain, how the wrongly binned rates can be obtained from the correctly binned ones. E.g. for the signal, the formula is

$$\tilde{S}_i^A(b) = (1+b)[(S_{\lfloor\delta(i)\rfloor+1} - S_{\lfloor\delta(i)\rfloor})(\delta(i) - \lfloor\delta(i)\rfloor) + S_{\lfloor\delta(i)\rfloor}], \tag{3.7}$$

where

$$\delta(i) = b \cdot (i + t_0 + \frac{1}{2}) + i \tag{3.8}$$

and S_i are the correctly binned rates. For the different backgrounds, the calculation is done in the same way (see Ref. [57]). In Eq. (3.8), t_0 is the energy threshold of the detector (expressed in units of the bin width) and $\lfloor\cdot\rfloor$ is the Gauß bracket. If the obtained energy is not exactly equal to one of the discrete bin energies, linear interpolation is used between the events in bin $\lfloor\delta(i)\rfloor + 1$ and those in $\lfloor\delta(i)\rfloor$, which is essentially what is done by Eq. (3.7). For very small calibration errors b, it is clear from Eq. (3.8) that $\lfloor\delta(i)\rfloor = i$, which means that the energy calibration does not change by more than a bin width. If some events are shifted outside the energy window of the simulation (e. g. are below threshold), then the signal rates for these particular events are assumed to be zero. The pre–factor $(1 + b)$ finally accounts for the change in the bin width, which would also be caused by a wrong energy calibration.

3.3 Analytical estimates for the best baseline

The purpose of the numerical simulation is to determine the sensitivity of an LLSD to the solar parameters of neutrino oscillations for different baselines. Before doing this, it is useful to consider an analytical estimation for the best baseline to be able to check if the results of the numerics are reliable and to get a better understanding of the χ^2 function.
For θ_{12}, this estimation can be done easily, but first one has to simplify Eq. (3.5) a bit: to avoid writing a summation in every term, one performs only a total rate analysis, which is equivalent to having one large energy bin, $n = 1$. Additionally, we use the 2–flavour approximation Eq. (3.4) for the oscillation probability. If we furthermore neglect the backgrounds and the systematical uncertainties, we will finally arrive at the simple expression,

$$\chi^2 = \frac{\left[N\left(1 - \overline{s}^2 \sin^2 \overline{\Delta}\right) - N\left(1 - s^2 \sin^2 \Delta\right)\right]^2}{N\left(1 - s^2 \sin^2 \Delta\right)}. \tag{3.9}$$

Here, the abbreviations $s \equiv \sin 2\theta_{12}$, $\overline{s} \equiv \sin 2\overline{\theta}_{12}$, $\Delta \equiv \Delta m^2_{\odot} L/(4E)$, and $\overline{\Delta} \equiv \overline{\Delta m^2_{\odot}} L/(4E)$ have been used. The barred quantities stand for the theoretical predictions of the corresponding parameters, while the ones without bars are the "true" parameter values. Hence, Eq. (3.9) is again the usual comparison between theoretical and observed event rates.

The rates N stand for the unoscillated event rates at the position of the detector, so taking into account that the initial number of particles N_0 originating from the reactor scales with the baseline L according to the geometrical inverse square law, one can write $N = N_0/L^2$. One can also neglect correlations between the solar parameters and hence assume that the mass square difference is fixed, $\Delta m^2_\odot = \overline{\Delta m^2_\odot}$. Taking all that into account, the χ^2 function becomes:

$$\chi^2 = \frac{N_0 \sin^4 \Delta}{L^2(1 - s^2 \sin^2 \Delta)}(\overline{s}^2 - s^2)^2. \tag{3.10}$$

The quantity that shall be measured, is the oscillation amplitude $s^2 = \sin^2 2\theta_{12}$. Taking a look at Eq. (3.4), it is clear that, for having the largest effect, the second sine function should be close to one and hence, Δ should be close to $\frac{\pi}{2}$[3]. Then, by using a Taylor expansion in the small quantity $(\Delta - \frac{\pi}{2})$, one gets

$$\begin{aligned} \sin\Delta &= \sin\left(\frac{\pi}{2} + \left(\Delta - \frac{\pi}{2}\right)\right) \approx 1 - \frac{1}{2}\left(\Delta - \frac{\pi}{2}\right)^2, \\ \sin^2\Delta &\approx 1 - \left(\Delta - \frac{\pi}{2}\right)^2, \quad \text{and} \quad \sin^4\Delta \approx 1 - 2\left(\Delta - \frac{\pi}{2}\right)^2. \end{aligned} \tag{3.11}$$

Applying these approximations, Eq. (3.10) becomes

$$\chi^2 \approx \frac{N_0}{L^2} \frac{1 - 2\left(\Delta - \frac{\pi}{2}\right)^2}{1 - s^2\left(1 - \left(\Delta - \frac{\pi}{2}\right)^2\right)}(s^2 - \overline{s}^2)^2. \tag{3.12}$$

Now, the χ^2 function has to be minimized for getting the best baseline, which means taking the derivative of Eq. (3.12) with respect to the baseline L and setting the result equal to zero, which, by skipping overall factors which do not depend on L, gives

$$\begin{aligned} 0 = \frac{\partial\chi^2}{\partial L} \propto \{ &-\frac{2}{L^3}\frac{1 - 2\left(\Delta - \frac{\pi}{2}\right)^2}{1 - s^2\left(1 - \left(\Delta - \frac{\pi}{2}\right)^2\right)} + \frac{1}{L^2}\frac{1}{\left[1 - s^2\left(1 - \left(\Delta - \frac{\pi}{2}\right)^2\right)\right]^2} \times \\ &\times (\Delta - \frac{\pi}{2})\frac{\Delta m^2_\odot}{4E}\left[-4 \cdot \left(1 - s^2\left(1 - \left(\Delta - \frac{\pi}{2}\right)^2\right)\right) - \left(1 - 2\left(\Delta - \frac{\pi}{2}\right)^2\right) \cdot 2s^2\right]\}. \end{aligned} \tag{3.13}$$

Now one can multiply Eq. (3.13) with $L^2\left[1 - s^2\left(1 - \left(\Delta - \frac{\pi}{2}\right)^2\right)\right]$ to get

$$-\frac{2}{L}\left(1 - 2\left(\Delta - \frac{\pi}{2}\right)^2\right) - (\Delta - \frac{\pi}{2})\frac{\Delta m^2_\odot}{E} - (\Delta - \frac{\pi}{2})\frac{\Delta m^2_\odot}{2E}s^2\frac{1 - 2\left(\Delta - \frac{\pi}{2}\right)^2}{1 - s^2\left(1 - \left(\Delta - \frac{\pi}{2}\right)^2\right)} = 0. \tag{3.14}$$

[3]Only mathematically, it could be any odd–integer multiple of $\frac{\pi}{2}$, but one should keep in mind that the neutrino flux scales with L^{-2}, so one should better choose the closest possible baseline, which corresponds to $\Delta \approx \frac{\pi}{2}$.

The last denominator can be approximated using $\frac{1}{1+x} \approx 1-x$ for a small x:

$$\frac{1}{1-s^2\left(1-\left(\Delta-\frac{\pi}{2}\right)^2\right)} = \frac{1}{1-s^2}\frac{1}{1+\frac{s^2}{1-s^2}(\Delta-\frac{\pi}{2})^2} \approx \frac{1}{1-s^2}\left[1-\frac{(\Delta-\frac{\pi}{2})^2 s^2}{1-s^2}\right]. \tag{3.15}$$

Putting this into Eq. (3.14) gives

$$-\frac{2}{L}\left(1-2\left(\Delta-\frac{\pi}{2}\right)^2\right)-(\Delta-\frac{\pi}{2})\frac{\Delta m^2_\odot}{E}- \\ -(\Delta-\frac{\pi}{2})\frac{\Delta m^2_\odot}{2E}\frac{s^2}{1-s^2}\left[1-2\left(\Delta-\frac{\pi}{2}\right)^2\right]\left[1-\frac{(\Delta-\frac{\pi}{2})^2 s^2}{1-s^2}\right]=0.$$

The last two terms in the brackets give simply a factor 1, since all other contributions would lead to terms of the order of $\mathcal{O}\left((\Delta-\frac{\pi}{2})^3\right)$ or higher. Keeping only the lowest order terms in $(\Delta-\frac{\pi}{2})$, we arrive at

$$\frac{2}{L}+\frac{\Delta m^2_\odot}{E}\left(\frac{\Delta m^2_\odot L}{4E}-\frac{\pi}{2}\right)\left(1+\frac{1}{2}\cdot\frac{s^2}{1-s^2}\right)=0. \tag{3.16}$$

This is now a simple polynomial equation of second order in L, as can be seen by multiplying Eq. (3.16) by L and using $s^2/(1-s^2) = s^2/c^2 = t^2$, where $c \equiv \cos 2\theta_{12}$ and $t \equiv \tan 2\theta_{12}$ are defined similarly to s:

$$\frac{(\Delta m^2_\odot)^2}{4E^2}\cdot L^2 - \frac{\pi}{2}\frac{\Delta m^2_\odot}{E}\left(1+\frac{t^2}{2}\right)\cdot L + 2 = 0. \tag{3.17}$$

Eq. (3.17) can by solved easily by using the well–known formula. Taking into account, that only the plus–solution is self–sonsistent with our initial assumption $\Delta \approx \frac{\pi}{2}$, this gives for the best baseline

$$L_{\text{best}} \approx \frac{2E^2}{(\Delta m^2_\odot)^2}\{\frac{\pi}{2}\frac{\Delta m^2_\odot}{E}\left(1+\frac{t^2}{2}\right)+\sqrt{\left(\frac{\pi}{2}\frac{\Delta m^2_\odot}{E}\left(1+\frac{t^2}{2}\right)\right)^2-\frac{(2\Delta m^2_\odot)^2}{E^2}}\} = \\ = \frac{\pi E}{\Delta m^2_\odot}\left(1+\sqrt{1-\frac{8}{\pi^2(1+\frac{1}{2}t^2)}}\right). \tag{3.18}$$

Using $\Delta m^2_\odot = 7.9\cdot 10^{-5}\text{eV}^2$ and $\sin^2 2\theta_{12} = 0.86$ as true values – as done in the simulation (cf. Eq. (3.19)) – one gets for an energy of 4 MeV a best baseline of approximately 55 km.

Unfortunately, an estimation of the best baseline for a measurement of $\Delta m^2_\odot$ is not so easy. One reason is that, in the χ^2 function, the baseline L appears inside the $\sin\Delta$ terms as well as outside, and hence $(\Delta m^2_\odot - \overline{\Delta m^2_\odot})$ cannot be extracted. However, one can still estimate that the strongest effect of $\Delta m^2_\odot$ should be there for a Δ equal to an odd–integer multiple of $\frac{\pi}{4}$, since $\Delta m^2_\odot$

occurs strongly related to the slope of the squared sine function in Eq. (3.4), which can be seen by taking the derivative of the oscillation probability with respect to L/E. Again, lower multiples of $\frac{\pi}{4}$ are favoured by better statistics, but since a value of $\Delta m^2_\odot$ different from the true value implies a stretching of the squared sine function, the effect of such a deviation will be stronger for larger baselines (simply because then the neutrinos have propagated the oscillation length more often). This discussion shows, that in this case, one really needs a numerical calculation to be able to say something about the sensitivity to $\Delta m^2_\odot$.

3.4 Scenarios and details of the numerical simulation

Now that we roughly know what to expect, it is time to describe the details of the numerical simulation. The used software is a modified version of the GLoBES software package [47]. "Modified" means that we have implemented our own χ^2 function and we also use some functions of the GSL library [58]. As already mentioned, the GLoBES software is used to perform a comparison between event rates calculated using different test values for the oscillation parameters and the systematical errors and the event rates calculated using the "true" parameter values. For our simulation, these true values are according to (2.32)

$$\begin{aligned} \Delta m^2_{\text{atm}} &= 2.2 \cdot 10^{-3}\text{eV}^2, & \sin^2 2\theta_{23} &= 1, \\ \Delta m^2_\odot &= 7.9 \cdot 10^{-5}\text{eV}^2, & \sin^2 2\theta_{12} &= 0.86, \\ \delta &= \tfrac{\pi}{2}, & \sin^2 2\theta_{13} &= 0. \end{aligned} \tag{3.19}$$

The variation over the test values for minimizing the χ^2 function runs over all oscillation parameters except the atmospheric mixing angle θ_{23} and the CP–violating phase δ, which do not play any role for the considered oscillation (cf. Eq. (3.3)). Of course, the parameter of the χ^2 function, θ_{12} resp. $\Delta m^2_\odot$, is also fixed in the particular simulation. The baselines are scanned from 25 to 100 km in steps of 5 km and for each baseline the 90%–range for the considered parameter is determined. This determination is done by setting the χ^2 function equal to 2.7, which corresponds to a confidence level of 90%. The χ^2 expression is essentially a parabola and it is numerically easier to determine the zeros of the function $2.7 - \chi^2$, because then one can simply start one time from the left and one time from the right hand side to find the respective roots. E.g. for $\sin^2 2\theta_{12}$, the true value is 0.86, so one can savely start in one case from $\sin^2 2\theta_{12} = 0.0$ and in the other one from 1.0 to be able to determine the roots to a certain accuracy (e. g. 10^{-4} is the absolute accuracy in the case of $\sin^2 2\theta_{12}$). Numerically, this is done using the "fsolver" algorithm of the GSL library, which seems to work stable and give accurate results.

For the systematical errors we used the same values as in Ref. [49], which are based on [59,60], as summarized in Table 3.1. As example for an LLSD, the

Reactor Neutrino Flux	2.0%
Detector Normalization	2.0%
Detector Energy Calibration	2.0%
Normalization of reactor background	2.0%
Normalization of Geo–ν background from U	no BG/10.0%/100.0%
Normalization of Geo–ν background from Th	no BG/10.0%/100.0%

Table 3.1: Systematical errors in our simulations (based on [49, 59, 60]).

proposed LENA detector at the possible site in Pyhäsalmi/Finland has been taken. This detector is expected to have an energy resolution of $\delta E/E = 0.091(E[\text{MeV}])^{-1/2}$ [54] and a position resolution of $\delta r = 25\,\text{cm}(E[\text{MeV}])^{-1/2}$, which leads, taking into account the geometry of the detector and the density of the scintillator PXE, to a fiducial mass of 45 kt [48, 61]. As energy window, the threshold for inverse beta decay (1.8 MeV) and the approximate end of the reactor spectrum (10 MeV) have been taken as suitable for this kind of experiment.

The reactor background has been calculated using the 20 closest reactors to the Pyhäsalmi mine, which are listed in Table 3.2. This yields about 850 events of a diffuse reactor backgound per year. By taking into account all nuclear power reactors in the world, this rate would be approximately doubled [62]. The other background are Geo–neutrinos and they turn out to be important for the determination of the best baseline. This is why we treat them in a more sophisticated way. Basics on Geo–neutrinos can e. g. be found in Ref. [65, 66]. The terrestrial neutrinos above threshold originate from the three elements uranium, thorium, and potassium and give about 1450 $\overline{\nu}_e$–events per year, which is a good example value for a detector like LENA as can be seen in Refs. [66–68], but one should keep in mind that there are still uncertainties in the values of the Geo–neutrino fluxes, depending on the type of crust and the particular Earth model. For us, only the Geo–neutrinos from the U– and the Th–chain are relevant, since the neutrinos stemming from K are below the energy threshold, as can be seen from the Geo–neutrino spectrum in Fig. 3.2 which used data from Ref. [67]. The spectrum also shows that the highest energy of Geo–neutrinos is approximately 3.3 MeV, while the reactor spectrum goes up to about 10 MeV (cf. Fig. 3.1). Hence, Geo–neutrinos only perturb the low energy part of the spectrum, because if a neutrino has an energy larger than 3.3 MeV, one can be sure that it cannot come from the interior of the Earth. In addition to the uncertainties in the fluxes, the exact ratio of the uranium and thorium abundances is also not known. To implement that in the simulation, we let the minimizer also run over the corresponding

Reactor	Baseline [km]	Power [GW_{th}]	Events per year
TVO 1	475.9	2.6	67.1
TVO 2	475.9	2.5	66.3
TVO 3 (2009)	475.9	5.2	131.1
Loviisa 1 & 2	346.8	2×1.4	137.7
Forsmark 1 & 2	800.0	2×3.0	55.5
Forsmark 3	800.0	3.6	33.0
Leningrad 1-4	521.6	4×2.9	253.7
Kola 1-4	829.0	4×1.3	44.3
Kola 5 & 6	829.0	2×3.0	51.1

Table 3.2: The 20 closest reactors [63, 64] to the Pyhäsalmi site with the corresponding distances to the experiment (baselines), reactor power, and expected event rates as calculated with GLoBES including oscillations.

normalization factors and take as central value an abundance of thorium which is by a factor of 3.9 larger than the one for uranium, according to Ref. [65].
To take into account the uncertainties in the Geo–neutrino fluxes in our simulations, we consider three different situations, which somehow cover the range of various possibilities:

- **No Geo–neutrinos:** The only background is the one caused by neighbouring reactors. Geo–neutrinos are completely neglected.
- **Geo–neutrinos with 10% uncertainty:** Geo–neutrinos are present additionally to the reactor background and the uncertainty in their fluxes is taken to be 10%.
- **Geo–neutrinos with 100% uncertainty:** Geo–neutrinos are present additionally to the reactor background and the uncertainty in their fluxes is taken to be 100%.

Furthermore, two different scenarios are considered for the measurement: the first one (*"small"*) is a small nuclear reactor with a thermal power of 0.5 GW_{th} which runs for 2 years. This could e. g. be a mobile reactor, such as the SSTAR design [70]. The other scenario (*"LARGE"*) is a power reactor with 10 GW_{th} that runs for 5 years. Of course, no one would build a detector like LENA voluntarily in the direct neighbourhood of such a power station, since the neutrino flux coming from this reactor would dominate all other events by other neutrino sources and the detector would be effectivly blind for types of experiments different from LBLs. However, if the reactor is scheduled to be shut down after the first years of data taking with the LLSD or if it is just planned to be built but there is enough time left to take data for the other measurements with the detector, this will not cause any

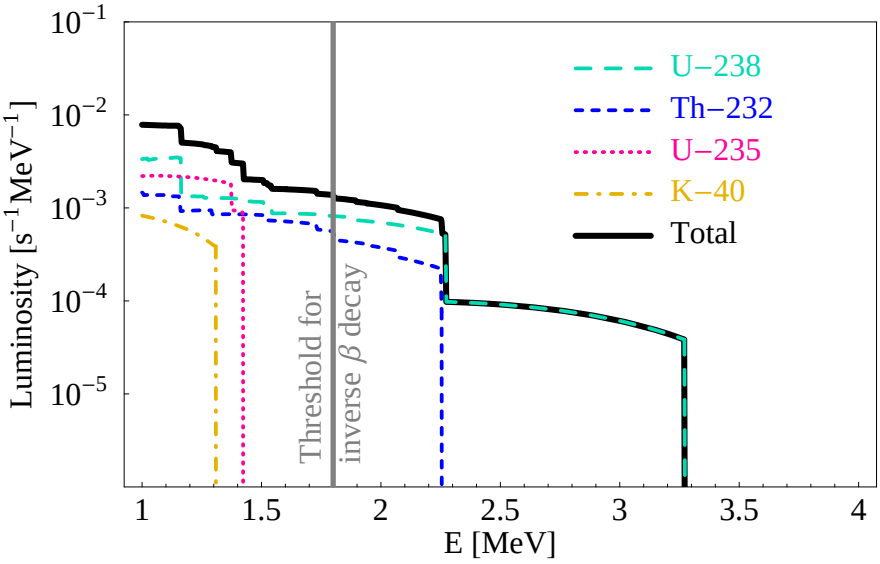

Figure 3.2: The Geo–neutrino spectrum as a function of the neutrino energy in MeV. (Figure taken from Ref. [69].)

problems. In both cases, the baseline is variable. For a mobile reactor, this will be oviously the case, but it also makes sense for the *LARGE* scenario, since the Pyhäsalmi mine in Finland is not the only possible site for an LLSD. In fact, currently there exist no old power station close to Pyhäsalmi that could do this job, but for other locations it may be possible to have an experimental site like that, so it is worth to consider it in the simulations.

3.5 The numerical results

The result of our numerical calculation can be seen in Fig. 3.3. Let us start with the discussion of the determination of $\sin^2 2\theta_{12}$, which is plotted in the upper panel of the figure, where the inner curves correspond to the *LARGE* scenario, while the outer ones are otained using the *small* scenario. For the latter, the best baseline turns out to be at about 50 to 70 km with Geo–neutrinos and 40 to 60 km without. Already from that, one can see, that our estimation of approximately 55 km obtained by Eq. (3.18) has not been that bad. The effect of Geo–neutrinos is a broadening of the confidence region for small baselines and a shift of the optimum baseline to higher values. This can be easily understood if ones takes into account that Geo–neutrinos can only perturb the low energy part of the reactor neutrino spectrum (cf. Figs. 3.2 & 3.1). Since the oscillation probability has its characteristic L/E–dependence, lower energies correspond to shorter

baselines, and hence a measurement at such baselines gets worsend, which is exactly what can be seen in Fig. 3.3.
For $\Delta m^2_\odot$, the results are similar: Geo–neutrinos shift the best baseline and perturb shorter baselines. Here, the *LARGE* scenario also leads to a great precision and the optimum baselines turn out to lie around 50 km without and between 70 and 90 km with Geo–neutrinos.
For both parameters, the relative accuracies for the *small* scenario turn out to be around $\pm 5\%$ and less than 1% for *LARGE*. The exact values for the particular best baselines as well as the 90%–ranges and bounds can be found in Table 3.3. Of course, the numerical values for the bounds and unrealistically accurate, but having a look at these values, one can see how much the precision of the experiment changes for different scenarios. The *LARGE* scenario also yields extremely precise results for the determination of $\Delta m^2_\odot$, which clearly comes from the power of the reactor. In this scenario, the exact baseline is not so important (as long as one is far away enough to resolve the solar oscillation), since the perturbation due to Geo–neutrinos is not large due to the high signal rates.
Our results are in agreement with those obtained in Ref. [71] and even – already for the *small* scenario – competitive with them, which becomes clear by taking into account that we present here the 90% and not the 1σ–range. Definitely, an LLSD like LENA could be a good instrument to achieve a completely new precision level in the measurements of the solar oscillation parameters. A good knowlegde of θ_{12} would be crucial for e. g. the distinction between the two different mass hierarchies in $0\nu\beta\beta$–experiments [72, 73] (cf. Chapter 5.4) and via the day–night effect for solar neutrinos [74], or for testing new ideas, such as quark–lepton complementarity [75], and could be achieved with such an experiment as described here.

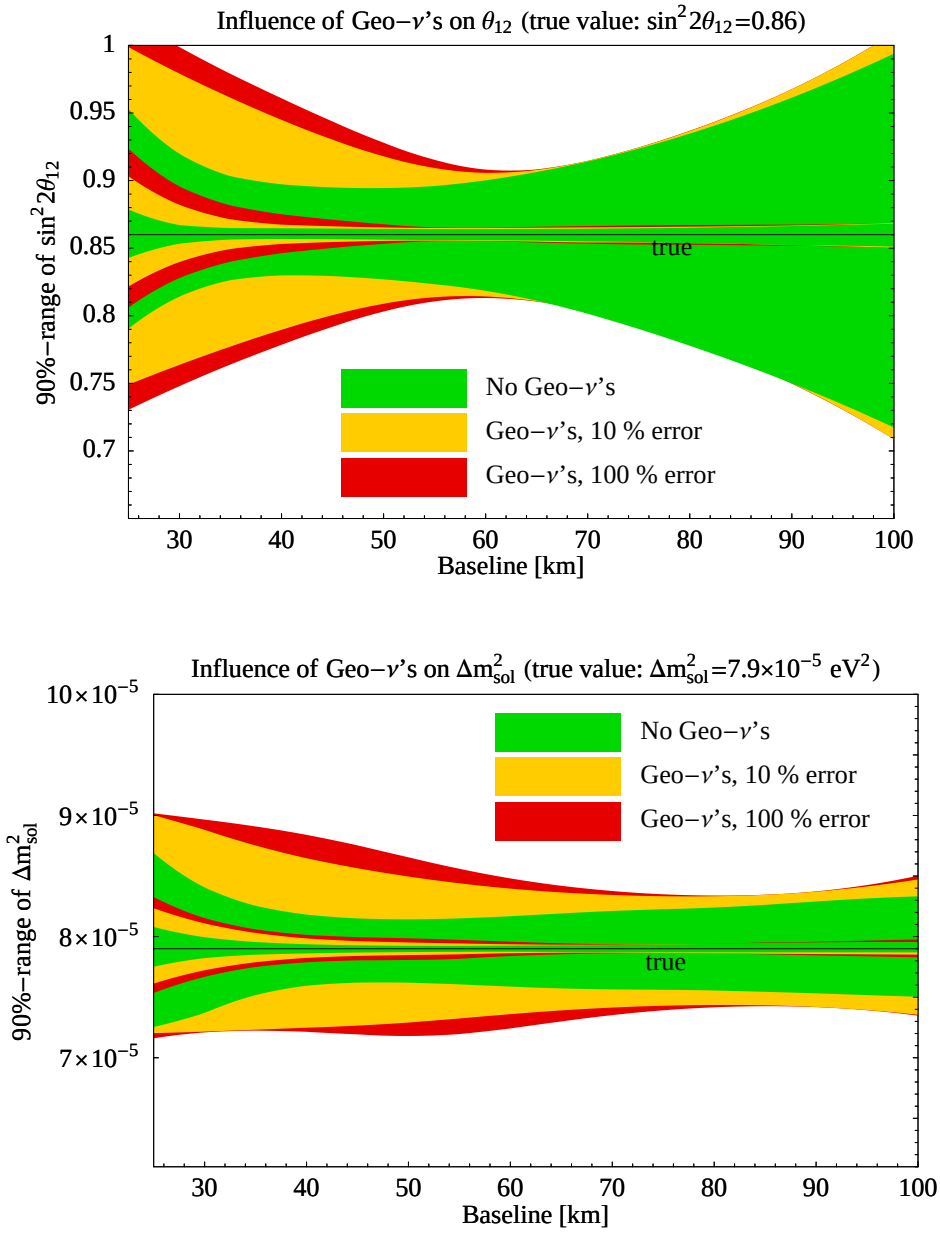

Figure 3.3: Achievable precision for the parameters $\sin^2 2\theta_{12}$ (upper panel) and $\Delta m^2_{\odot}$ (lower panel) at the 90% confidence level as a function of the baseline. The outer curves correspond to the *small* scenario, while the inner ones show the achievable precision with the *LARGE* scenario. The true values we have chosen are indicated by the horizontal lines.

$\sin^2 2\theta_{12}$	*small*	Best BL	Lower	Upper	90%-range
	No Geo-ν's	44.8 km	0.829	0.895	0.066
	10% error	59.6 km	0.814	0.906	0.091
	100% error	61.2 km	0.813	0.908	0.095
$\sin^2 2\theta_{12}$	*LARGE*	Best BL	Lower	Upper	90%-range
	No Geo-ν's	43.2 km	0.857	0.865	0.008
	10% error	55.2 km	0.856	0.865	0.009
	100% error	58.0 km	0.855	0.865	0.010
$\Delta m^2_\odot$ [eV^2]	*small*	Best BL	Lower	Upper	90%-range
	No Geo-ν's	48.7 km	$7.62{\cdot}10^{-5}$	$8.14{\cdot}10^{-5}$	$5.22{\cdot}10^{-6}$
	10% error	78.9 km	$7.44{\cdot}10^{-5}$	$8.33{\cdot}10^{-5}$	$8.97{\cdot}10^{-6}$
	100% error	82.8 km	$7.42{\cdot}10^{-5}$	$8.34{\cdot}10^{-5}$	$9.17{\cdot}10^{-6}$
$\Delta m^2_\odot$ [eV^2]	*LARGE*	Best BL	Lower	Upper	90%-range
	No Geo-ν's	55.5 km	$7.87{\cdot}10^{-5}$	$7.92{\cdot}10^{-5}$	$4.89{\cdot}10^{-7}$
	10% error	67.8 km	$7.87{\cdot}10^{-5}$	$7.93{\cdot}10^{-5}$	$6.55{\cdot}10^{-7}$
	100% error	73.7 km	$7.86{\cdot}10^{-5}$	$7.94{\cdot}10^{-5}$	$7.17{\cdot}10^{-7}$

Table 3.3: Best baselines and 90% confidence regions (widths with lower and upper bounds) for both parameters and both scenarios. Note that for the *LARGE* scenario, the exact baseline is not so important since one always has extremely high rates. The (hypothetical) true values used in the simulations are $\sin^2 2\theta_{12} = 0.86$ and $\Delta m^2_\odot = 7.9 \cdot 10^{-5}$ eV^2 (cf. Eq. (3.19)). Typical event rates are some thousands for the *small* and some ten thousands for the *LARGE* scenario.

Chapter 4

Present and upcoming direct measurements of the neutrino mass

The best known approaches to get a clue of the real nature of neutrinos are neutrino oscillations, kinematical measurements of the neutrino mass, and neutrinoless double beta decay ($0\nu\beta\beta$). Oscillations have already been introduced (see Chapters 2, 3). So, in this chapter, we will at first explain the kinematical measurement of the neutrino mass and show, how results obtained by such an experiment are influenced by the mass square differences and the mixing angles we get from the oscillation experiments. Afterwards we will explain, how neutrinoless double beta decay $0\nu\beta\beta$ works and what the difficulties are, and discuss possible alternatives to such a type of experiment.

4.1 Kinematical measurement of the neutrino mass

Let us at first discuss the kinematical measurement of the "electron–neutrino mass"[1] by β^-–decay, as already shortly introduced in Chapter 1. More precisely, this is done using the reaction

$$B(Z, A) \rightarrow C(Z + 1, A) + e^- + \overline{\nu}_e, \tag{4.1}$$

where a parent nucleus $B(Z, A)$ decays into a daughter nucleus $C(Z + 1, A)$ and emits an electron and an electron–antineutrino.
To see how the neutrino mass can be measured from this process, it is useful at first to make an easy consideration of what happens: to determine the

[1] In fact, the electron–neutrino is no mass eigenstate at all but a mixture of all of them and – being exact – there cannot exist a definite mass of this state, since the mixing angles with the flavours are non–zero.

neutrino mass m_ν, one has to determine its momentum $\vec{p}_\nu$ as well as its energy E_ν. Then one can use the simple 4–vector scalar product $m_\nu^2 = E_\nu^2 - p_\nu^2$ with $p_\nu = |\vec{p}_\nu|$ to determine m_ν. Taking into account that all nuclei are much heavier than a neutrino (and of course also much heavier than an electron), one can, already from that, conclude that for the kinematics only the leptons will play a role. Now, in an experiment, one can measure the energy E_e as well as the momentum $\vec{p}_e$ of the electron. The electron mass is known, but there are still two variables left, namely the energy and the momentum of the neutrino. Hence one can, in general, not determine the neutrino mass from such a measurement except in the one case that the neutrino is completely at rest, because then $\vec{p}_\nu = \vec{0}$ and $m_\nu = E_\nu$. Taking now into account, that the electron is still much heavier than the neutrino, it is already intuitively clear, that this configuration will not occur very often, as will be shown next. Now we can take a closer look at the kinematics. At first,

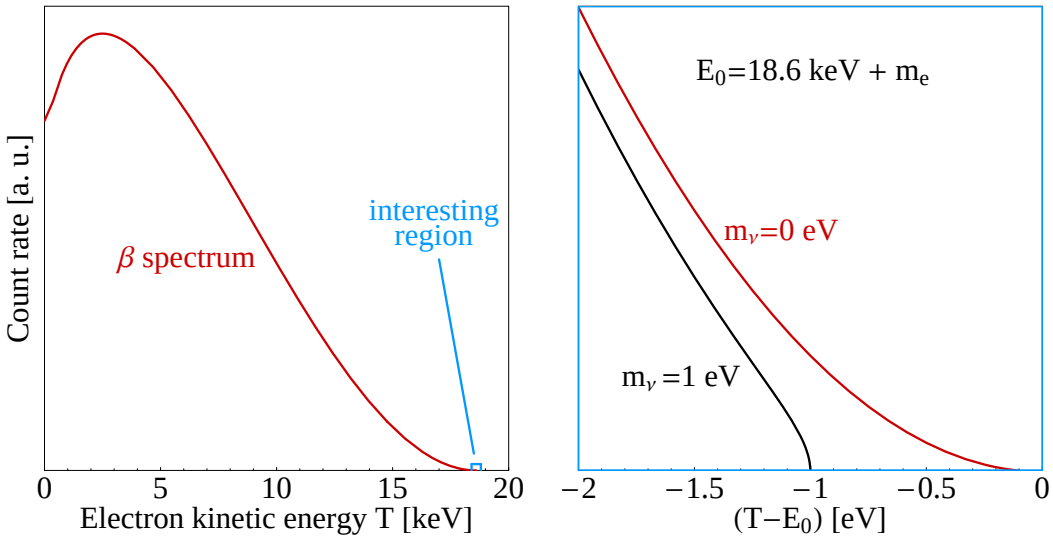

Figure 4.1: The energy spectrum of the electrons from β^-–decay. The interesting region for the determination of the neutrino mass is shown in more detail on the right panel. Since the effect of a non–zero neutrino mass is very tiny (note that the second plot is shown in the eV–scale), this kind of experiment is extremely challenging.

since all existing nuclei are much heavier than neutrinos and electrons, it is clear that they will only carry a completely negligible kinetic energy in this process. However, they are necessary for the conservation of 3–momentum, since the daughter nucleus will carry the "rest" of the momentum which is not carried away by the leptons. Since this is the case, there will be no correlation between the lepton momenta, which means that, in the calculation of the phase space, there arise two independent factors, one from the

electron and one from the (anti–) neutrino. Normalizing the volume to 1, the infinitesimal number of states can be written as:

$$d^2N = \frac{d^3p_e}{(2\pi)^3}\frac{d^3p_\nu}{(2\pi)^3}. \tag{4.2}$$

Since the directions of both particles are not correlated (due to the nuclear recoil), one can write $d^3p_i = p_i^2 dp_i d\Omega$ for both factors and integrate over the solid angle, which leads to

$$d^2N = \frac{1}{4\pi^4}p_e^2 dp_e p_\nu^2 dp_\nu. \tag{4.3}$$

The rest of the calculation is very easy: one applies the identity $p_i dp_i = E_i dE_i$ and uses $p_\nu^2 = E_\nu^2 - m_\nu^2$. To get the differential rate depending on the elctron energy, one can intergrate over all possible final neutrino energies with the condition of energy conservation, $E_0 = E_e + E_\nu$, where E_0 is the total decay energy, which is done simply by multiplying Eq. (4.3) by the corresponding δ–function. Having done all that, one finally arrives at:

$$\frac{dN}{dE_e} \propto p_e E_e \cdot \sqrt{(E_0 - E_e)^2 - m_\nu^2}(E_0 - E_e). \tag{4.4}$$

From this, the continuous energy spectrum is obtained as it is shown in Fig. 1.1. The neutrino mass appears only in the square root, where also the electron and the total decay energy are present. Since the latter is larger than the electron mass, the only way to have a small $(E_0 - E_e)^2$, which is necessary to have a stronger effect of a non–zero neutrino mass, is to take a nucleus with a very small E_0. In a real experiment, the best candidate is the β–decay of tritium,

$$^3H \;\rightarrow\; ^3He + e^- + \overline{\nu}_e, \tag{4.5}$$

for which $E_0 = m_e + 18.6$ keV. This values is still much larger than the neutrino mass and the kinetic energy of the electron has a wide range in "neutrino scales", so it is clear that a kinematical measurement of the neutrino mass is, even for the best possible case, challenging. Eq. (4.4) can be generalized taking into account the Coulomb interaction of the electron with the nucleus, which is done using the corresponding Fermi function F. Taking into account all proportinality factors as well as the nuclear matrix element M, the electron energy spectrum is [76]

$$\frac{dN}{dE_e} = \frac{G_F^2 m_e^5 \cos^2\theta_C}{2\pi^3}|M|^2 F(Z,E) p_e E_e \cdot \sqrt{(E_0 - E_e)^2 - m_\nu^2}(E_0 - E_e)\Theta(E_0 - E_e - m_\nu). \tag{4.6}$$

Here, the step function $\Theta(E_0 - E_e - m_\nu)$ simply ensures the conservation of energy. Taking additionally into account that neutrinos mix, Eq. (4.6)

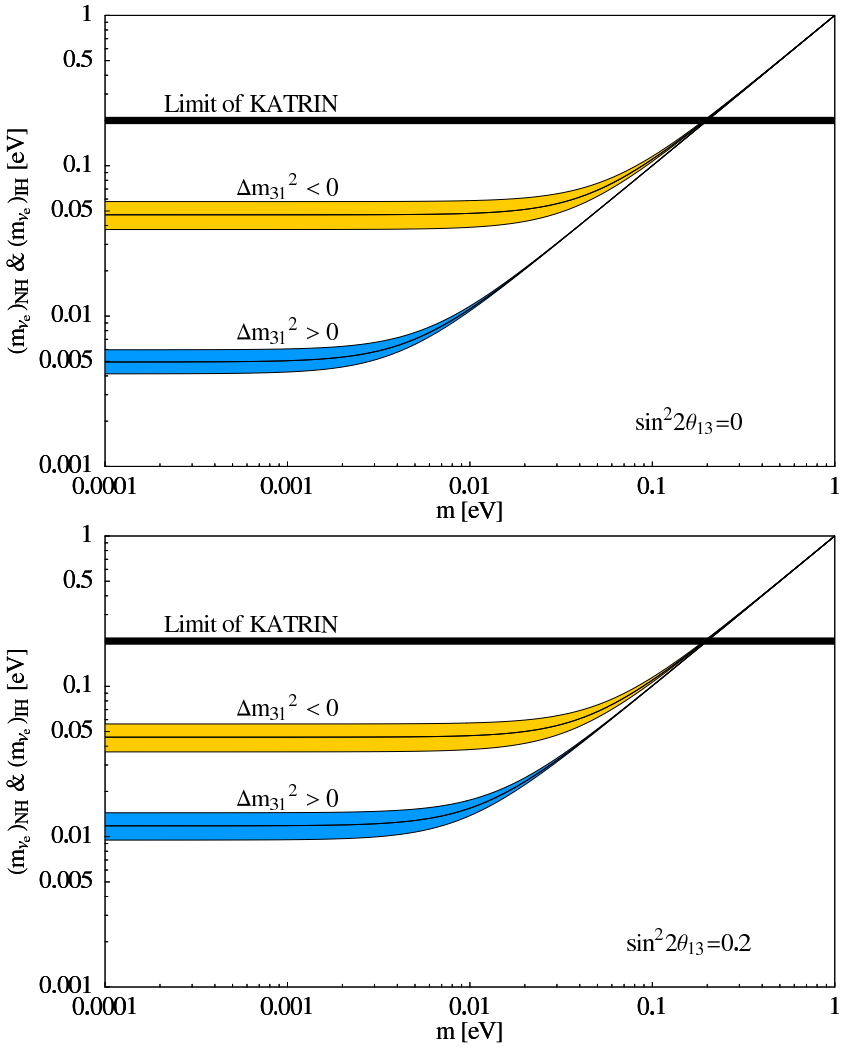

Figure 4.2: The electron–neutrino mass $m(\nu_e)$ as measured in β–decay. One can clearly see the width caused by the lack of knowledge of the oscillation parameters (best–fit values compared to 3σ–ranges). The expected sensitivity of KATRIN is also inducated, which shows that even the next generation experiments will not be able to resolve the hierarchy of the neutrino masses and can only detect a finite neutrino mass in the case of quasi–degeneracy (QD).

finally becomes

$$\frac{dN}{dE_e} \propto F(Z,E)p_eE_e(E_0-E_e)\cdot\sum_{i=1}^{3}|U_{ei}|^2\sqrt{(E_0-E_e)^2-m_i^2}\Theta(E_0-E_e-m_i), \tag{4.7}$$

where the constant factors have been skipped (they are the same as in Eq. (4.6)). The PMNS matrix elements $|U_{ei}|^2$ are given by Eq. (2.27). Having a look at the spectra (Fig. 4.1), it is even more obvious that only a very tiny fraction of all decays (approximately $2 \cdot 10^{-13}$) is relevant.
The neutrino mass, as measured with a future kinematical experiment like for example KATRIN, is [76, 77]

$$m^2(\nu_e) = \sum_{i=1}^{3} |U_{ei}|^2 \cdot m_i^2. \tag{4.8}$$

Of course, the quality of this measurement depends on two things: the knowledge of the mixing angles contained in $|U_{ei}|^2$ as well as the mass square differences and the hierarchy in m_i^2. For normal hierarchy (NH), this ν_e–mass is quite sensitive to the value of the reactor mixing angle θ_{13}, while for an inverted hierarchy (IH), this is not the case ($m^{\mathrm{NH}}(\nu_e) \simeq \sqrt{s_{12}^2 c_{13}^2 \Delta m_{\odot}^2 + s_{13}^2 \Delta m_{\mathrm{atm}}^2} \ll m^{\mathrm{IH}}(\nu_e) \simeq \sqrt{c_{13}^2 \Delta m_{\mathrm{atm}}^2}$). Plotting this mass against the smallest neutrino mass (m_1 for NH resp. m_3 for IH), and including the 3σ errors for all parameters, one can clearly see that there will be a certain width for the determination of the smallest neutrino mass (and hence also for all the other neutrino masses), even if a measurement of $m(\nu_e)$ is successful (cf. Fig. 4.2). KATRIN will be the most advanced experiment for measuring the ν_e–mass. At the moment, there exist only upper bounds on $m(\nu_e)$ of e. g. 2.3 eV from the Mainz experiment [78] or 2.5 eV from the Troitsk experiment [79] (both at 95% C.L.). KATRIN will improve this limit down to about 0.2 eV, or even measure the neutrino mass, if it is large enough. But it can be seen from the plots that even this experiment will not be able to resolve the hierarchy of neutrino masses except for a "large" neutrino mass in the case of quasi–degenerate (QD) neutrinos ($\Delta m_{\mathrm{atm}}^2 \ll m_1 \approx m_2 \approx m_3$).

4.2 Neutrinoless double beta decay

One of the most exciting tests for the nature of neutrinos is neutrinoless double beta decay ($0\nu\beta\beta$), since it can yield information on the possible Majorana nature of the neutrino, on lepton number violation (and hence on physics beyond the Standard Model), and on the absolute value of the neutrino mass simultaneously (for a nice review, see e. g. [81, 82]). This is the decay of a nucleus (Z, A) to a nucleus $(Z + 2, A)$ with the emission of only two electrons,

$$(Z, A) \to (Z + 2, A) + 2e^-. \tag{4.9}$$

This process clearly violates lepton number conservation (there is no lepton on the left hand side of Eq. (4.9) while there are two of them on the right hand side). So it is clearly forbidden in the Standard Model, since there

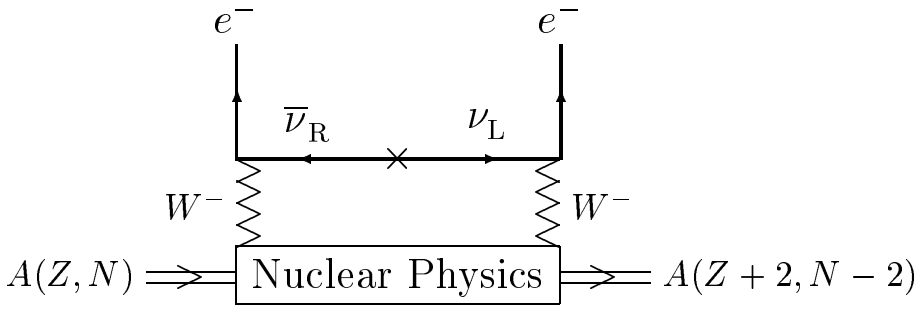

Figure 4.3: The "lobster" diagram for neutrinoless double beta decay ($0\nu\beta\beta$). At the left vertex, a right–handed (anti–) neutrino is emitted. Then its helicity gets flipped (indicated by the cross) and it is then, as left–handed neutrino, absorbed by a second virtual W^- and produces a second electron. The "black box" of nuclear physics indicates the difficulties in the calculations of the nuclear matrix elements. (Figure taken from [80].)

exist no lepton number violating terms. However, this conservation is just an empirical one and currently there is no symmetry known which would force this number to be conserved. In Section 2.1.2, we have discussed the possibility for a neutrino to be its own antiparticle, which is possible due to its neutralness. In fact, the mass term Eq. (2.15) does violate the lepton number, and if one assumed the neutrino to be a Majorana particle, then there should be processes which indeed violate the lepton number. One of them is $0\nu\beta\beta$, as shown in Fig. 4.3: at first, a neutron decays as described in Chapter 1 according to $n^0 \rightarrow p^+ + e^- + \overline{\nu}_e$. But now, the $\overline{\nu}_e$ is identical to the ν_e. Hence, there is a certain probability that this $\overline{\nu}_e$ is not emitted by the nucleus but re–absorbed (and hence virtual) by another neutron, which induces a second β–decay according to $\nu_e + n^0 \rightarrow e^- + p^+$. From this, one can already see that, since the decay energy must be a constant value as long as the daughter nucleus is not in an excited state, which depends only on the considered nucleus, the sum of the energies of the two emitted electrons in $0\nu\beta\beta$ has to be constant, while for the intrinsic background process, analogously denoted $2\nu\beta\beta$, energy is also carried away by the neutrinos and hence the sum of energies of the two electrons will have a continous spectrum in this case.

The problem with $0\nu\beta\beta$ is, that it is strongly suppressed: at first, it is a second order weak process and hence the transition matrix element is proportinal to G_F^2 (G_F is the Fermi constant – a very small number). Additionally, there is another suppression: since the weak interaction is chiral, which means that it can only couple to left–handed particles as well as to right–handed anti–particles, the helicity of the neutrino has to be flipped in this process (since, even for particle identical to anti–particle, the helicity

will distinguish if the neutrino can take part in a weak process, or not). Every massive particle has a small admixture of "wrong–helicity states" proportional to $(1-\beta)$ with $\beta = v/c$. This is also true for the vitual neutrino in Fig. 4.3, but since nuclear decay energies are much larger than the neutrino mass (which is at most about 1 eV), the virtual neutrino will be ultra–relativistic in most cases and hence $\beta \approx 1$. This fact makes it very difficult to really observe a $0\nu\beta\beta$–process, since the approximate lifetime for such a decay is of the order 10^{24}–10^{25} years [83].
In fact, what is measured in $0\nu\beta\beta$, is the lifetime of the nucleus, which is inversely proportional to the decay width [84]:

$$\frac{1}{T_{1/2}^{0\nu\beta\beta}} = G^{0\nu}(E_0, Z)|M^{0\nu}|^2|m_{ee}|^2. \tag{4.10}$$

This is in turn proportional to the effective mass of the neutrino that is measured in this decay process,

$$|m_{ee}| = \Big|\sum_{i=1}^{3} U_{ei}^2 m_i\Big|. \tag{4.11}$$

Hence, the observation of neutrinoless double beta decay gives no direct information on the absolute value of the neutrino mass, but this information can be extracted from the measurement using Eq. (4.11) together with the oscillation parameters. A detailed phenomenological analysis of this effective mass will be given in Chapter 5.
A further complication arises from the fact that the process in Eq. (4.9) also involves nuclear physics. While the calculation of the phase space factor $G^{0\nu}(E_0, Z)$ is fairly easy, the calculation of nuclear matrix elements $M^{0\nu}$ is a very sophisticated task and in spite of the fact that there has been a lot of progress in the last years, the uncertainties ζ are still of $\mathcal{O}(1)$ [85, 86]. The currently best limit on the effective mass comes from the Heidelberg–Moscow experiment [87],

$$|m_{ee}| \leq 0.35\zeta \text{ eV}. \tag{4.12}$$

Other ongoing and planned experiments on $0\nu\beta\beta$ are e. g. IGEX [88], COBRA [89], or GERDA [90].

4.3 Alternative double beta processes

Interestingly, there are possible alternatives to neutrinoless double beta decay. Besides possible tests of the other mass matrix elements, there are also other ways to measure $|m_{ee}|$. In principle, every way of reversing some of the legs of the "lobster" in Fig. 4.3 would do this job. Such candidates are e. g. [91, 92] neutrinoless double β^+–decay (emission of two positrons),

neutrinoless electron capture with simultaneous emission of a positron, or neutrinoless double electron capture. All these processes can basically occur for the same nuclei (if the Q–values are positive), good candidates would e. g. be Ni–58, Zn–64, or Er–162.
Especially the last case,

$$0\nu 2\mathrm{EC}: \quad B(Z,A) + e^-_{\mathrm{bound}} + e^-_{\mathrm{bound}} \rightarrow C(Z-2,A) + \gamma, \tag{4.13}$$

is interesting, since it is energetically most favored and exhibits an extremely nice signature: "normal" double electron capture would be accompanied by two neutrinos, which would escape the detector. Hence, one would at most see characteristic X–rays of the daughter element. However, in the neutrinoless case, energy conservation would not be possible without the emission of an additional particle, which can, for the possible candidate nuclei, only be a photon. This, of course, can be detected, and would have a characteristic energy that could be observed together with the transition of a nucleus B to another nucleus C. Furthermore, in this radiative case, there could be an additional resonance effect, which would maybe even increase the decay rate up to about 10^{-25} per nucleus and year [93].
All these cases are less often discussed in the literature than "normal" neutrinoless double beta decay. However, e. g. the COBRA proposal [89] also discusses such processes from the experimental point of view. They suggest using CdTe semiconductor detectors, which would allow the simultaneous measurement of 5 $\beta^-\beta^-$– and 4 $\beta^+\beta^+$–emitters (where the latter also includes double EC and EC/β^+ modes).

Chapter 5

The neutrino mass matrix in future experiments

In this chapter, a detailed analysis of the effective neutrino mass $|m_{ee}|$ will be given and its role in future measurements will be pointed out. Special focus is put on the impact of an improved limit on the still unknown small neutrino mixing angle θ_{13}. To determine this angle with a good precision, there are several upcoming neutrino experiments scheduled (e. g. Double Chooz [94]) and there are intensive studies going on for future experiments or possible upgrades of present experiments (e. g. Triple Chooz [59]). Another interesting connection is that one can, by measuring a certain value of the effective mass in neutrinoless double beta decay, also constrain the sum Σ of all neutrino masses and hence get an inference on cosmology, too (cf. Section 2.3.1). All these aspects will be treated in this chapter and numerical results will be presented. For the oscillation parameters, we use the values taken from [28], as well as in the previous chapters. The work presented here is based on [73] and [95].

5.1 The effective mass

The effective mass that can be measured using neutrinoless double beta decay is given by

$$|m_{ee}| \text{ where } m_{ee} = |m_{ee}^{(1)}| + |m_{ee}^{(2)}|e^{2i\alpha} + |m_{ee}^{(3)}|e^{2i\beta}. \tag{5.1}$$

Having a look at Eq. (4.11), one could think that the effective mass should also depend on the CP–phase δ. However, this is not true, as can be explained in two ways: at first, one can simply absorb the complex phase $e^{i\delta}$ into the definition of the mass eigenstate m_3. But, the more intuitive explanation can be understood by visualizing the effective mass as done in Fig. 5.1. The effective mass m_{ee} is essentially a sum of three complex numbers, which can be represented as vectors. Then the phases are simply the

rotation angles of the vectors associated with $|m_{ee}^{(2)}|$ and $|m_{ee}^{(3)}|$, and it is clear that they can only rotate from 0 to 360°, which is already covered by varying α and β from 0 to π. Furthermore, only the absolute value of the effective mass can be measured. Hence, it will also be possible to let the vector associated with $|m_{ee}^{(1)}|$ point in the positive real direction. Since $0\nu\beta\beta$ is not sensitive to off–diagonal elements of the neutrino mass matrix, this variation of the Majorana phases is enough (for a process that is sensitive to off–diagonal elements, it would be necessary to vary α and β between 0 to 2π). Of course, the Dirac phase δ, which is measurable in oscillation (appearance) experiments, can still be non–zero.

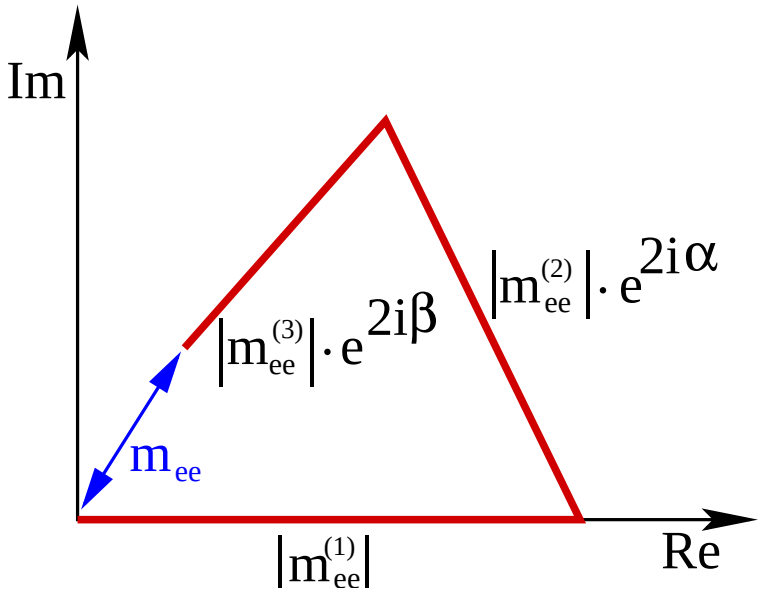

Figure 5.1: The effective mass as sum of three complex numbers. Since the variations of the Majorana phases already cover the whole physical range, one cannot gain anything new by including the CP–phase δ in the definition of the effective mass. (Figure taken from [73].)

The absolute values of the three vectors expressed by the neutrino mass eigenvalues m_1, m_2, and m_3 as well as by the mixing angles are given by

$$\begin{aligned} |m_{ee}^{(1)}| &= m_1 \, |U_{e1}|^2 = m_1 \, c_{12}^2 \, c_{13}^2 \; , \\ |m_{ee}^{(2)}| &= m_2 \, |U_{e2}|^2 = m_2 \, s_{12}^2 \, c_{13}^2 \; , \\ |m_{ee}^{(3)}| &= m_3 \, |U_{e3}|^2 = m_3 \, s_{13}^2 \; . \end{aligned} \tag{5.2}$$

We give every result as function of the smallest neutrino mass eigenvalue. For a normal mass ordering ($m_1 < m_2 < m_3$), this is m_1, while for an inverted ordering ($m_3 < m_1 < m_2$) this will be m_3. The first mass eigenvalue

Case	Majorana phases	$\lvert m_{ee}\rvert_{\min}$
$--$	$\alpha=\beta=\frac{\pi}{2}$	$\left\lvert m_1 c_{12}^2 c_{13}^2 - \sqrt{m_1^2+\Delta m_\odot^2}\, s_{12}^2 c_{13}^2 - \sqrt{m_1^2+\Delta m_{\rm atm}^2}\, s_{13}^2\right\rvert$
$-+$	$\alpha=\frac{\pi}{2}$, $\beta=0$	$\left\lvert m_1 c_{12}^2 c_{13}^2 - \sqrt{m_1^2+\Delta m_\odot^2}\, s_{12}^2 c_{13}^2 + \sqrt{m_1^2+\Delta m_{\rm atm}^2}\, s_{13}^2\right\rvert$
$+-$	$\alpha=0$, $\beta=\frac{\pi}{2}$	$\left\lvert m_1 c_{12}^2 c_{13}^2 + \sqrt{m_1^2+\Delta m_\odot^2}\, s_{12}^2 c_{13}^2 - \sqrt{m_1^2+\Delta m_{\rm atm}^2}\, s_{13}^2\right\rvert$

Table 5.1: Minimal values of $|m_{ee}|$ for dominance of one of the $|m_{ee}^{(i)}|$.

is known to be smaller than the second one, since from matter effects the sign of $\Delta m_\odot^2 = m_2^2 - m_1^2$ is known to be positive (cf. Sec. 2.2.2). However, from $\Delta m_{\rm atm}^2 = |m_3^2 - m_1^2|$, only the absolute value is known and not the sign, so $m_3 < m_1$ is still possible. For these two types of ordering, the masses are then given by

$$\begin{aligned} \text{normal}: &\quad m_1 = \text{lightest}; && m_2 = \sqrt{m_1^2+\Delta m_\odot^2}; && m_3 = \sqrt{m_1^2+\Delta m_{\rm atm}^2} \\ \text{inverted}: &\quad m_1 = \sqrt{m_3^2+\Delta m_{\rm atm}^2}; && m_2 = \sqrt{m_3^2+\Delta m_{\rm atm}^2+\Delta m_\odot^2}; && m_3 = \text{lightest} \end{aligned} \tag{5.3}$$

Most interesting are the following three different extreme cases:

$$\begin{aligned} \text{normal hierarchy (NH)}: &\quad |m_1| \ll \sqrt{\Delta m_\odot^2} \simeq |m_2| \ll \sqrt{\Delta m_{\rm atm}^2} \simeq |m_3|, \\ \text{inverted hierarchy (IH)}: &\quad |m_3| \ll \sqrt{\Delta m_{\rm atm}^2} \simeq |m_1| \simeq |m_2|, \\ \text{quasi}-\text{degeneracy (QD)}: &\quad \sqrt{\Delta m_{\rm atm}^2} \ll m_0 \equiv |m_1| \simeq |m_2| \simeq |m_3|. \end{aligned} \tag{5.4}$$

To determine the whole range of $|m_{ee}|$, one can simply look at the ranges of the three "sticks" $|m_{ee}^{(i)}|$ and imagine the geometrical shape: the maximal $|m_{ee}|$ will always be obtained, if all three vectors exactly add up, which happens for $\alpha = \beta = 0$. Note that from considerations like that, it could also be possible to get an experimental hint on the Majorana phases, at least for some extreme cases. When trying to find the minimum value of $|m_{ee}|$, one can realize two different cases: either, one can form a triangle out of the three parts (then, $|m_{ee}| \equiv 0$), which will be possible for $|m_{ee}^{(i)}| + |m_{ee}^{(j)}| \geq |m_{ee}^{(k)}|$ (with unequal $i,j,k = 1,2,3$), or one has to substract the two smaller pieces from the larger one, which will be the case for $|m_{ee}^{(i)}| + |m_{ee}^{(j)}| < |m_{ee}^{(k)}|$ and results in $|m_{ee}| > 0$. In this case we label the dominance of the first with "$--$", the one of the second term with "$-+$", and for the third term with "$+-$" (cf. Table 5.1). Simply adding or subtracting the different contributions is equivalent to having trivial values for the Majorana phases, i.e. 0 or $\pi/2$, which means conservation of CP [96]. This is exactly the case for the maximum or minimum (non–vanishing) values of $|m_{ee}|$.

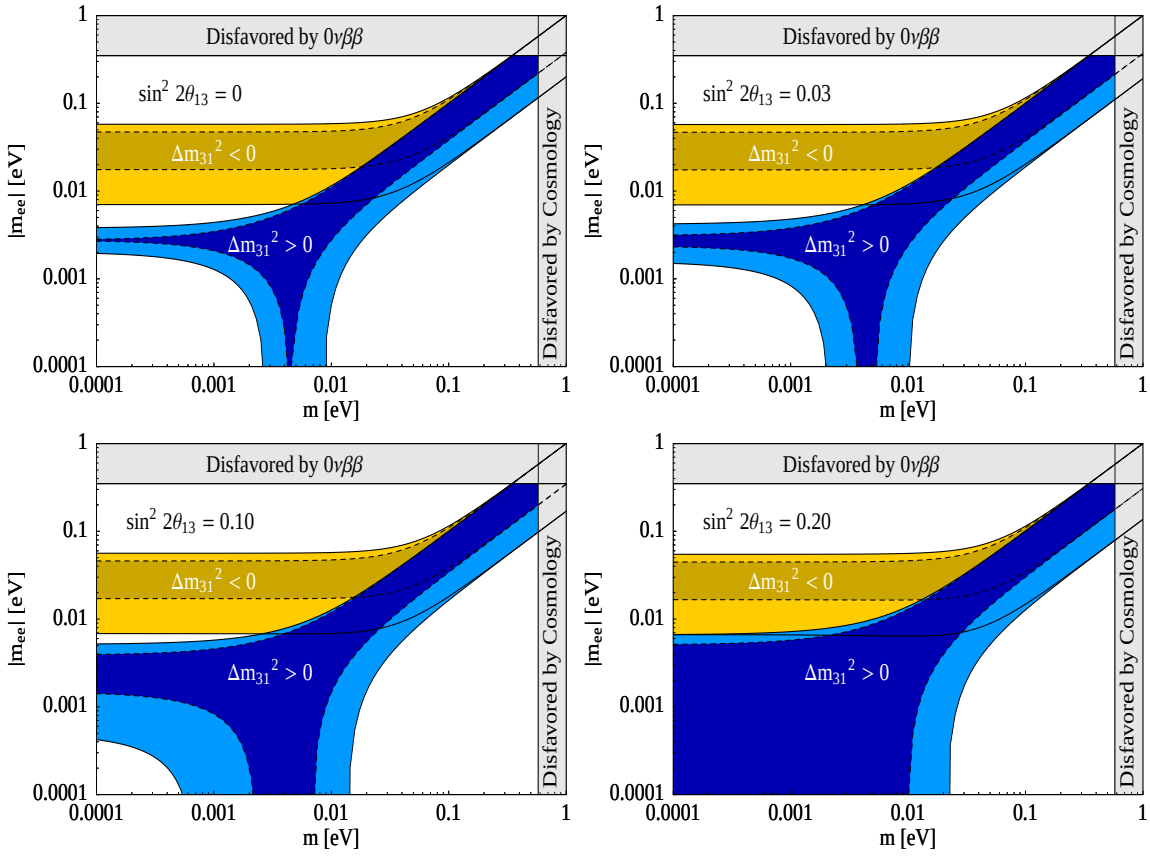

Figure 5.2: The effective mass (in eV) as measured in $0\nu\beta\beta$ for the normal and inverted mass ordering as a function of the smallest neutrino mass (in eV) for different values of $\sin^2 2\theta_{13}$. The prediction for the best–fit values of the oscillation parameters (inner bands) and for the 3σ ranges (outer bands) is given. A typical bound from cosmology and the limit on the effective mass from Eq. (4.12) are indicated.

We have plotted the effective mass for four different values of $\sin^2 2\theta_{13}$ in Fig. 5.2, namely 0, 0.03, 0.1, and 0.2. Some regions, which are disfavored, are also marked: the upper bound on $|m_{ee}|$ coming from Eq. (4.12) for setting $\zeta \equiv 1$ and the bound on the sum $\Sigma = \sum_i m_i$ of all neutrino masses of 1.74 eV coming from cosmology derived by the SDSS collaboration [40]. Note that both of these bounds are no strict exclusions, since in the case of $0\nu\beta\beta$ one still has to take into account the uncertainty in the nuclear matrix elements and in cosmology one has unknown systematical errors. Having a look at these plots, one can easily identify certain behaviors:

1. For normal mass ordering, the effective mass is in general smaller and

can, for certain parameter values, even vanish completely. The corresponding range of m_1 for $|m_{ee}| = 0$ increases with $\sin^2 2\theta_{13}$.

2. For small values of m_1, $|m_{ee}|_{\rm min}$ becomes smaller with increasing $\sin^2 2\theta_{13}$ and the gap between the effective mass for normal and for inverted mass ordering shrinks.

3. For inverted mass ordering, there is nearly no effect visible due to the much larger values of $|m_{ee}|$.

What will follow, is a detailed analysis of all these features and drawing conclusions what can be gained by certain limits on θ_{13}. A concise summary of the presented work is given in Fig. 5.3.

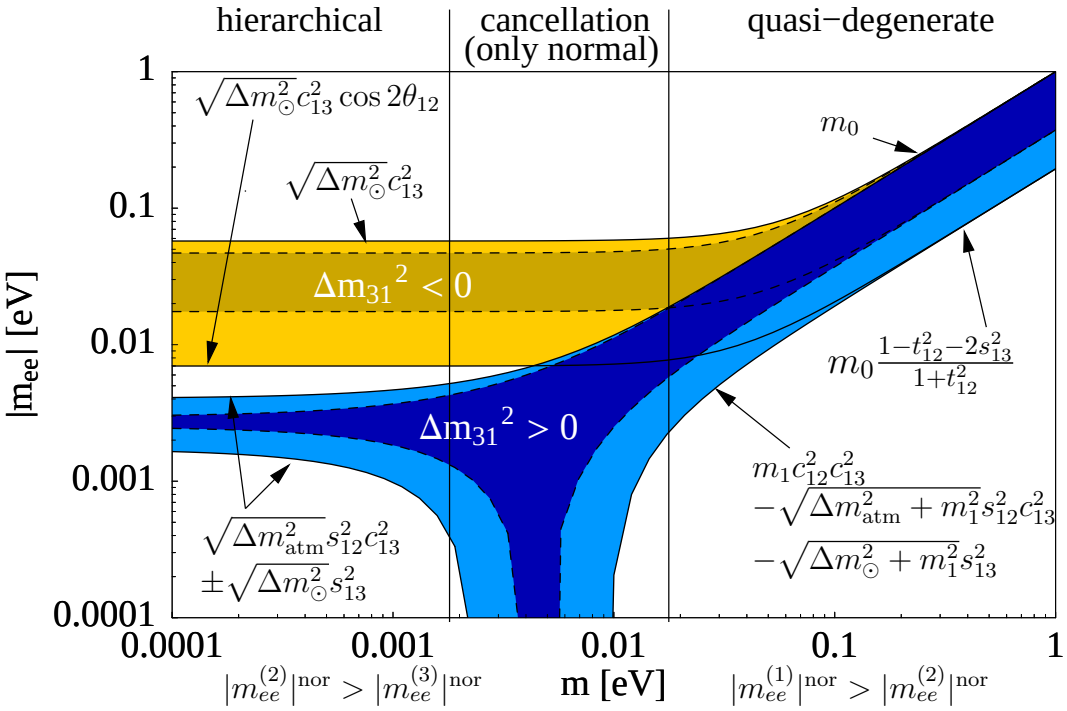

Figure 5.3: A summary of the main properties of $|m_{ee}|$ as function of the smallest neutrino mass. We have indicated the relevant formulae and the important regimes: hierarchical, cancellation (only possible for normal mass ordering), and quasi–degeneracy. The value of $\sin^2 2\theta_{13} = 0.02$ has been chosen, we take $t_{12}^2 \equiv \tan^2\theta_{12}$, and m_0 is the common mass scale (measurable in KATRIN or by cosmology via $\Sigma/3$) for quasi-degenerate neutrinos $m_0 \equiv m_1 \simeq m_2 \simeq m_3$.

5.2 The effective mass for normal mass ordering

Let us now start the analysis with the case of normal mass ordering, $m_1 < m_2 < m_3$. In this case, the effective neutrino mass as measured in neutrinoless double beta decay is given by

$$|m_{ee}^{\rm nor}| = \left| m_1 c_{12}^2 c_{13}^2 + \sqrt{m_1^2 + \Delta m_\odot^2}\, s_{12}^2 c_{13}^2 e^{2i\alpha} + \sqrt{m_1^2 + \Delta m_{\rm atm}^2}\, s_{13}^2 e^{2i\beta} \right|. \tag{5.5}$$

For the maximum value of this quantity, one simply adds up all three conributions ($\alpha = \beta = 0$), which gives:

$$|m_{ee}|_{\rm max}^{\rm nor} = m_1 c_{12}^2 c_{13}^2 + \sqrt{m_1^2 + \Delta m_\odot^2}\, s_{12}^2 c_{13}^2 + \sqrt{m_1^2 + \Delta m_{\rm atm}^2}\, s_{13}^2. \tag{5.6}$$

This will be maximal if all parameters involved, namely $\Delta m_\odot^2$, $\Delta m_{\rm atm}^2$, s_{12}^2, and s_{13}^2, are maximal. Numerically, the best–fit (1σ, and 3σ ranges of the) oscillation parameters give $|m_{ee}|_{\rm max}^{\rm nor} = 0.10$ (0.10, 0.10) eV for $m_1 = 0.1$ eV, 0.011 (0.012, 0.014) eV for $m_1 = 0.01$ eV, and 0.0066 (0.0073, 0.0096) eV for $m_1 = 0.005$ eV.
However, for $|m_{ee}|_{\rm min}^{\rm nor}$, it is not always that easy to find an analytical expression except for very large or very small values of the lightest neutrino mass eigenvalue. Especially for $|m_{ee}|$ smaller than about 0.001 eV, at least two of the $|m_{ee}^{(i)}|$'s have nearly the same size which means that small variations of the oscillation parameters or the smallest mass can exchange the role of the dominant term. Numerical examples are given in Table 5.2. For an m_1 larger than 0.01 eV, the first term always dominates, while for values smaller than 0.001 this is mostly the second term. This last dominance is true except for rather extreme cases (if $\Delta m_\odot^2$ and θ_{12} have their 3σ minima and $\Delta m_{\rm atm}^2$ its 3σ maximum, then this dominance will not be given for $\sin^2 2\theta_{13} > 0.13$, which is still less than the upper 3σ bound of $\sin^2 2\theta_{13} = 0.18$).

5.2.1 The strictly hierarchical part: $m_1 \to 0$

The first part to be discussed is the region where the smallest mass m_1 is very tiny. In this case, since $m_1 \ll \Delta m_\odot^2 \ll \Delta m_{\rm atm}^2$, one has the extreme case of a normal hierarchy (NH), which corresponds to the "hierarchical regime" in Fig. 5.3. As already shown in Table 5.2, for small m_1 and $\sin^2 2\theta_{13} \lesssim 0.1$, the term $m_{ee}^{(2)}$ will dominate the other two ones. If this is the case, $|m_{ee}|$ will be minimal for $\alpha = \pi/2$ and $\beta = 0$ ($-+$, cf. Table 5.1):

$$|m_{ee}|_{\rm min}^{\rm nor} = \sqrt{m_1^2 + \Delta m_\odot^2}\, s_{12}^2 c_{13}^2 - m_1 c_{12}^2 c_{13}^2 - \sqrt{m_1^2 + \Delta m_{\rm atm}^2}\, s_{13}^2. \tag{5.7}$$

Taking the best–fit and 1σ parameters, one gets $|m_{ee}|_{\rm min}^{\rm nor} = 0.0021$ (0.0011) eV for $m_1 = 0.001$ eV and $|m_{ee}|_{\rm min}^{\rm nor} = 0.0024$ (0.0015) eV for $m_1 = 0.0005$ eV.

m_1 [eV]	$\sin^2 2\theta_{13}$	$\lvert m_{ee}^{(1)}\rvert$ [eV]	$\lvert m_{ee}^{(2)}\rvert$ [eV]	$\lvert m_{ee}^{(3)}\rvert$ [eV]
0.1	0	**0.060–0.076**	0.024–0.040	0.0000
	0.05	**0.059–0.075**	0.024–0.040	0.0014–0.0015
	0.2	**0.057–0.072**	0.023–0.038	0.0056–0.0061
0.01	0	**0.0060–0.0076**	0.0031–0.0055	0.0000
	0.05	**0.0059–0.0076**	0.0031–0.0054	$(4.9–7.4)\cdot10^{-4}$
	0.2	**0.0057–0.0072**	0.0030–0.0052	0.0020–0.0031
0.001	0	$(6.0–7.6)\cdot10^{-4}$	**0.0020–0.0038**	0.0000
	0.05	$(5.9–7.5)\cdot10^{-4}$	**0.0020–0.0037**	$(4.7\text{-}7.3)\cdot10^{-4}$
	0.2	$(5.7–7.2)\cdot10^{-4}$	0.0019–0.0036	0.0020–0.0030
0.0001	0	$(6.0–7.6)\cdot10^{-5}$	**0.0020–0.0038**	0.0000
	0.05	$(5.9–7.5)\cdot10^{-5}$	**0.0020–0.0037**	$(4.7–7.3)\cdot10^{-5}$
	0.2	$(5.7–7.2)\cdot10^{-5}$	0.0019–0.0036	0.0020–0.0030

Table 5.2: The ranges of $|m_{ee}^{(i)}|$ for a 3σ variation of the oscillation parameters. Bold faced numbers indicate the dominance of the corresponding term in the whole parameter range.

Since m_1^2 is small, it can be neglected compared to $\Delta m^2_{\rm atm}$ and $\Delta m^2_\odot$, which gives the approximate formula

$$|m_{ee}|^{\rm nor}_{\rm min,max} \simeq \sqrt{\Delta m^2_\odot} s^2_{12} c^2_{13} \mp \sqrt{\Delta m^2_{\rm atm}} s^2_{13}, \tag{5.8}$$

which simply leads to a band for $|m_{ee}|$ that should, in lowest order approximation, not change with a variation of m_1. This is indeed the case in Fig. 5.2. However, with increasing θ_{13} the width of the band increases, too. If θ_{13} vanishes completely, one will simply have $|m_{ee}|^{\rm nor}_{\rm min,max} \simeq \sqrt{\Delta m^2_\odot} s^2_{12}$, which means that the band collapses to a line for definite values of $\Delta m^2_\odot$ and $\sin^2\theta_{12}$. The precise value using the best–fit parameters is 2.8 meV. All these properties can be seen in the plots. If θ_{13} is non–zero, then $|m_{ee}|^{\rm nor}_{\rm min} = |\sqrt{\Delta m^2_\odot} s^2_{12} c^2_{13} - \sqrt{\Delta m^2_{\rm atm}} s^2_{13}|$ can vanish for $s^2_{13} \simeq s^2_{12}\sqrt{\Delta m^2_\odot / \Delta m^2_{\rm atm}}$. This is between 0.034 to 0.090 for the 3σ ranges of $\Delta m^2_\odot$, $\Delta m^2_{\rm atm}$, and $\sin^2\theta_{12}$, and lies partly in the 3σ range of s^2_{13} (0–0.046). For $s^2_{13} \lesssim 0.034$, $|m_{ee}^{(2)}|$ is dominant, which means that the point $\sqrt{\Delta m^2_\odot} s^2_{12} c^2_{13}$, where the NH–band reaches the $|m_{ee}|$–axis, is nearly constant, since the cosine of θ_{13} varies only with the square of its argument. However, the width $2\sqrt{\Delta m^2_{\rm atm}} s^2_{13}$ of this band is – in this range – directly proportional to $|U_{e3}|^2$, since $\sin\theta_{13} \approx \theta_{13}$

for a small angle. If $s^2_{13} \gtrsim 0.034$, $|m^{(3)}_{ee}|$ will dominate and then the center of the band is at $\sqrt{\Delta m^2_{\rm atm}} s^2_{13}$ while the width will be $2\sqrt{\Delta m^2_{\odot}} s^2_{12} c^2_{13}$.

5.2.2 Nearly vanishing $|m_{ee}|$

This is maybe the most interesting case, since, going to the flavour basis, a very small resp. vanishing $|m_{ee}|$ would correspond to a texture zero in the neutrino mass matrix. From the model building perspective, this would be good, since such a texture would be a hint to some underlying symmetry. On the other hand, experimentally, this case would be quite a bad one, since the $0\nu\beta\beta$ lifetime is inversly proportional to the effective mass (cf. Eq. (4.10)) which means that, for a vanishing $|m_{ee}|$, neutrinoless double beta decay would never be observed, and as long as no other tests are available, one would not be able to decide, if this non–observation is due to a vanishing effective mass or due to the (still possible) Dirac nature of neutrinos.
But let us now discuss this case: for not too large values of $\sin^2 2\theta_{13}$ (up to ≈ 0.1), there exists only a limited certain region for m_1, where $|m_{ee}|$ can vanish (the "cancellation regime" in Fig. 5.3), which would also have phenomenological consequences [72, 80, 97]. Going back to the geometrical interpretation of $|m_{ee}|$, this means that we have the case, when $|m^{(1)}_{ee}|$, $|m^{(2)}_{ee}|$, and $|m^{(3)}_{ee}|$ just form a triangle. If $m_1 \neq 0$ and also $\theta_{13} \neq 0$ (this means that none of the $|m^{(i)}_{ee}|$'s vanishes), one can, for known m_1, calculate the two Majorana phases α and β by simple geometry using the law of cosines (cf. Fig. 5.1), which gives

$$\begin{aligned}\cos 2\alpha &= \frac{m^{(1)}_{ee}|^2 + |m^{(2)}_{ee}|^2 - |m^{(3)}_{ee}|^2}{2|m^{(1)}_{ee}||m^{(2)}_{ee}|} = \\ &= \frac{m_1^2\left(c^4_{13}\left(s^4_{12}+c^4_{12}\right)-s^4_{13}\right)+\Delta m^2_{\odot} s^4_{12} c^4_{13} - \Delta m^2_{\rm atm} s^4_{13}}{2m_1\sqrt{m_1^2+\Delta m^2_{\odot}}\, s^2_{12} c^2_{12} c^4_{13}}\end{aligned} \tag{5.9}$$

and

$$\begin{aligned}\cos 2\beta &= \frac{|m^{(3)}_{ee}|^2 + |m^{(2)}_{ee}|^2 - |m^{(1)}_{ee}|^2}{2|m^{(2)}_{ee}||m^{(3)}_{ee}|} = \\ &= \frac{m_1^2\left(c^4_{13}\left(s^4_{12}-c^4_{12}\right)+s^4_{13}\right)+\Delta m^2_{\odot} s^4_{12} c^4_{13} + \Delta m^2_{\rm atm} s^4_{13}}{2\sqrt{m_1^2+\Delta m^2_{\odot}}\sqrt{m_1^2+\Delta m^2_{\rm atm}}\, s^2_{12} s^2_{13} c^2_{13}}.\end{aligned} \tag{5.10}$$

Now one can consider several special cases for $|m_{ee}| \approx 0$:

- For $\theta_{13} = 0$, $m^{(3)}_{ee} = 0$, and $|m_{ee}|$ will be zero if the remaining two terms exactly cancel each other ($\alpha = \pi/2$). Then it follows e. g. from

Eq. (5.7) that

$$m_1 = \tan^2\theta_{12}\sqrt{\frac{\Delta m^2_\odot}{1-\tan^4\theta_{12}}} = \sin^2\theta_{12}\sqrt{\frac{\Delta m^2_\odot}{\cos 2\theta_{12}}}, \tag{5.11}$$

which is 4.5 meV for the best–fit parameters (1σ: 3.7-5.1 meV, 3σ: 2.8-8.4 meV), as can be seen in Fig. 5.2. As soon as the parameters have fixed values, the width of this band will be zero, since the point $|m_{ee}| = 0$ will exactly discriminate between the dominance of $|m^{(1)}_{ee}|$ and of $|m^{(2)}_{ee}|$.

- The case of $m_1 = 0$ is exactly the same as in Sec. 5.2.1, where $|m^{(1)}_{ee}| = 0$, and $|m^{(2)}_{ee}|$ and $|m^{(3)}_{ee}|$ have to cancel, which happens for $\alpha = 0$ and $\beta = \pi/2$ or vice versa. As already mentioned, θ_{13} has to be quite large for $|m_{ee}| = 0$, namely

$$\sin^2 2\theta_{13} = 4\frac{\sin^2\theta_{12}\sqrt{\Delta m^2_\odot}}{\sqrt{\Delta m^2_{\rm atm}}+\sin^2\theta_{12}\sqrt{\Delta m^2_\odot}} \simeq 4\sin^2\theta_{12}\sqrt{\frac{\Delta m^2_\odot}{\Delta m^2_{\rm atm}}}. \tag{5.12}$$

  For best–fit (1σ, 3σ) parameters, this gives 0.24 (0.19-0.28, 0.14-0.40).

- Dominance of $|m^{(2)}_{ee}|$ occurs for values of m_1 and θ_{13} which are small enough to suppress the third term. Since $|m_{ee}|$ vanishes, one still can approximate $\sqrt{m_1^2+\Delta m^2_{\rm atm}} \approx \sqrt{\Delta m^2_{\rm atm}}$, which leads to

$$|m_{ee}|^{\rm nor}_{\rm min} \simeq \sqrt{m_1^2+\Delta m^2_\odot}s^2_{12}c^2_{13} - m_1 c^2_{12}c^2_{13} - \sqrt{\Delta m^2_{\rm atm}}s^2_{13}. \tag{5.13}$$

  Setting this to zero, one gets by linearizing in m_1 and using $s^4_{13} \simeq 0$:

$$m_1 \simeq \frac{\Delta m^2_\odot s^4_{12}}{2\sqrt{\Delta m^2_{\rm atm}}c^2_{12}\tan^2\theta_{13}}. \tag{5.14}$$

  For $\sin^2 2\theta_{13} = 0.02$ this gives 0.023 eV for the best–fit parameters (1σ: 0.016 eV, 3σ: 0.009 eV), and 0.047 eV for $\sin^2 2\theta_{13} = 0.01$ (1σ: 0.032 eV, 3σ: 0.019 eV). Since this case is very specific, here, the lower 1σ and 3σ values have been inserted in order not to lose the dominance of the second term.

- The last case is the dominance of $|m^{(3)}_{ee}|$, which also needs large θ_{13}–values. One can again apply $\sqrt{m_1^2+\Delta m^2_{\rm atm}} \approx \sqrt{\Delta m^2_{\rm atm}}$, which gives

$$|m_{ee}|^{\rm nor}_{\rm min} \simeq \sqrt{\Delta m^2_{\rm atm}}s^2_{13} - \sqrt{m_1^2+\Delta m^2_\odot}s^2_{12}c^2_{13} - m_1 c^2_{12}c^2_{13}, \tag{5.15}$$

and, linearizing in m_1, leads to

$$m_1 \simeq \frac{\Delta m^2_{\rm atm} s^4_{13} - \Delta m^2_{\odot} s^4_{12} c^4_{13}}{2\sqrt{\Delta m^2_{\rm atm}} s^2_{13} c^2_{13} s^2_{12}} = \frac{\Delta m^2_{\rm atm} \tan^2\theta_{13} - \Delta m^2_{\odot} s^4_{12} \cot^2\theta_{13}}{2\sqrt{\Delta m^2_{\rm atm}} s^2_{12}}. \tag{5.16}$$

In general, the "$|m_{ee}| = 0$"–region, that has its origin in the variation of the oscillation parameters, gets larger (cf. Fig. 5.2) with increasing θ_{13} and the width of the band also grows with $|m_{ee}|$, e. g. the width is 3.6 $(5.0,\ 12) \cdot 10^{-3}$ eV for $|m_{ee}| = 10^{-3}$ eV and $\sin^2 2\theta_{13} = 0$ $(0.02,\ 0.2)$, while it is 0.4 $(1.7,\ 10) \cdot 10^{-3}$ eV for $|m_{ee}| = 10^{-4}$ eV and $\sin^2 2\theta_{13} = 0$ $(0.02,\ 0.2)$ (in both cases, the best–fit values of the oscillation parameters have been used).

5.2.3 Cosmological consequences of very small $|m_{ee}|$

Now it is time to consider an application of this width of the band for very small values of $|m_{ee}|$. Let us suppose that (sometime in the future) one has a very stringent limit on the effective neutrino mass and one additionally knows that neutrinos indeed are Majorana particles (this knowledge could come from rare decays other than $0\nu\beta\beta$, e. g. the Kaon decay $K^+ \to \pi^-\mu^+\mu^+$ [98]). Then one would know, that there can be no inverted mass ordering, because in that case, one would have already seen $0\nu\beta\beta$ at some point. Additionally one would have, depending on the value of $\sin^2 2\theta_{13}$ (and, of course, on the oscillation parameters), just a certain allowed range for the smallest neutrino mass m_1, and this is exactly where cosmology comes in: since there, one measures the sum Σ of all neutrino masses. This can be parametrized under the assumption that we indeed have only three neutrinos:

$$\Sigma = m_1 + m_2 + m_3 = m_1 + \sqrt{m_1^2 + \Delta m^2_{\odot}} + \sqrt{m_1^2 + \Delta m^2_{\rm atm}}. \tag{5.17}$$

We have calculated the possible values for Σ by taking the width of the "tube" (the range of m_1 for normal mass ordering and a certain value of $|m_{ee}|$, cf. Figs. 5.2, 5.3) and the 1σ and 3σ values of $\Delta m^2_{\odot}$ and $\Delta m^2_{\rm atm}$. The results for different values of θ_{13} can be seen in Fig. 5.4 and read off from Table 5.3. The sum Σ is always of order 0.01 eV and the range increases for a larger θ_{13}. This is due to the growing width of the tube, which corrsponds to larger intervals for m_1 (cf. Sec 5.2.2), but the major broadening comes simply from the ranges of the oscillation parameters. However, an important conclusion is, that reaching a limit of 0.001 eV on $|m_{ee}|$ is already enough to conclude that $\Sigma \approx 0.01$ eV, which would have a large impact on cosmology. As already shown in Sec. 2.3.1, the current cosmological limit on Σ lies, depending on the group which has done the analysis and on the data that has been used, between 0.17 and 1.8 eV. Even the conservative limit is just one order of magnitude larger than e. g. the 1σ range of Σ (roughly 0.05-0.08 eV)

$\lvert m_{ee}\rvert = 0.001$ eV				
$\sin^2 2\theta_{13}$	s^2_{13}	Best-fit	1σ ranges	3σ ranges
0	0	$(5.9 - 6.5) \cdot 10^{-2}$ eV	$(5.5 - 6.9) \cdot 10^{-2}$ eV	$(4.7 - 8.5) \cdot 10^{-2}$ eV
0.03	0.008	$(5.8 - 6.6) \cdot 10^{-2}$ eV	$(5.4 - 7.2) \cdot 10^{-2}$ eV	$(4.7 - 8.9) \cdot 10^{-2}$ eV
0.05	0.01	$(5.8 - 6.7) \cdot 10^{-2}$ eV	$(5.4 - 7.3) \cdot 10^{-2}$ eV	$(4.6 - 9.1) \cdot 10^{-2}$ eV
0.2	0.05	$(5.6 - 7.6) \cdot 10^{-2}$ eV	$(5.3 - 8.4) \cdot 10^{-2}$ eV	$(4.5 - 11.7) \cdot 10^{-2}$ eV
$\lvert m_{ee}\rvert = 0.0001$ eV				
$\sin^2 2\theta_{13}$	s^2_{13}	Best-fit	1σ ranges	3σ ranges
0	0	$(6.1 - 6.2) \cdot 10^{-2}$ eV	$(5.7 - 6.7) \cdot 10^{-2}$ eV	$(4.9 - 8.0) \cdot 10^{-2}$ eV
0.03	0.008	$(6.0 - 6.3) \cdot 10^{-2}$ eV	$(5.6 - 6.8) \cdot 10^{-2}$ eV	$(4.8 - 8.2) \cdot 10^{-2}$ eV
0.05	0.01	$(6.0 - 6.4) \cdot 10^{-2}$ eV	$(5.6 - 6.9) \cdot 10^{-2}$ eV	$(4.8 - 8.4) \cdot 10^{-2}$ eV
0.2	0.05	$(5.6 - 7.1) \cdot 10^{-2}$ eV	$(5.2 - 7.9) \cdot 10^{-2}$ eV	$(4.6 - 10.6) \cdot 10^{-2}$ eV

Table 5.3: The ranges of Σ for different values of $|m_{ee}|$ and θ_{13}.

implied by a very small $|m_{ee}|$. Such an improvement of the cosmological measurement is discussed in the literature (see e. g. [99]), so one could also be able to test the $0\nu\beta\beta$–prediction for the sum of all neutrino masses. Hence, even a negative search for $|m_{ee}|$ would have testable consequences for cosmology, which a positive search would have anyway (e. g. [100,101]), and one is in a win–win situation by performing a $0\nu\beta\beta$–experiment.

5.2.4 The transition to the quasi–degenerate region

For large m_1 ($\gtrsim 0.03$ eV), the neutrino masses are very similar ($m_1 \approx m_2 \approx m_3$), since the scale of the masses is in this case much larger than all mass square differences ($m_0 \gg \sqrt{\Delta m^2_{\text{atm}}}$), which can consequently be neglected. This region is called quasi–degenerate ("QD") regime (cf. Fig. 5.3). The approximate formula for the effective mass is then

$$m^{\text{nor}}_{ee} \simeq m_1 \left(c^2_{12} c^2_{13} + s^2_{12} c^2_{13} e^{2i\alpha} + s^2_{13} e^{2i\beta} \right). \tag{5.18}$$

$|m_{ee}|$ scales with m_1, which leads to a linear behavior in this region of the plots. This is indeed the case (cf. Fig. 5.2). To figure out the maximum value of $|m_{ee}|$, one just has to take $\alpha = \beta = 0$, which just gives m_1. For QD, one knows for sure that $|m^{(3)}_{ee}| \ll |m^{(2)}_{ee}| < |m^{(1)}_{ee}|$, since m_1 can be factorized out. Analogously, the minimum value of $|m_{ee}|$ will be given by

$$|m_{ee}|^{\text{nor}}_{\text{min}} = m_1 c^2_{12} c^2_{13} - \sqrt{m^2_1 + \Delta m^2_{\odot}}\, s^2_{12} c^2_{13} - \sqrt{m^2_1 + \Delta m^2_{\text{atm}}}\, s^2_{13} \tag{5.19}$$

$$\simeq m_1 \left(|U_{e1}|^2 - |U_{e2}|^2 - |U_{e3}|^2 \right) = m_1 \frac{1 - \tan^2\theta_{12} - 2\sin^2\theta_{13}}{1 + \tan^2\theta_{12}} \equiv m_1 f(\theta_{12}, \theta_{13}),$$

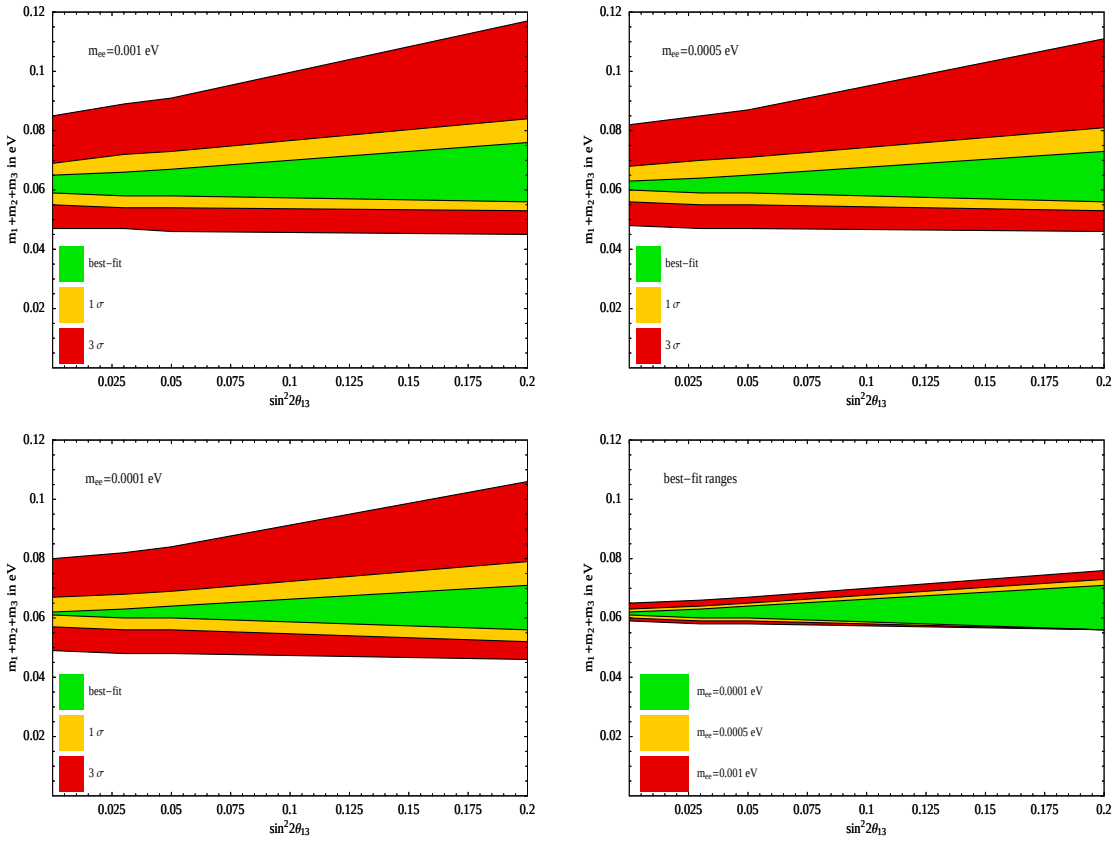

Figure 5.4: The ranges of the sum Σ of all neutrino masses for a certain very small $|m_{ee}|$ (and hence for a normal mass ordering) and different values of θ_{13} calculated using Eq. (5.17) and the best–fit, 1σ, and 3σ values of the oscillation parameters.

which is obtained by $\alpha = \beta = \pi/2$ ($--$, cf. Table 5.1). The function $f(\theta_{12}, \theta_{13})$ is discussed in Ref. [72]. Its best–fit value (1σ, 3σ range) is 0.38 (0.32-0.44, 0.15-0.52), and $m_1(1 - f(\theta_{12}, \theta_{13}))$ is the width of the band in the QD regime.

5.3 The effective mass for inverted mass ordering

Let us now turn to inverted mass ordering, where the smallest mass eigenvalue is m_3. Taking this mass as parameter, one gets

$$m_{ee}^{\rm inv} = \sqrt{m_3^2 + \Delta m^2_{\rm atm}}\, c_{12}^2 c_{13}^2 + \sqrt{m_3^2 + \Delta m^2_{\odot} + \Delta m^2_{\rm atm}}\, s_{12}^2 c_{13}^2 e^{2i\alpha} + m_3 s_{13}^2 e^{2i\beta}. \tag{5.20}$$

This will again be maximal for $\alpha = \beta = 0$, namely

$$|m_{ee}|^{\text{inv}}_{\text{max}} = \sqrt{m_3^2 + \Delta m^2_{\text{atm}}} c_{12}^2 c_{13}^2 + \sqrt{m_3^2 + \Delta m^2_{\odot} + \Delta m^2_{\text{atm}}} s_{12}^2 c_{13}^2 + m_3 s_{13}^2 . \tag{5.21}$$

This will be largest for inserting the maximum values of Δm^2_{atm}, $\Delta m^2_{\odot}$, and s^2_{12}, and the minimum value of s^2_{13}. In fact, the dependence of this expression on s^2_{12} is only small, since its contribution is proportional to $\left(\sqrt{m_3^2 + \Delta m^2_{\text{atm}} + \Delta m^2_{\odot}} - \sqrt{m_3^2 + \Delta m^2_{\text{atm}}}\right)$, which is always small, independent of m_3.

In contrast to normal mass ordering, it is here not difficult to calculate an analytical expression for the minimal $|m_{ee}|$. It holds that $\Delta m^2_{\text{atm}} \gg \Delta m^2_{\odot}$, which gives, for every m_3,

$$\frac{|m^{(2)}_{ee}|}{|m^{(1)}_{ee}|} \simeq \tan^2 \theta_{12} \quad \text{and} \quad \frac{|m^{(3)}_{ee}|}{|m^{(2)}_{ee}|} = \frac{m_3}{\sqrt{m_3^2 + \Delta m^2_{\text{atm}}}} \frac{s^2_{13}}{s^2_{12} c^2_{13}}, \tag{5.22}$$

so $|m^{(2)}_{ee}|/|m^{(1)}_{ee}|$ is always smaller than one within the parameter range and $|m^{(3)}_{ee}|/|m^{(2)}_{ee}|$ even much smaller, which gives $|m^{(3)}_{ee}| \ll |m^{(2)}_{ee}| \ll |m^{(1)}_{ee}|$. This corresponds to the case "$--$" in Table 5.1 ($\alpha = \beta = \pi/2$):

$$|m_{ee}|^{\text{inv}}_{\text{min}} = \sqrt{m_3^2 + \Delta m^2_{\text{atm}}} c_{12}^2 c_{13}^2 - \sqrt{m_3^2 + \Delta m^2_{\odot} + \Delta m^2_{\text{atm}}} s_{12}^2 c_{13}^2 - m_3 s_{13}^2 . \tag{5.23}$$

This will be minimal for minimal Δm^2_{atm} and the largest values of $\Delta m^2_{\odot}$, s^2_{12}, and s^2_{13}, and defines, together with Eq. (5.21), the band in Fig. 5.2 for inverted mass ordering.

5.3.1 The strictly hierarchical part: $m_3 \to 0$

For a negligible m_3 (hierarchical regime in Fig. 5.3), Eq. (5.20) simplifies to (see e. g. Ref. [102])

$$m^{\text{inv}}_{ee} \simeq \sqrt{\Delta m^2_{\text{atm}}} c^2_{13} \left(c^2_{12} + s^2_{12} e^{2i\alpha}\right) . \tag{5.24}$$

Then, the mass scale of $|m_{ee}|$ is always $\sqrt{\Delta m^2_{\text{atm}}}$, and $|m_{ee}|^{\text{inv}}$ lies between $\sqrt{\Delta m^2_{\text{atm}}} c^2_{13} \cos 2\theta_{12}$ and $\sqrt{\Delta m^2_{\text{atm}}} c^2_{13}$, which leads to a width of $2\sqrt{\Delta m^2_{\text{atm}}} s^2_{12}$. This width is 0.03 eV for the best–fit parameters (1σ: 0.025–0.034 eV, 3σ: 0.018–0.046 eV). The dependence of this width on s^2_{13} is very weak (since it is just proportional to $(1 - s^2_{13})$), and it never vanishes in the allowed parameter ranges, which shows that – in this regime – $|m_{ee}|$ does not contain much information about the yet unknown mixing angle θ_{13}.

5.3.2 The transition to the quasi–degenerate region

This is exactly the same as for normal mass ordering, which has been presented in Sec. 5.2.4. The only difference is that m_1 has to be replaced by m_3 to switch from normal to inverted mass ordering, but in this regime all mass eigenvalues are equal to m_0 anyway.

5.4 The possible distinction between normal and inverted mass ordering

One of the most exciting possible results of a $0\nu\beta\beta$–experiment is the distinction between normal and inverted mass ordering [72, 102, 103]. Therefore, one can have a look at the dependence of the gap between the bands for the two different orderings on θ_{13}. From Fig. 5.2, one can already see that the width of the gap decreases for increasing $\sin^2 2\theta_{13}$. Now it is time to investigate this behaviour in more detail. Obviously, the larger the gap the better the chance to distingiush between both orderings. Intuitively, one would expect this distinction to be more difficult for a worse knowlegde of the oscillation parameters, which turns out to be true by looking at the figures: using the 3σ range of the neutrino oscillation parameters narrows the gap compared to the best–fit values. Of course, in case that neutrino masses are quasi–degenerate in their masses, the possibility of distinction between the two ordering must also be washed out, which is true since for QD one just has a band of values which shows no difference between both possibilities. Hence we assume the hierarchical regime for the rest of this section.
Another point has not yet been included in our analysis, but mentioned in Sec. 4.2: the uncertainty ζ in the calculation of the nuclear matrix elements. This can be implemented here by using the following form for the gap $\Delta|m_{ee}|$ between inverted and normal mass ordering:

$$\Delta|m_{ee}| \equiv |m_{ee}|^{\text{inv}}_{\text{min}} - \zeta |m_{ee}|^{\text{nor}}_{\text{max}}. \tag{5.25}$$

Then, this $\Delta|m_{ee}|$ represents the largest experimental uncertainty in the determination of $|m_{ee}|$ [72]. In case of larger uncertainties, a discrimination between normal and inverted mass ordering will not be possible. Here, $|m_{ee}|^{\text{nor}}_{\text{max}}$ is given by Eq. (5.6) and $|m_{ee}|^{\text{inv}}_{\text{min}}$ by Eq. (5.23). In general, this has the explicit form

$$\begin{aligned}\Delta|m_{ee}| = &\left(\sqrt{m_{\text{sm}}^2 + \Delta m_{\text{atm}}^2} - \zeta m_{\text{sm}}\right) c_{12}^2 c_{13}^2 - \\ &- \left(\sqrt{m_{\text{sm}}^2 + \Delta m_{\odot}^2 + \Delta m_{\text{atm}}^2} + \zeta \sqrt{m_{\text{sm}}^2 + \Delta m_{\odot}^2}\right) s_{12}^2 c_{13}^2 - \\ &- \left(\zeta \sqrt{m_{\text{sm}}^2 + \Delta m_{\text{atm}}^2} + m_{\text{sm}}\right) s_{13}^2,\end{aligned} \tag{5.26}$$

where $m_{\rm sm}$ is the smallest neutrino mass eigenvalue. The most important dependence of $\Delta|m_{ee}|$ is the one on s^2_{13}. Since the first two lines of in Eq. (5.26) depend only on c^2_{13}, which only varies slowly in the possible range for θ_{13}, the shape of this function should be in principle linearly decreasing in s^2_{13}. A larger ζ then simply increases the negative slope of this line. This is shown for $m_{\rm sm} = 0.005$ eV and different values of s^2_{12} and ζ in Fig. 5.5, which exactly shows the expected behavior.
The value $\Delta|m_{ee}|$ of the gap is in general of the order $\mathcal{O}(\sqrt{\Delta m^2_{\rm atm}}c^2_{13})$, which can be shown by expanding it in the small quantities

$$R \equiv \frac{\Delta m^2_\odot}{\Delta m^2_{\rm atm}} \quad \text{and} \quad \eta \equiv \frac{m_{\rm sm}}{\sqrt{\Delta m^2_{\rm atm}}}. \tag{5.27}$$

Then, Eq. (5.26) reads

$$\begin{aligned}\Delta|m_{ee}| = \sqrt{\Delta m^2_{\rm atm}}c^2_{13}\Big(c^2_{12}\Big(\sqrt{1-\eta^2}-\eta\zeta\Big) - \\ -s^2_{12}\Big(\sqrt{1-\eta^2+R}+\zeta\sqrt{R+\eta^2}\Big) \\ -\Big(\eta+\sqrt{1-\eta^2}\zeta\Big)\tan^2\theta_{13}\Big).\end{aligned} \tag{5.28}$$

To zeroth order in all small quantities R, ζ, and θ_{13}, it turns out that $\Delta|m_{ee}| \simeq \sqrt{\Delta m^2_{\rm atm}}\cos 2\theta_{12} = |m_{ee}|^{\rm inv}_{\rm min}$. In the limit $m_{\rm sm} \to 0$, and neglecting $\Delta m^2_\odot$ compared to $\Delta m^2_{\rm atm}$, $\Delta|m_{ee}|$ simplifies to

$$\Delta|m_{ee}|(m_{\rm sm}\to 0) \simeq \sqrt{\Delta m^2_{\rm atm}}\left(c^2_{13}(c^2_{12}-s^2_{12}) - \zeta s^2_{13}\right) - \zeta\sqrt{\Delta m^2_\odot}s^2_{12}c^2_{13}. \tag{5.29}$$

This is now exactly a linear function in s^2_{13}: for no nuclear uncertainty ($\zeta = 1$), it decreases, using the best–fit parameters, monotonously from 15.0 meV at $s^2_{13} = 0$ to 12.0 meV at $s^2_{13} = 0.05$. For a larger value of ζ, the point where the graph intersects the "$\theta_{13} = 0$"–axis gets shifted to a lower value (last term in Eq. (5.29)) and the negative slope increases (part of the term in parantheses). E.g. for $\zeta = 2$, the width of the gap decreases from 12.3 meV at $s^2_{13} = 0$ to 7.0 meV at $s^2_{13} = 0.05$. The dependence of $\Delta|m_{ee}|$ on θ_{12} is quite strong [72], which is reflected here by using different values of this angle. E.g. for $s^2_{12} = 0.24$ (lower 3σ bound), the width decreases from 22.3 meV to 18.8 meV, while for the upper bound of 0.40 i t does so from 5.8 meV to 3.2 meV, both for $\zeta = 1$ (cf. Fig. 5.5, where also the dependence on ζ is illustrated).
The physical message that can be extracted from all these numerics is, that $0\nu\beta\beta$ and neutrino oscillation experiments play a complementary role for the determination of the neutrino mass ordering: a small value of θ_{13} of course makes it difficult to measure this angle in an oscillation experiment, since the oscillation amplitude then will also be very small (cf. Eq. (2.30)). This is the reason that this small angle is still unknown, while θ_{12} and θ_{23}

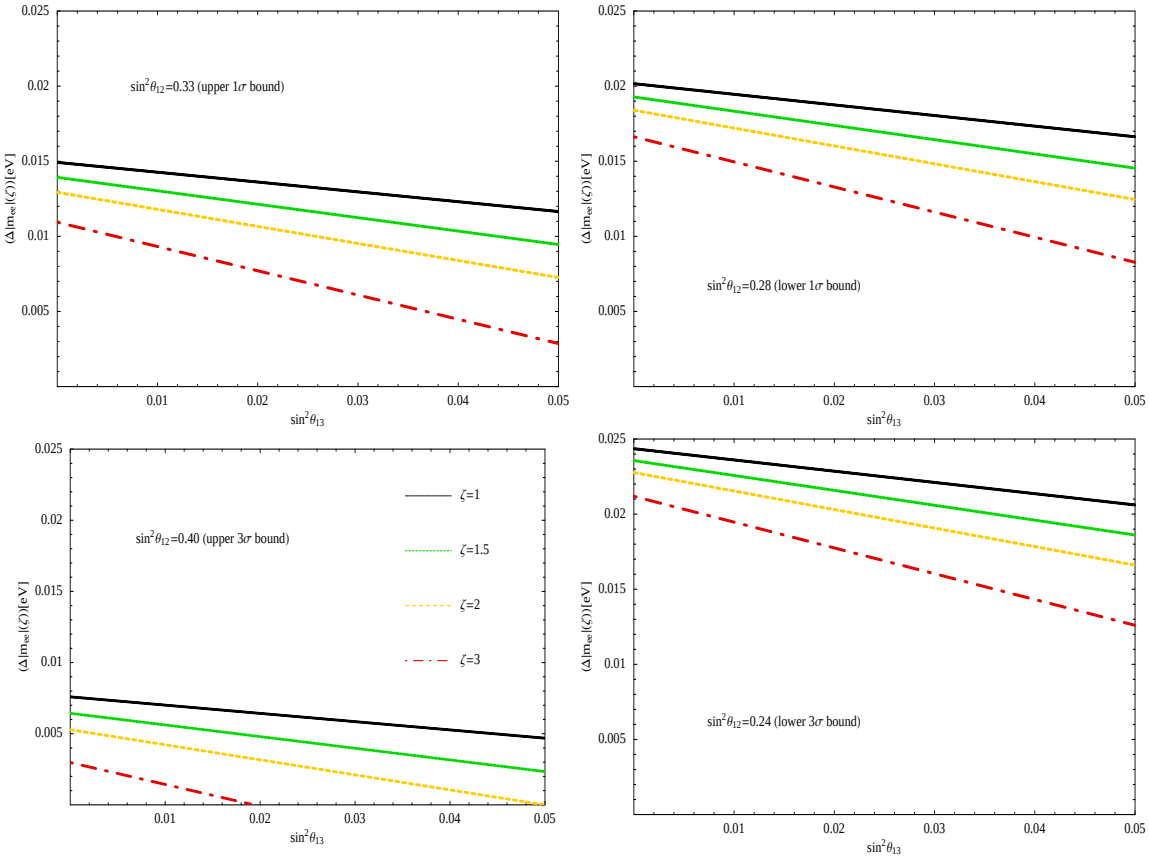

Figure 5.5: The gap $\Delta|m_{ee}|$ between $|m_{ee}|^{\rm inv}_{\rm min}$ and $\zeta|m_{ee}|^{\rm nor}_{\rm max}$ as a function of $\sin^2\theta_{13}$ for an illustrative value of $m_{\rm sm} = 0.005$ eV, different sets of oscillation parameters, and different nuclear matrix element uncertainties ζ.

are at least measured with a certain accuracy. Since already the detection of the oscillation is difficult in this case, it is clear that this will also affect the determination of the mass orderings. On the other hand, from Fig. 5.5, one can see that the width of the gap between normal and inverted mass ordering shrinks for a larger θ_{13}, which makes it more difficult to distinguish normal and inverted ordering by a $0\nu\beta\beta$-experiment. In turn, a larger mixing angle will be better for oscillation experiments. Both methods are affected by a bad knowledge of the oscillation parameters as well as some model–dependence (e. g. the assumption that neutrinos are Majorana particles for $0\nu\beta\beta$).

5.5 Other elements of the mass matrix

As already mentioned in Secs. 4.3 and 5.2.3, neutrinoless double beta decay as in Eq. (4.9) is not the only lepton number or flavour violating process

that could occur. Rare processes like muon–electron conversion or some Kaon decays are possible, but current experiments are not yet sensitive to them [98, 104, 105]. But in principle, just as in $0\nu\beta\beta$, a decay like $K^+ \to \pi^-\mu^+\mu^+$ would have a branching ratio proportional to $|m_{\mu\mu}|^2$. Also for model–builders it can be interesting to have a detailed analysis of other neutrino mass matrix elements and not just $|m_{ee}|$. The rest of the matrix elements can be classified in the ones with electron flavour contribution ($m_{e\mu}$ and $m_{e\tau}$) and the ones without ($m_{\mu\mu}$, $m_{\tau\tau}$, and $m_{\mu\tau}$). The former ones yield some correlations for IH or QD while the latter ones are only interesting for QD–neutrinos. The work in this section is based on [95].

5.5.1 The mass matrix elements $m_{e\mu}$ and $m_{e\tau}$

The general expression for the $e\mu$–element of the neutrino mass matrix is

$$m_{e\mu} = c_{13}\left(\left(e^{2i\alpha}m_2 - m_1\right)s_{12}c_{12}c_{23} + e^{i\delta}\left(e^{2i\beta}m_3 - e^{2i\alpha}m_2 s_{12}^2 - m_1 c_{12}^2\right)s_{23}s_{13}\right). \tag{5.30}$$

This form is more complicated than the one for m_{ee}, which comes from the chosen parametrisation for the PMNS–matrix. Note that here, we have an off–diagonal element of the mass matrix. The CP–phase δ cannot be eliminated and it has (as well as the two Majorana phases α and β) to be varied from $-\pi$ to π. This variation is plotted for the best–fit and the 3σ oscillation parameters in Fig. 5.6.
One can now have a look at some extreme cases, namely $\theta_{13} = 0$ and $\theta_{23} = \pi/4$:

- $\theta_{13} = 0$: The $e\mu$–element of the mass matrix looks like

$$(m_{e\mu})_{\theta_{13}=0} = \left(e^{2i\alpha}m_2 - m_1\right)s_{12}c_{12}c_{23}, \tag{5.31}$$

which gives as lower limits

$$|m_{e\mu}|_{\theta_{13}=0} \gtrsim \begin{cases} s_{12}c_{12}c_{23}\sqrt{\Delta m^2_{\odot}} & = 0.003 \text{ eV} \quad \text{NH}, \\ s_{12}c_{12}c_{23}\frac{\Delta m^2_{\odot}}{2\sqrt{\Delta m^2_{\text{atm}}}} & = 0.0003 \text{ eV} \quad \text{IH}, \\ s_{12}c_{12}c_{23}\frac{\Delta m^2_{\odot}}{2m_0} & = 2.6\cdot 10^{-5} \text{ eV} \quad \text{QD}, \end{cases} \tag{5.32}$$

with the best–fit parameters and $m_0 = 0.5$ eV for QD. This means that, for vanishing θ_{13}, the $e\mu$–element of the mass matrix cannot vanish exactly, but it can be very close to zero. The corresponding upper limits are

$$|m_{e\mu}|_{\theta_{13}=0} \lesssim s_{12}c_{12}c_{23}\begin{cases} \sqrt{\Delta m^2_{\odot}} & = 0.003 \text{ eV} \quad \text{NH}, \\ \sqrt{\Delta m^2_{\text{atm}}} & = 0.014 \text{ eV} \quad \text{IH}, \\ m_0 & = 0.15 \text{ eV} \quad \text{QD}, \end{cases} \tag{5.33}$$

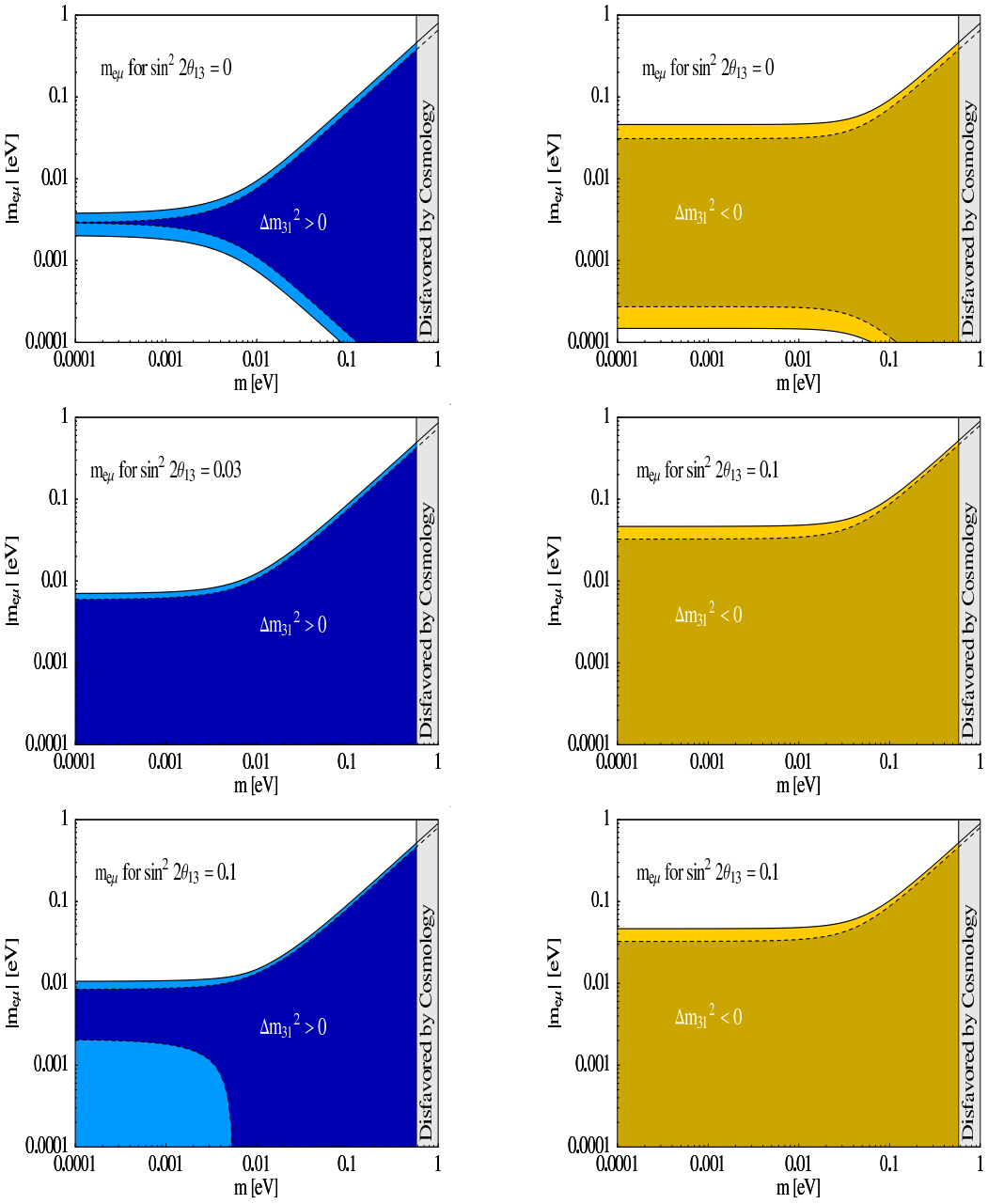

Figure 5.6: The absolute value of the $e\mu$–element of the neutrino mass matrix for three example values of θ_{13} (left: normal, right: inverted mass ordering) and the best–fit and 3σ oscillation parameters. All three phases are varied from $-\pi$ to π. Because of $\mu\tau$–symmetry, a plot of $|m_{e\tau}|$ looks practically identical.

which explains the narrow band for NH as well as the broadening for IH. Approximate expressions in the different regimes are

$$|m_{e\mu}|_{\theta_{13}=0} \simeq \begin{cases} \frac{1}{2}\sqrt{\Delta m^2_\odot}\, c_{23} \sin 2\theta_{12} & \text{NH}, \\ c_{23} \sin 2\theta_{12} \sqrt{\Delta m^2_{\text{atm}}} \sin\alpha & \text{IH}, \\ m_0 c_{23} \sin 2\theta_{12} \sin\alpha & \text{QD}. \end{cases} \tag{5.34}$$

This also explains the broader range for $|m_{e\mu}|_{\theta_{13}=0}$ in the cases of IH and QD: the Majorana phase term $\sin\alpha$ can take any value between -1 and 1, which is not the case for NH, where the scale is roughly $\sqrt{\Delta m^2_\odot}/\sqrt{8}$. This is about 0.002 eV for the best–fit parameters.

- $\theta_{23} = \frac{\pi}{4}$: Here, the mass matrix element is

$$(m_{e\mu})_{\theta_{23}=\pi/4} = \frac{c_{13}}{\sqrt{2}}\Big[\left(e^{2i\alpha} m_2 - m_1\right) s_{12} c_{12} + \\ + e^{i\delta}\left(e^{2i\beta} m_3 - e^{2i\alpha} m_2 s_{12}^2 - m_1 c_{12}^2\right) s_{13}\Big]. \tag{5.35}$$

The absolute values are with best–fit (1σ, 3σ) parameters 2.9 (0–7.1, 0–12.3) meV for NH, 0–30.7 (0–34.8, 0–40.6) meV for IH, and 0–0.33 (0–0.38, 0–0.43) eV for QD and $m_0 = 0.5$ eV. Values of $\sin^2 2\theta_{13}$ around 0.03 allow for complete cancellation even for NH (cf. the first two best–fit plots on the left panel in Fig. 5.6). This comes because for these specific values, the two leading terms, namely $\sqrt{\Delta m^2_\odot} s_{12} c_{12}$ and $\sqrt{\Delta m^2_{\text{atm}}} s_{13}$, happen to be almost identical. For smaller values of $\sin^2 2\theta_{13}$, the first term dominates, and for larger ones, the second term does so. In IH and QD, the matrix element can always practically vanish for $\sin\alpha \simeq 0$, which could also be seen in $0\nu\beta\beta$:

$$|m_{ee}|^{m_{e\mu}=0}_{\theta_{13}\neq 0} \simeq \begin{cases} \sqrt{\Delta m^2_{\text{atm}}}\, c_{13}^2 & \text{IH}, \\ m_0 c_{13}^2 & \text{QD}. \end{cases} \tag{5.36}$$

In Fig. 5.7, some observable parameters are plotted in the case that $m_{e\mu}$ vanishes. On the left, there is a scatter plot of the smallest neutrino mass (denoted m here) against the Majorana phase α. As expected for inverted mass ordering, α is equal to 0 or $\pm\pi$, which causes $\sin\alpha$ to vanish, and hence the effective mass is essentially given by $\sqrt{\Delta m^2_{\text{atm}}}$ for IH and m_0 for QD. This is exactly what causes the band for the effective mass on the right of Fig. 5.7 to be very narrow, since only those cases with $\sin\alpha \simeq 0$ lead to a vanishing $e\mu$–element of the mass matrix. Accordingly, if we knew the value for $|m_{e\mu}|$, a discrimination between normal and inverted mass ordering would be much easier than just by measuring $|m_{ee}|$.

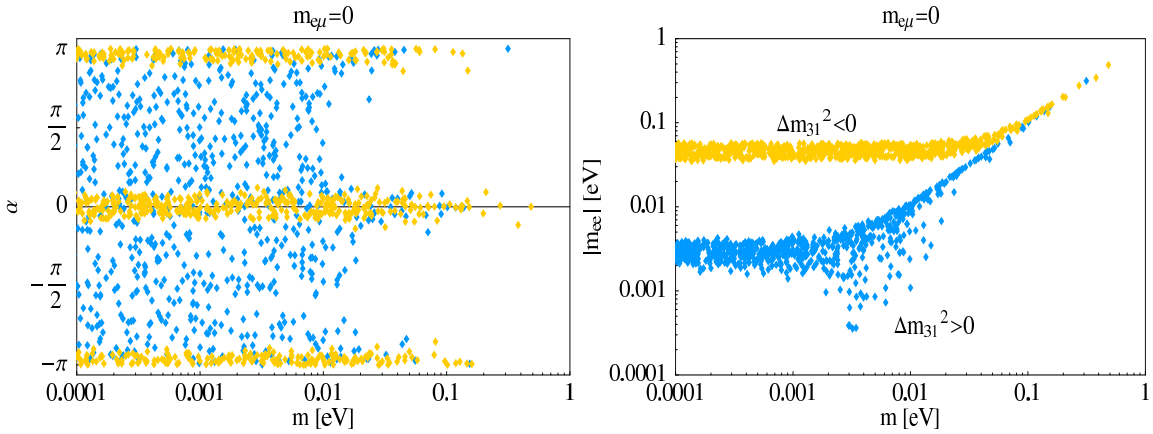

Figure 5.7: Possible observables for $m_{e\mu} = 0$. The left plot shows the smallest neutrino mass m against the Majorana phase α, and the right one shows the smallest against the effective mass. In both cases, the blue (dark) dots indicate normal, and the yellow (light) ones indicate inverted mass ordering. The oscillation parameters are varied within their 3σ ranges.

Finally, the $e\tau$–element of the mass matrix is

$$m_{e\tau} = c_{13}\left(\left(m_1 - e^{2i\alpha}m_2\right)s_{12}c_{12}s_{23} + e^{i\delta}\left(e^{2i\beta}m_3 - e^{2i\alpha}m_2 s_{12}^2 - m_1 c_{12}^2\right)c_{23}s_{13}\right), \tag{5.37}$$

which is nothing than $m_{e\mu}$ with the replacements $s_{23} \to c_{23}$ and $c_{23} \to -s_{23}$. Due to the $\mu\tau$–symmetry [106, 107], a plot of this matrix element would be practically indistinguishable from Fig. 5.6.

5.5.2 The mass matrix elements $m_{\mu\mu}$, $m_{\tau\tau}$, and $m_{\mu\tau}$

Let us start with $m_{\mu\mu}$ which reads

$$\begin{aligned} m_{\mu\mu} = {} & m_1\left(c_{23}\,s_{12} + e^{i\delta}c_{12}s_{13}s_{23}\right)^2 + \\ & + e^{2i\alpha}m_2\left(c_{12}c_{23} - e^{i\delta}s_{12}s_{13}s_{23}\right)^2 + e^{2i(\beta+\delta)}m_3 c_{13}^2 s_{23}^2. \end{aligned} \tag{5.38}$$

This is plotted in Fig. 5.8 as function of the smallest neutrino mass for both mass orderings and for the best–fit parameters as well as their 3σ ranges. Again, there are two special cases:

- $\theta_{13} = 0$: Then, the $\mu\mu$–element is

$$(m_{\mu\mu})_{\theta_{13}=0} = c_{23}^2\left(e^{2i\alpha}m_2 c_{12}^2 + m_1 s_{12}^2\right) + e^{2i(\beta+\delta)}m_3 s_{23}^2. \tag{5.39}$$

In the three different regimes, this gives

$$|m_{\mu\mu}|_{\theta_{13}=0} \simeq \begin{cases} s_{23}\sqrt{\Delta m^2_{\text{atm}} s^2_{23} + 2\sqrt{\Delta m^2_{\odot}\Delta m^2_{\text{atm}}}c^2_{12}c^2_{23}\cos 2(\alpha-\beta-\delta)} & \text{NH,} \\ \sqrt{\Delta m^2_{\text{atm}}}c^2_{23}\sqrt{1-\sin^2 2\theta_{12}\sin^2\alpha} & \text{IH,} \\ m_0\left|c^2_{23}\left(e^{2i\alpha}c^2_{12}+s^2_{12}\right)+e^{2i(\beta+\delta)}s^2_{23}\right| & \text{QD,} \end{cases} \tag{5.40}$$

Hence, the scale of $m_{\mu\mu}$ in the hierarchical regime for vanishing θ_{13} is roughly $\sqrt{\Delta m^2_{\text{atm}}}/2 \simeq 0.02$ eV (note that for IH, cancellations up to 50% are possible due to the phase–term, which plays only a minor role for NH, where the first term under the square root is dominant). Numerically, the best–fit (1σ, 3σ) oscillation parameters give 20.2–26.3 (15.8–31.1, 6.4–41.3) meV for NH, 8.9–23.5 (6.6–27.9, 2.4–37.9) meV for IH, and 0.0–0.5 (0.0–0.5, 0.0–0.5) eV for QD and $m_0 = 0.5$ eV.

For $\theta_{13} = 0$, $m_{\mu\mu}$ cannot vanish for NH and IH (cf. Fig. 5.8). For NH, the $\mu\mu$–element is centered around $\sqrt{\Delta m^2_{\text{atm}}}/2$ and for IH, it is equal to $|m_{ee}|$ multiplied with c^2_{23}. In this case, also $m_{e\mu}$ and $m_{e\tau}$ would be known to be quite small. Hence, if one for sure has an inverted hierarchy, e. g. by measuring an $|m_{ee}|$ around 0.05 eV in a $0\nu\beta\beta$–experiment, one can also determine other elements of the mass matrix without the need to know the Majorana phase α. This clearly shows, that already the knowledge of the neutrino mass hierarchy would greatly improve our knowledge about the nature of neutrinos, since the ordering implies a definite structure in the neutrino mass matrix.

In the case of QD–neutrinos, Eq. (5.40) implies that $|m_{\mu\mu}|$ will be zero, if only the term inside the modulus vanishes. However, looking at Fig. 5.8, one can see that this is not true for normal mass ordering, at least for using the best–fit oscillation parameters. It looks especially strange, that the curves for normal and inverted ordering seem to be so different in that case. However, this can be easily understood by defining the small quantities $2r_{\odot} \equiv \Delta m^2_{\odot}/m^2_0$ and $2r_{\text{atm}} \equiv \Delta m^2_{\text{atm}}/m^2_0$, which allow to write $m_1 = m_0$, $m_2 \simeq m_0(1+r_{\odot})$, and $m_3 \simeq m_0(1+r_{\text{atm}})$ for NH, and $m_1 \simeq m_0(1+r_{\text{atm}})$, $m_2 \simeq m_0(1+r_{\odot}+r_{\text{atm}})$, and $m_3 = m_0$ for IH (cf. Eq. (5.3)). For $m_{\mu\mu}$ in the QD regime with $\theta_{13} = 0$ and $\theta_{23} = \pi/4$, this gives approximately

$$m_{\mu\mu} \approx \begin{cases} \frac{m_0}{2}\left(s^2_{12}+c^2_{12}e^{2i\alpha}(1+r_{\odot})+e^{2i(\beta+\delta)}(1+r_{\text{atm}})\right) & \text{normal,} \\ \frac{m_0}{2}\left(s^2_{12}(1+r_{\text{atm}})+c^2_{12}e^{2i\alpha}(1+r_{\text{atm}}+r_{\odot})+e^{2i(\beta+\delta)}\right) & \text{inverted.} \end{cases} \tag{5.41}$$

In both cases, the term proportional to $e^{2i(\beta+\delta)}$ dominates, but for inverted mass ordering, the sum of the two subdominant terms can exceed the value of the dominating one. For normal mass ordering, this

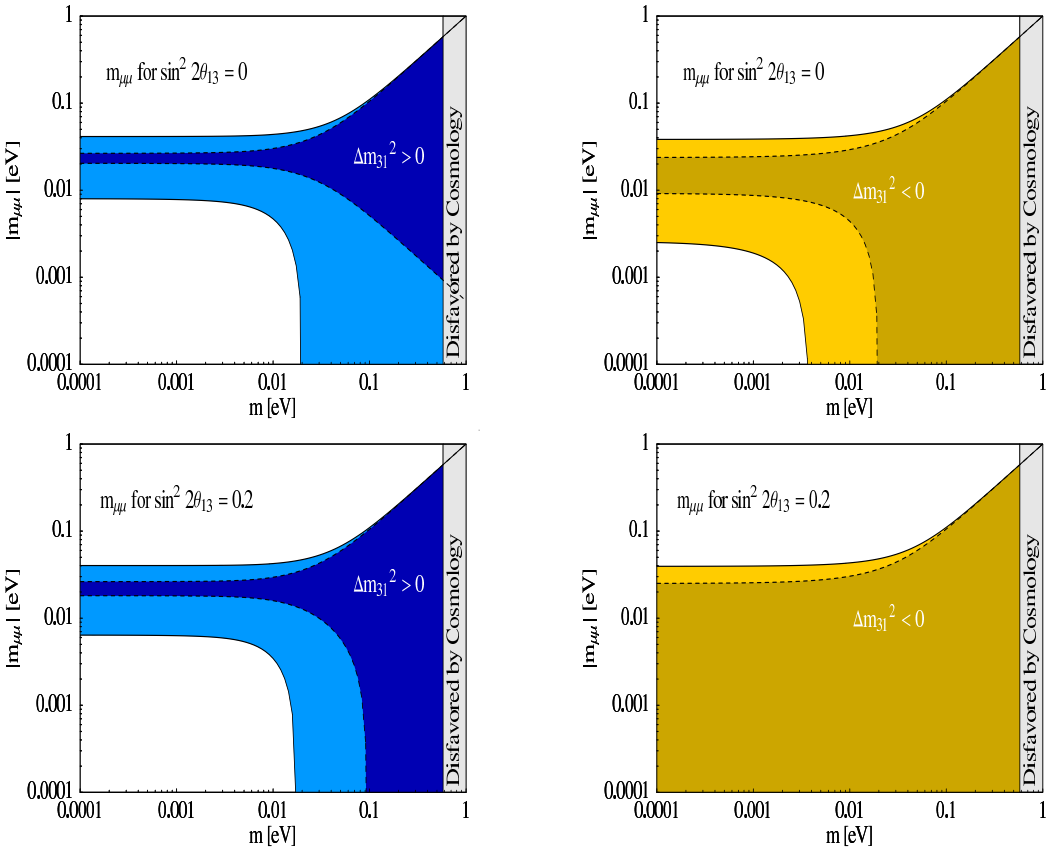

Figure 5.8: The absolute value of the $\mu\mu$–element of the neutrino mass matrix for two example values of θ_{13} (left: normal, right: inverted mass ordering) and the best–fit and 3σ oscillation parameters. All three phases are varied from $-\pi$ to π. Because of $\mu\tau$–symmetry, a plot of $|m_{\tau\tau}|$ looks practically identical.

is not possible due to the different dependence of the particular terms on the mass square differences. Hence, the $\mu\mu$–element of the neutrino mass matrix can only vanish for an inverted mass ordering, as long as the best–fit values of the oscillation parameters are somehow accurate. For normal ordering, the minimal value of $|m_{\mu\mu}|$ (and the difference between normal and inverted mass ordering in the QD regime) is given by $\frac{1}{2}m_0(r_{\text{atm}} - c_{12}^2 r_\odot)$. This is about 0.0018 eV for $m_0 = 0.3$ eV, which is in agreement with Fig. 5.8. In principle, a difference of this order also occurs for other matrix elements, like $|m_{ee}|$, where this difference is approximately $m_0 r_{\text{atm}}$, but there the absolute values of the particular element are orders larger than this difference, and hence, it is not visible in the associated plots (cf. Fig. 5.3).

Anyway, the approximate expression for $|m_{\mu\mu}|$ can lead to an interesting correlation between θ_{23} and the Majorana phase α, as will be shown at the end of this section.

- $\theta_{23} = \frac{\pi}{4}$: In this case,

$$(m_{\mu\mu})_{\theta_{23}=\pi/4} = \frac{1}{2}\left(m_1 \Big(s_{12} + e^{i\delta} c_{12} s_{13} \Big)^2 + \right.$$
$$\left. + e^{2i\alpha} m_2 \Big(c_{12} - e^{i\delta} s_{12} s_{13} \Big)^2 + e^{2i(\beta+\delta)} m_3 c_{13}^2 \right), \quad (5.42)$$

which gives numerically, again for the usual different parameter ranges, 0.9–1.2 (0.8–1.4, 0.1–1.8) meV for NH, 8.9–23.5 (2.9–25.9, 0–31.1) meV for IH, and 0–0.50 (0–0.50, 0–0.51) eV for QD and $m_0 = 0.5$ eV. The only important thing is, that now $m_{\mu\mu}$ can also vanish for IH in contrast to the case where $\theta_{13} = 0$ (cf. last picture for best–fit values on the right panel of Fig. 5.8).

Going to $m_{\tau\tau}$ should again not cause a big difference, due to $\mu\tau$–symmetry. This element reads

$$m_{\tau\tau} = m_1 \Big(e^{i\delta} c_{12} s_{13} c_{23} - s_{23} s_{12} \Big)^2 +$$
$$+ e^{2i\alpha} m_2 \Big(c_{12} s_{23} + e^{i\delta} s_{12} s_{13} c_{23} \Big)^2 + e^{2i(\beta+\delta)} m_3 c_{13}^2 c_{23}^2. \quad (5.43)$$

A plot would look identical to Fig. 5.8.
The remaining element is $m_{\mu\tau}$. Its absolute value looks most complicated:

$$|m_{\mu\tau}| = \frac{1}{2} \cos 2\theta_{23} e^{i\delta} \left(m_1 - e^{2i\alpha} m_2 \right) \sin 2\theta_{12} s_{13} -$$
$$- \frac{1}{2} \sin 2\theta_{23} \left(e^{2i\alpha} m_2 c_{12}^2 + m_1 \, s_{12}^2 - \right.$$
$$\left. - \, e^{2i\delta} \left(e^{2i\beta} m_3 c_{13}^2 + \left(m_1 c_{12}^2 + e^{2i\alpha} m_2 s_{12}^2 \right) s_{13}^2 \right) \right). \quad (5.44)$$

Note that the first term is suppressed due to the smallness of θ_{13} and due to the close–to–maximal value of θ_{23}. This element is plotted in Fig. 5.9, which looks not much different from $m_{\mu\mu}$ and $m_{\tau\tau}$. Important is that, for vanishing θ_{13}, this element can only be zero for an inverted mass ordering, even if all oscillation parameters are varied within their full 3σ ranges. The reason for this is again the interplay of the terms with the mass square differences. In the strongly hierarchical regime, this element can never be zero, even if θ_{13} is relatively large.
To finish this section, let us mention one interesting correlation, that can occur in the QD regime for vanishing (or nearly vanishing) $m_{\mu\mu}$, $m_{\tau\tau}$, or

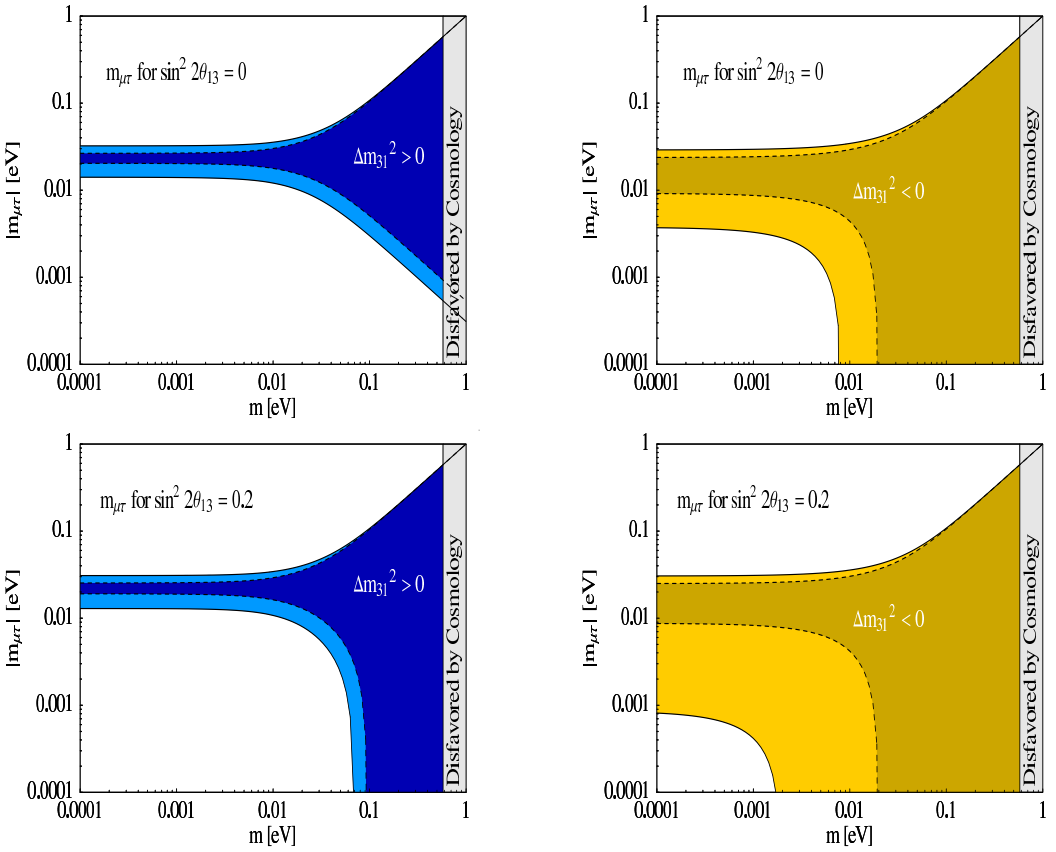

Figure 5.9: The absolute value of the $\mu\tau$–element of the neutrino mass matrix for two example values of θ_{13} (left: normal, right: inverted mass ordering) and the best–fit and 3σ oscillation parameters. All three phases are varied from $-\pi$ to π.

$m_{\mu\tau}$. The approximate expressions for all three elements in this case with $\theta_{13} = 0$ are

$$
\begin{aligned}
|m_{\mu\mu}|^{\mathrm{QD}} &\simeq m_0 \left| c_{23}^2 \left(e^{2i\alpha} c_{12}^2 + s_{12}^2 \right) + e^{2i(\beta+\delta)} s_{23}^2 \right| , \\
|m_{\tau\tau}|^{\mathrm{QD}} &\simeq m_0 \left| s_{23}^2 \left(e^{2i\alpha} c_{12}^2 + s_{12}^2 \right) + e^{2i(\beta+\delta)} c_{23}^2 \right| , \\
|m_{\mu\tau}|^{\mathrm{QD}} &\simeq m_0 c_{23} s_{23} \left| \left(e^{2i\alpha} c_{12}^2 + s_{12}^2 \right) - e^{2i(\beta+\delta)} \right| . \qquad (5.45)
\end{aligned}
$$

Note that the $\mu\tau$–element cannot vanish for normal mass ordering if $\theta_{13} = 0$, but in all other cases, this works, and this is illustrated in Fig. 5.10. A zero $m_{\mu\mu}$ is not possible for $\sin^2 2\theta_{23} > 1$, and accordingly $m_{\tau\tau}$ cannot vanish for $\sin^2 2\theta_{23} < 1$. This is reflected in the visible symmetry of the associated points in the figure. Exactly maximal θ_{23} will lead to vanishing $m_{\mu\mu}$ and

$m_{\tau\tau}$ if $\sin\alpha = 0$ or $\sin(\beta+\delta) = 1$.
Hence, also for the elements presented here, some correlations are possible in certain special cases.

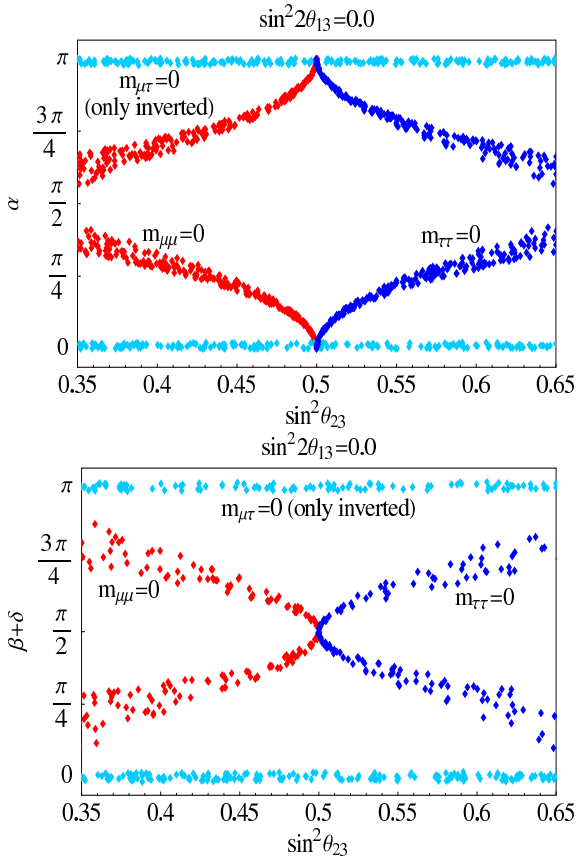

Figure 5.10: The correlation between θ_{23} and α (top) and between θ_{23} and $\beta+\delta$ (bottom) for QD neutrinos and $\theta_{13} = 0$ in case that particular elements of the neutrino mass matrix vanish. For the $\mu\tau$–element, there is no dependence on θ_{23}, as expected from Eq. (5.45), since θ_{23} does not appear inside the absolute value. All parameters except θ_{13} are varied within their 3σ ranges.

Chapter 6

Conclusions

We have started with an introduction of some pieces of neutrino physics, which are relevent for this work. Therefore, we have explained mass terms of Dirac and Majorana type, as well as the seesaw mechanism, which could be a natural explanation for the astonishing smallness of neutrino masses. Afterwards, we have turned to neutrino oscillations, which are only possible for massive neutrinos. Hence, the detection of this phenomenon is an evidence that not all neutrino masses can be zero. Meanwhile, neutrino oscillations are accepted and well understood, but the parameters are not yet known to a very good precision, which makes it at some points difficult to discriminate between different theoretical models. As closure of Chapter 2, the cosmological methods to get bounds on neutrino masses as well as the time–of–flight measurements of neutrinos coming from supernova explosions have been discussed.

In Chapter 3, a possible method to perform a precision measurement of the solar parameters of neutrino oscillation, θ_{12} and $\Delta m^2_{\odot}$, has been presented. One could use a Large Liquid Scintillator Detector (LLSD) like the proposed 45 kt LENA experiment. Since this detector has a large fiducial mass, it is possible to take a small (in fact mobile) reactor for such a measurement to get good results. We have performed a detailed statistical analysis of such a configuration using the χ^2 approach. Some estimates can be made analytically (under certain assumptions), but reliable results are only possible with a numerical simulation. This has been done using the GLoBES software package. As backgrounds, some neighbouring nuclear reactors as well as Geo–neutrinos have been taken into account. Due to its uncertainties, the latter background needs an accurate treatment, which has been done by having a look at different Geo–neutrino scenarios and by a careful implementation in the minimization algorithm. As a result, the optimum baselines turn out to be roughly around 50 km. Geo–neutrinos shift the best baselines to higher values (70–80 km). For a mobile reactor, the precision of a measurement of θ_{12} or $\Delta m^2_{\odot}$ turns out to be around 5%, while with a

large reactor even a precision on the sub–percent level would be possible.
Then, in Chapter 4, we have reviewed the known methods for a direct measurement of the neutrino mass, which are possible in a laboratory. First, the kinematical measurement using the β^-–decay of tritium has been introduced. Such experiments have already been performed, but until now, there exists only an upper bound of the "$\overline{\nu}_e$–mass" of e. g. 2.3 eV at 95% C.L. from the Mainz experiment. The upcoming KATRIN experiment will improve this limit to 0.2 eV. A different way of measuring the neutrino mass would be by neutrinoless double beta decay ($0\nu\beta\beta$), which is the simultaneous emission of two electrons by one nucleus without the emission of the associated neutrinos. This process can only happen for Majorana neutrinos and would hence also be a test for the fundamental nature of neutrinos as well as for a possible violation of the lepton number, but has not been observed yet due to the large lifetime ($\sim 10^{24}$ years). What would be measured in this decay, is the so–called effective neutrino mass $|m_{ee}|$, which has been discussed in the following chapter. At the end, we have also presented possible alternatives to $0\nu\beta\beta$, such as neutrinoless double electron capture as well as neutrinoless single electron capture together with simultaneous emission of a positron.
Finally, in Chapter 5, we have dealt with the neutrino mass matrix and have analyzed its entries. The most important one of these is the effective mass $|m_{ee}|$ as measured in neutrinoless double beta decay. This mass has been discussed in detail and all possible cases for both hiearchies and with special focus on a future improved limit on the not yet measured mixing angle θ_{13} are presented. The effective mass shows quite characteristic features, that could help to distingiush between the two possible mass orderings of neutrino masses, normal ($m_1 < m_2 < m_3$) and inverted ($m_3 < m_1 < m_2$). Unfortunately, for normal mass ordering, this effective mass could even vanish and since it is inversely proportional to the lifetime of $0\nu\beta\beta$, this would make the observation of such a process impossible. In that situation, one might not be able to decide if this non–observation comes from the fact that neutrinos are indeed Dirac particles or simply from the effective mass being zero. However, if one knew from some other measurement that neutrinos are indeed Majorana particles, one could derive very stringent bound from this "negative" result on the sum Σ of all neutrino masses, which can be tested by cosmological observations. For the sake of completeness, also the other elements of the neutrino mass matrix are discussed and possible implications of some of them being zero are presented.
Crucial for all possible results is a good knowledge of the neutrino oscillation parameters. One can hope that we will soon enter an era of precision measurements on neutrino properties to be able to distinguish between different models and to learn more about the nature of these fascinating objects called neutrinos Wolgang Pauli has "invented" already more than 70 years ago.

Acknowledgments

Writing this thesis would have never been possible in this form without the help of some very important people. Now it's time to express my thank to (hopefully) all of them. Already now, I also say sorry to those I have forgotten to mention!!! If you know me, you will know that this never happened on purpose!
First of all, I want to express my sincere thank to my supervisor Manfred Lindner. He has affiliated me as group member and he has given me the chance to work on exciting topics. During this diploma thesis (and before), I have learned a lot, and I am grateful for this opportunity. He has supported me in having own ideas and had so often time for questions – even when he has been extremely busy. I also want to say thank you for the chance to participate in the Young Scientists' Workshop on "Hot topics in particle and astro–particle physics" at Ringberg Castle, the ISAPP summer school on "Neutrinos in Physics, Astrophysics and Cosmology" in Munich, as well as in the WE–Heraeus–Seminar on "Massive Neutrinos" in Bad Honnef.
Of course, I also want to thank my collaborators Joachim F. Kopp, Manfred Lindner, Werner Rodejohann, and Mark "Marc" Rolinec for the nice work together. For interesting discussions on a lot of things related to work here (and beyond) and also for work done together, I additionally want to thank Naoyuki Haba, Toshihiko Ota, and Walter Potzel.
I want to thank "the experimental guys" Jean–Côme Lanfranchi, Teresa Marrodán–Undagoitia, Lothar Oberauer, Walter Potzel, and Michael Wurm for providing me with a lot of information on experimental issues and for being patient with a theorist, who cannot understand anything without having giant formulae to help.
For having time for all my stupid questions I want to thank Naoyuki Haba, Claudia Hagedorn, Toshihiko Ota, Werner Rodejohann, and Michael A. Schmidt.
I'm especially grateful to Patrick Huber for awaking my interest in neutrinos and being my first contact to this really cool group.
For endless patience with me being an absolute dummy concerning computers I want to thank Stefan Recksiegel and especially Markus Michael Müller.
For proof–reading this work, I want to thank Joachim Kopp, Mark Rolinec,

and Michael Schmidt.
My former office mate Florian Plentinger has just left Munich and is now a Ph. D.–student in Würzburg – Flo, thank you for the funny time together and for the bets you have lost against me. By the way: you still owe me a beer! ;-)
For contributing to the nice atmosphere here, I want to thank all people who have been part of this group during my hitherto time here and whom I have not yet mentioned: Evgeny Akhmedov, Florian Bauer, Alexander Blum, Marc–Thomas Eisele, Mathias Garny, Srubabati Goswami, Andreas Hohenegger, Toshifumi Jittoh, Michael Ratz, Rabindra Mohapatra, Joe Sato, Yoshio Sato, and Alexei Yu. Smirnov.
Special thanks goes to the adorable ladies: AMANDA, GERDA, KATRIN, LENA, ... and Double Chooz (?!?).
Danke den Sekretärinnen Laura Darabas, Alexandra Füldner und Karin Ramm dafür, dass sie mich immer mit so wichtigen Sachen wie Papier und Stiften versorgt haben, und für die Hilfe bei solch komplizierten Tätigkeiten wie dem Senden von Faxen und dem Verschicken von Paketen.
Für viele lustige Stunden in der Uni (und außerhalb) danke ich Yvonne Gawlina, Daniela Lindner, Sebastian Schöll und Michael Wurm. Vorletzterem, zusammen mit Alexander Penger und Marius Schulte, danke ich auch noch für viele spannende Snooker–Abende.
Vielen vielen Dank an die besten Freunden auf dieser Welt: Daniel Czap, Bettina Prüller, Andreas Regler, Lukas Sennefelder und Matthias Stecher. Es ist echt verdammt cool, dass ihr es immer noch mit mir aushalten könnt!

Der allergrößte Dank gebührt jedoch meinen Eltern Franz und Katharina Merle. Ohne Euch wäre dieses Studium nie möglich gewesen – und vieles andere auch nicht. Vielen Dank für Eure Unterstützung und dafür, dass Ihr immer hinter mir steht. Ich liebe Euch, Ihr seid beide ganz große Klasse!!!

Bibliography

[1] N. Schmitz, *Neutrinophysik*, first ed., Teubner-Studienbücher, Stuttgart, 1997.

[2] P. A. Tipler, *Physik*, first ed., Spektrum Akademischer Verlag, Heidelberg, 2000.

[3] *Celebrating the Neutrino*, Special Issue of Los Alamos Science **25** (1997).

[4] M. Lindner, `http://users.physik.tu-muenchen.de/lindner/neutrinos.html`.

[5] M. Fukugita and T. Yanagida, *Physics of Neutrinos and Applications to Astrophysics*, first ed., Springer Verlag, Berlin Heidelberg, 2003.

[6] M. E. Peskin and D. V. Schroeder, *An Introduction to Quantum Field Theory*, first ed., Westview Press, 1995.

[7] B. Kayser, *The New World of Neutrino Physics*, 2006, Presented at the International School on Particle and Astroparticle Physics (ISAPP06) on "Neutrinos in Particle Physics and Astrophysics", Max-Planck-Institut für Physik, Munich, Germany, 24-31 May 2006.

[8] E. Akhmedov, *Neutrino Oscillations: Phenomenology, results, future*, 2006, Presented at the International School on Particle and Astroparticle Physics (ISAPP06) on "Neutrinos in Particle Physics and Astrophysics", Max-Planck-Institut für Physik, Munich, Germany, 24-31 May 2006.

[9] C. Giunti and C. W. Kim, *Quantum mechanics of neutrino oscillations*, Found. Phys. Lett. **14** (2001), 213–229, `hep-ph/0011074`.

[10] R. Davis, *A review of the Homestake solar neutrino experiment*, Prog. Part. Nucl. Phys. **32** (1994), 13–32.

[11] OPERA, `http://operaweb.web.cern.ch/operaweb/index.shtml`.

[12] OPERA, F. Di Capua, *Status of the OPERA experiment*, PoS **HEP2005** (2006), 177.

[13] SNO, S. N. Ahmed et al., *Measurement of the total active B-8 solar neutrino flux at the Sudbury Neutrino Observatory with enhanced neutral current sensitivity*, Phys. Rev. Lett. **92** (2004), 181301, nucl-ex/0309004.

[14] SNO, Q. R. Ahmad et al., *Direct evidence for neutrino flavor transformation from neutral-current interactions in the Sudbury Neutrino Observatory*, Phys. Rev. Lett. **89** (2002), 011301, nucl-ex/0204008.

[15] SNO, Q. R. Ahmad et al., *Measurement of day and night neutrino energy spectra at SNO and constraints on neutrino mixing parameters*, Phys. Rev. Lett. **89** (2002), 011302, nucl-ex/0204009.

[16] KamLAND, K. Eguchi et al., *First results from KamLAND: Evidence for reactor anti- neutrino disappearance*, Phys. Rev. Lett. **90** (2003), 021802, hep-ex/0212021.

[17] KamLAND, T. Araki et al., *Measurement of neutrino oscillation with KamLAND: Evidence of spectral distortion*, Phys. Rev. Lett. **94** (2005), 081801, hep-ex/0406035.

[18] L. Wolfenstein, *Neutrino oscillations in matter*, Phys. Rev. **D17** (1978), 2369.

[19] S. P. Mikheev and A. Y. Smirnov, *Resonance enhancement of oscillations in matter and solar neutrino spectroscopy*, Sov. J. Nucl. Phys. **42** (1985), 913–917.

[20] Super-Kamiokande, Y. Fukuda et al., *Evidence for oscillation of atmospheric neutrinos*, Phys. Rev. Lett. **81** (1998), 1562–1567, hep-ex/9807003.

[21] Super-Kamiokande, S. Fukuda et al., *Determination of solar neutrino oscillation parameters using 1496 days of Super-Kamiokande-I data*, Phys. Lett. **B539** (2002), 179–187, hep-ex/0205075.

[22] K2K, K. Kaneyuki, *Recent results from K2K*, Nucl. Phys. Proc. Suppl. **145** (2005), 124–127.

[23] K2K, L. Ludovici, *K2K preliminary ν_μ oscillation analysis of the full data set*, Nucl. Phys. Proc. Suppl. **155** (2006), 160–161.

[24] MINOS, N. Tagg, *First MINOS results from the NuMI beam*, (2006), hep-ex/0605058.

[25] MINOS, R. Plunkett, *Status of MINOS after one year of running*, (2006), Presented at 3rd International Workshop on NO-VE: Neutrino Oscillations in Venice: 50 Years after the Neutrino Experimental Discovery, Venice, Italy, 7-10 Feb 2006.

[26] CHOOZ, M. Apollonio et al., *Limits on neutrino oscillations from the CHOOZ experiment*, Phys. Lett. **B466** (1999), 415–430, hep-ex/9907037.

[27] V. Barger, D. Marfatia, and K. Whisnant, *Progress in the physics of massive neutrinos*, Int. J. Mod. Phys. **E12** (2003), 569–647, hep-ph/0308123.

[28] T. Schwetz, *Neutrino oscillations: Current status and prospects*, Acta Phys. Polon. **B36** (2005), 3203–3214, hep-ph/0510331.

[29] G. L. Fogli, E. Lisi, A. Marrone, and D. Montanino, *Status of atmospheric $\nu_\mu \to \nu_\tau$ oscillations and decoherence after the first K2K spectral data*, Phys. Rev. **D67** (2003), 093006, hep-ph/0303064.

[30] J. N. Bahcall, M. C. Gonzalez-Garcia, and C. Pena-Garay, *Solar neutrinos before and after Neutrino 2004*, JHEP **08** (2004), 016, hep-ph/0406294.

[31] A. Bandyopadhyay, S. Choubey, S. Goswami, S. T. Petcov, and D. P. Roy, *Update of the solar neutrino oscillation analysis with the 766-Ty KamLAND spectrum*, Phys. Lett. **B608** (2005), 115–129, hep-ph/0406328.

[32] M. Maltoni, T. Schwetz, M. A. Tortola, and J. W. F. Valle, *Status of global fits to neutrino oscillations*, New J. Phys. **6** (2004), 122, hep-ph/0405172.

[33] C. Giunti, *Absolute neutrino masses*, Acta Phys. Polon. **B36** (2005), 3215–3226, hep-ph/0511131.

[34] G. L. Fogli, E. Lisi, A. Marrone, and A. Palazzo, *Global analysis of three-flavor neutrino masses and mixings*, (2005), hep-ph/0506083.

[35] S. M. Bilenky, C. Giunti, J. A. Grifols, and E. Masso, *Absolute values of neutrino masses: Status and prospects*, Phys. Rept. **379** (2003), 69–148, hep-ph/0211462.

[36] S. Hannestad, *Neutrinos and Cosmology*, 2006, Presented at the International School on Particle and Astroparticle Physics (ISAPP06) on "Neutrinos in Particle Physics and Astrophysics", Max-Planck-Institut für Physik, Munich, Germany, 24-31 May 2006.

[37] J. C. Mather, D. J. Fixsen, R. A. Shafer, C. Mosier, and D. T. Wilkinson, *Calibrator Design for the COBE Far Infrared Absolute Spectrophotometer (FIRAS)*, Astrophys. J. **512** (1999), 511–520, astro-ph/9810373.

[38] 2dFGRS, O. Lahav, *The 2dF Galaxy Redshift Survey: Cosmological Parameters and Galaxy Biasing*, (2002), astro-ph/0205382.

[39] U. Seljak, A. Slosar, and P. McDonald, *Cosmological parameters from combining the Lyman-α forest with CMB, galaxy clustering and SN constraints*, (2006), astro-ph/0604335.

[40] SDSS, M. Tegmark et al., *Cosmological parameters from SDSS and WMAP*, Phys. Rev. **D69** (2004), 103501, astro-ph/0310723.

[41] S. Pakvasa and K. Tennakone, *Neutrinos of Non-Zero Rest Mass*, Phys. Rev. Lett. **28** (1972), 1415.

[42] N. Cabibbo, L. Gratton, G. Salvini, N. Dallaporta, and F. Pacini, *Astrophysics and Elementary Particles, Common Problems*, Proceedings, International Meeting, ROME, ITALY, FEBRUARY 21-23, 1980, Accad. Naz. Lincei (1980) 311p.

[43] A. S. Dighe, M. T. Keil, and G. G. Raffelt, *Identifying earth matter effects on supernova neutrinos at a single detector*, JCAP **0306** (2003), 006, hep-ph/0304150.

[44] A. S. Dighe and A. Y. Smirnov, *Identifying the neutrino mass spectrum from the neutrino burst from a supernova*, Phys. Rev. **D62** (2000), 033007, hep-ph/9907423.

[45] T. J. Loredo and D. Q. Lamb, *Bayesian analysis of neutrinos observed from supernova SN 1987A*, Phys. Rev. **D65** (2002), 063002, astro-ph/0107260.

[46] D. N. Schramm, *Neutrinos from Supernova SN1987A*, Comments Nucl. Part. Phys. **17** (1987), 239.

[47] P. Huber, M. Lindner, and W. Winter, *Simulation of long-baseline neutrino oscillation experiments with* GLoBES, Comput. Phys. Commun. **167** (2005), 195, hep-ph/0407333, http://www.ph.tum.de/~globes.

[48] L. Oberauer, F. von Feilitzsch, and W. Potzel, *A large liquid scintillator detector for low-energy neutrino astronomy*, Nucl. Phys. Proc. Suppl. **138** (2005), 108–111.

[49] J. F. Kopp, M. Lindner, A. Merle, and M. Rolinec, *Reactor Neutrino Experiments with a Large Liquid Scintillator Detector*, (2006), hep-ph/0606151.

[50] C. L. Cowan, F. Reines, F. B. Harrison, H. W. Kruse, and A. D. McGuire, *Detection of the free neutrino: A Confirmation*, Science **124** (1956), 103–104.

[51] L. Oberauer and F. von Feilitzsch, *Neutrino oscillations*, Rept. Prog. Phys. **55** (1992), 1093–1163.

[52] H. Murayama and A. Pierce, *Energy spectra of reactor neutrinos at KamLAND*, Phys. Rev. **D65** (2002), 013012, `hep-ph/0012075`.

[53] P. Vogel and J. F. Beacom, *The angular distribution of the neutron inverse beta decay, $\overline{\nu}_e + p \to e^+ + n$*, Phys. Rev. **D60** (1999), 053003, `hep-ph/9903554`.

[54] T. M. Undagoitia et al., *Search for the proton decay $p \to K + \overline{\nu}$ in the large liquid scintillator low energy neutrino astronomy detector LENA*, Phys. Rev. **D72** (2005), 075014, `hep-ph/0511230`.

[55] M. Blennow, T. Ohlsson, and W. Winter, *Damping signatures in future neutrino oscillation experiments*, JHEP **06** (2005), 049, `hep-ph/0502147`.

[56] Particle Data Group, S. Eidelman et al., *Review of particle physics*, Phys. Lett. **B592** (2004), 1.

[57] P. Huber, M. Lindner, T. Schwetz, and W. Winter, *Reactor neutrino experiments compared to superbeams*, Nucl. Phys. **B665** (2003), 487–519, `hep-ph/0303232`.

[58] M. Galassi et al., *GNU Scientific Library Reference Manual*, second ed.

[59] P. Huber, J. Kopp, M. Lindner, M. Rolinec, and W. Winter, *From Double Chooz to Triple Chooz: Neutrino physics at the Chooz reactor complex*, (2006), `hep-ph/0601266`.

[60] F. Ardellier et al., *Letter of intent for double-CHOOZ: A search for the mixing angle θ_{13}*, (2004), `hep-ex/0405032`.

[61] L. Oberauer, private communication.

[62] M. Wurm, private communication.

[63] `http://www.insc.anl.gov/`.

[64] `http://www.icjt.org/nukestat/index.html`.

[65] F. Mantovani, L. Carmignani, G. Fiorentini, and M. Lissia, *Antineutrinos from the earth: The reference model and its uncertainties*, Phys. Rev. **D69** (2004), 013001, `hep-ph/0309013`.

[66] S. Enomoto, *Neutrino Geophysics and Observation of Geo-Neutrinos at KamLAND*, Ph.D. thesis, 2005.

[67] S. Enomoto, http://www.awa.tohoku.ac.jp/ sanshiro/geoneutrino/spectrum/.

[68] K. A. Hochmuth et al., *Probing the earth's interior with the Low Energy Neutrino Astronomy detector*, (2005), hep-ph/0509136.

[69] J. Kopp, M. Lindner, and A. Merle, *Self-Calibration of Neutrino Detectors using characteristic Backgrounds*, work in progress.

[70] J. Hecht, *US plans portable nuclear power plants*, New Scientist **2463** (2004).

[71] H. Minakata, H. Nunokawa, W. J. C. Teves, and R. Zukanovich Funchal, *Reactor measurement of θ_{12}: Principles, accuracies and physics potentials*, Phys. Rev. **D71** (2005), 013005, hep-ph/0407326.

[72] S. Choubey and W. Rodejohann, *Neutrinoless double beta decay and future neutrino oscillation precision experiments*, Phys. Rev. **D72** (2005), 033016, hep-ph/0506102.

[73] M. Lindner, A. Merle, and W. Rodejohann, *Improved limit on θ_{13} and implications for neutrino masses in neutrino-less double beta decay and cosmology*, Phys. Rev. **D73** (2006), 053005, hep-ph/0512143.

[74] M. Blennow, T. Ohlsson, and H. Snellman, *Day-night effect in solar neutrino oscillations with three flavors*, Phys. Rev. **D69** (2004), 073006, hep-ph/0311098.

[75] H. Minakata and A. Y. Smirnov, *Neutrino mixing and quark lepton complementarity*, Phys. Rev. **D70** (2004), 073009, hep-ph/0405088.

[76] KATRIN, A. Osipowicz et al., *KATRIN: A next generation tritium beta decay experiment with sub-eV sensitivity for the electron neutrino mass*, (2001), hep-ex/0109033.

[77] W. Rodejohann, *Neutrinoless double beta decay and the neutrino mass matrix*, 2006, Presented at the 2nd Scandinavian NeutrinO Workshop, AlbaNova University Center, Stockholm, Sweden, 2-6 May 2006.

[78] C. Kraus et al., *Final results from phase II of the Mainz neutrino mass search in tritium beta decay*, Eur. Phys. J. **C40** (2005), 447–468, hep-ex/0412056.

[79] V. M. Lobashev, *Study of the tritium beta-spectrum in experiment 'Troitsk nu-mass'*, Prog. Part. Nucl. Phys. **48** (2002), 123–131.

[80] Z.-z. Xing, *Vanishing effective mass of the neutrinoless double beta decay?*, Phys. Rev. **D68** (2003), 053002, hep-ph/0305195.

[81] S. R. Elliott and P. Vogel, *Double beta decay*, Ann. Rev. Nucl. Part. Sci. **52** (2002), 115–151, hep-ph/0202264.

[82] A. Faessler and F. Simkovic, *Double beta decay*, J. Phys. **G24** (1998), 2139–2178, hep-ph/9901215.

[83] S. R. Elliott and J. Engel, *Double beta decay*, J. Phys. **G30** (2004), R183, hep-ph/0405078.

[84] V. A. Rodin, A. Faessler, F. Simkovic, and P. Vogel, *On the uncertainty in the 0nu beta beta decay nuclear matrix elements*, Phys. Rev. **C68** (2003), 044302, nucl-th/0305005.

[85] O. Civitarese and J. Suhonen, *Light-neutrino masses and hierarchies and the observability of neutrinoless beta beta decay*, Nucl. Phys. **A729** (2003), 867–883, nucl-th/0208005.

[86] F. Simkovic, *The Nuclear Matrix Elements for Double Beta Decay*, 2006, Presented at Neutrino 2006, Santa Fe's Lensic Theater, Santa Fe, Mexico, 13-19 June 2006.

[87] H. V. Klapdor-Kleingrothaus et al., *Latest results from the Heidelberg-Moscow double-beta-decay experiment*, Eur. Phys. J. **A12** (2001), 147–154, hep-ph/0103062.

[88] IGEX, C. E. Aalseth et al., *The IGEX Ge-76 neutrinoless double-beta decay experiment: Prospects for next generation experiments*, Phys. Rev. **D65** (2002), 092007, hep-ex/0202026.

[89] K. Zuber, *COBRA: Double beta decay searches using CdTe detectors*, Phys. Lett. **B519** (2001), 1–7, nucl-ex/0105018.

[90] I. Abt et al., *A new Ge-76 double beta decay experiment at LNGS*, (2004), hep-ex/0404039.

[91] J. Bernabeu, A. De Rujula, and C. Jarlskog, *Neutrinoless double electron capture as a tool to measure the electron-neutrino mass*, Nucl. Phys. **B223** (1983), 15.

[92] M. Doi and T. Kotani, *Neutrinoless modes of double beta decay*, Prog. Theor. Phys. **89** (1993), 139–160.

[93] Z. Sujkowski and S. Wycech, *Neutrino-less double electron capture: A tool to search for Majorana neutrinos*, Phys. Rev. **C70** (2004), 052501, hep-ph/0312040.

[94] M. G. T. Lasserre, *Double Chooz: A search for the neutrino mixing angle θ_{13}*, (2006), hep-ex/0606025.

[95] A. Merle and W. Rodejohann, *The elements of the neutrino mass matrix: Allowed ranges and implications of texture zeros*, Phys. Rev. **D73** (2006), 073012, hep-ph/0603111.

[96] B. Kayser, *CPT, CP, and C phases and their Effects in Majorana Particle Processes*, Phys. Rev. **D30** (1984), 1023.

[97] S. Pascoli, S. T. Petcov, and L. Wolfenstein, *Searching for the CP-violation associated with Majorana neutrinos*, Phys. Lett. **B524** (2002), 319–331, hep-ph/0110287.

[98] K. Zuber, *Effective Majorana neutrino masses*, (2000), hep-ph/0008080.

[99] S. Hannestad, *Neutrino mass bounds from cosmology*, Nucl. Phys. Proc. Suppl. **145** (2005), 313–318, hep-ph/0412181.

[100] V. Barger, S. L. Glashow, D. Marfatia, and K. Whisnant, *Neutrinoless double beta decay can constrain neutrino dark matter*, Phys. Lett. **B532** (2002), 15–18, hep-ph/0201262.

[101] F. R. Joaquim, *Neutrino masses from beta decays after KamLAND and WMAP*, Phys. Rev. **D68** (2003), 033019, hep-ph/0304276.

[102] S. Pascoli, S. T. Petcov, and T. Schwetz, *The absolute neutrino mass scale, neutrino mass spectrum, Majorana CP-violation and neutrinoless double-beta decay*, Nucl. Phys. **B734** (2006), 24–49, hep-ph/0505226.

[103] S. Pascoli, S. T. Petcov, and W. Rodejohann, *On the neutrino mass spectrum and neutrinoless double-beta decay*, Phys. Lett. **B558** (2003), 141–156, hep-ph/0212113.

[104] W. Rodejohann, *Neutrino oscillation experiments and limits on lepton number and lepton flavor violating processes*, Phys. Rev. **D62** (2000), 013011, hep-ph/0003149.

[105] A. Atre, V. Barger, and T. Han, *Upper bounds on lepton-number violating processes*, Phys. Rev. **D71** (2005), 113014, hep-ph/0502163.

[106] A. S. Joshipura, *Universal 2-3 symmetry*, (2005), hep-ph/0512252.

[107] R. N. Mohapatra and W. Rodejohann, *Broken mu-tau symmetry and leptonic CP violation*, Phys. Rev. **D72** (2005), 053001, hep-ph/0507312.

Index